Calhoun
Institutional Archive of the Naval Postgraduate School

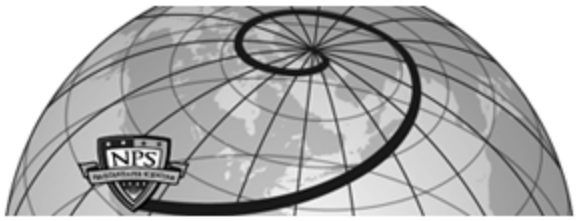

Author(s)	Humphrey, Matthew Donald
Title	Texture analysis of high resolution panchromatic imagery for terrain classification
Publisher	Monterey, California. Naval Postgraduate School
Issue Date	2003-06
URL	http://hdl.handle.net/10945/971

This document was downloaded on May 04, 2015 at 22:35:22

DUDLEY KNOX LIBRARY

http://www.nps.edu/library

Calhoun is a project of the Dudley Knox Library at NPS, furthering the precepts and goals of open government and government transparency. All information contained herein has been approved for release by the NPS Public Affairs Officer.

Dudley Knox Library / Naval Postgraduate School
411 Dyer Road / 1 University Circle
Monterey, California USA 93943

NPS PRAESTANTIA PER SCIENTIAM 1909

http://www.nps.edu/

NAVAL POSTGRADUATE SCHOOL
Monterey, California

THESIS

TEXTURE ANALYSIS OF HIGH RESOLUTION PANCHROMATIC IMAGERY FOR TERRAIN CLASSIFICATION

by

Matthew Donald Humphrey

June 2003

Thesis Advisor:	Richard C. Olsen
Second Reader:	Alan A. Ross

Approved for public release; distribution is unlimited

THIS PAGE INTENTIONALLY LEFT BLANK

REPORT DOCUMENTATION PAGE

Form Approved OMB No. 0704-0188

Public reporting burden for this collection of information is estimated to average 1 hour per response, including the time for reviewing instruction, searching existing data sources, gathering and maintaining the data needed, and completing and reviewing the collection of information. Send comments regarding this burden estimate or any other aspect of this collection of information, including suggestions for reducing this burden, to Washington headquarters Services, Directorate for Information Operations and Reports, 1215 Jefferson Davis Highway, Suite 1204, Arlington, VA 22202-4302, and to the Office of Management and Budget, Paperwork Reduction Project (0704-0188) Washington DC 20503.

1. AGENCY USE ONLY *(Leave blank)*	2. REPORT DATE	3. REPORT TYPE AND DATES COVERED
	June 2003	Master's Thesis

4. TITLE AND SUBTITLE Texture Analysis of High Resolution Panchromatic Imagery for Terrain Classification

5. FUNDING NUMBERS

6. AUTHOR (S) Matthew D. Humphrey

7. PERFORMING ORGANIZATION NAME(S) AND ADDRESS(ES)
Naval Postgraduate School
Monterey, CA 93943-5000

8. PERFORMING ORGANIZATION REPORT NUMBER

9. SPONSORING / MONITORING AGENCY NAME(S) AND ADDRESS(ES)

10. SPONSORING/MONITORING AGENCY REPORT NUMBER

11. SUPPLEMENTARY NOTES The views expressed in this thesis are those of the author and do not reflect the official policy or position of the U.S. Department of Defense or the U.S. Government.

12a. DISTRIBUTION / AVAILABILITY STATEMENT	12b. DISTRIBUTION CODE
Approved for public release; distribution is unlimited	A

13. ABSTRACT ***(maximum 200 words)***

Terrain classification is studied here using the tool of texture analysis of high-spatial resolution panchromatic imagery. This study analyzes the impact and effectiveness of texture analysis on terrain classification within the Elkhorn Slough Estuary and surrounding farmlands within the central California coastal region. Ikonos panchromatic (1 meter) and multispectral (4 meter) imagery data are examined to determine the impact of adding texture analysis to the standard MSI classification approaches. Spectral Angle Mapper and Maximum Likelihood classifiers are used. Overall accuracy rates increased with the addition of the texture processing. The classification accuracy rate rose from 81.0% for the MSI data to 83.9% when the additional texture measures were added. Modest accuracy (55%) was obtained from texture analysis alone. The addition of textural data also enhanced the classifier's ability to discriminate between several different woodland classes contained within the image.

14. SUBJECT TERMS	15. NUMBER OF PAGES
Remote Sensing, Multispectral, Ikonos, Texture Filters, Scene Classification, Imagery Interpretation	155
	16. PRICE CODE

17. SECURITY CLASSIFICATION OF REPORT	18. SECURITY CLASSIFICATION OF THIS PAGE	19. SECURITY CLASSIFICATION OF ABSTRACT	20. LIMITATION OF ABSTRACT
Unclassified	Unclassified	Unclassified	UL

NSN 7540-01-280-5500 **Standard Form 298 (Rev. 2-89)**
Prescribed by ANSI Std. 239-18

THIS PAGE INTENTIONALLY LEFT BLANK

Approved for public release; distribution is unlimited

TEXTURE ANALYSIS OF HIGH RESOLUTION PANCHROMATIC IMAGERY FOR TERRAIN CLASSIFICATION

Matthew Donald Humphrey
Lieutenant Commander, United States Navy
B.A., Virginia Military Institute, 1992

Submitted in partial fulfillment of the
requirements for the degree of

MASTER OF SCIENCE IN APPLIED PHYSICS

from the

NAVAL POSTGRADUATE SCHOOL
June 2003

Author: Matthew D. Humphrey

Approved by: Richard C. Olsen
Thesis Advisor

Alan A. Ross
Second Reader

William B. Maier, II
Chairman, Department of Physics

THIS PAGE INTENTIONALLY LEFT BLANK

ABSTRACT

Terrain classification is studied here using the tool of texture analysis of high-spatial resolution panchromatic imagery. This study analyzes the impact and effectiveness of texture analysis on terrain classification within the Elkhorn Slough Estuary and surrounding farmlands within the central California coastal region. Ikonos panchromatic (1 meter) and multispectral (4 meter) imagery data are examined to determine the impact of adding texture analysis to the standard MSI classification approaches. Spectral Angle Mapper and Maximum Likelihood classifiers are used. Overall accuracy rates increased with the addition of the texture processing. The classification accuracy rate rose from 81.0% for the MSI data to 83.9% when the additional texture measures were added. Modest accuracy (55%) was obtained from texture analysis alone. The addition of textural data also enhanced the classifier's ability to discriminate between several different woodland classes contained within the image.

THIS PAGE INTENTIONALLY LEFT BLANK

TABLE OF CONTENTS

I. INTRODUCTION 1

II. BACKGROUND 3
A. ELEMENTS OF RECOGNITION 3
B. USE OF TEXTURE 16
C. PREVIOUS WORK 18
1. Textural Features for Image Classification (Haralick, 1973). 18
2. Texture-Tone Analysis for Automated Land-Use Mapping (Hsu, 1978). 27
3. Spectral and Textural Features to Classify Elusive Land Cover at the Urban Fringe (Jensen, 1979). 31
4. Evaluation of the Grey-Level Co-Occurrence Matrix Method for Land-Cover Classification Using SPOT Imagery (Marceau et al., 1990) ... 37
5. Spectral and Textural Information of Multisensor Data for Land Use Classification in Metropolitan Area (Wikantika et al., 2000) 42
6. Texture-Based Segmentation of Temperate-Zone Woodland in Panchromatic IKONOS Imagery (Gagnon et al., 2003) 45
D. IKONOS REMOTE SENSING PLATFORM 50
E. AREA OF INVESTIGATION 53
1. Coverage area 53
2. Terrain within the study area 55
F. SPECTRAL CHARACTERISTICS OF VEGETATION 55
G. ENVI SOFTWARE 61
1. Texture Filters 61
2. Classifiers 62
a. Spectral Angle Mapper *64*
b. Maximum Likelihood Classifier *64*

III. METHODOLOGY 69
A. GENERAL PROCEDURES 69
B. MOSAIC IMAGES 70
C. TEXTURE FILTERS 72
D. REGIONS-OF-INTEREST CREATION 75
E. SPECTRAL ANGLE MAPPER (SAM) AND MAXIMUM LIKELIHOOD (ML) CLASSIFICATION PROCESS 77
F. POST-CLASSIFICATION PROCEDURES 77

IV. RESULTS 81
A. MOSAIC ANALYSIS 81
B. FULL IMAGE 83
V. SUMMARY AND CONCLUSIONS 95
APPENDIX A. TEXTURE FILTERED IMAGES 97
APPENDIX B. SAM CLASSIFIED IMAGES 115
APPENDIX C. ML CLASSIFIED IMAGES 117
APPENDIX D. CLASSIFICATION RESULTS 121
LIST OF REFERENCES 127
INITIAL DISTRIBUTION LIST 131

LIST OF SYMBOLS, ACRONYMS, AND ABBREVIATIONS

d	Angular orientation (within Marceau et al. study)
f	Window size (within Marceau et al. study)
f_1	Angular second moment (within Jensen study)
f_2	Contrast measure (within Jensen study)
f_3	Correlation measure (within Jensen study)
i	Training set
K	Kappa coefficient
N	Number of bands
N_g	Number of distinct gray tones in the quantized image
N_x	Number of column elements in image matrix
N_y	Number or row elements in image matrix
p	Step size (within Marceau et al. study)
P_c	Central control point
$\hat{P}_d(j)$	Value of index j of the normalized difference-histogram
P_h	Horizontal computation of GLCM
$P(i,j)$	(i,j)th entry in a normalized gray-tone spatial dependence matrix, = P(i,j) / R.
P_{ld}	Left-diagonal computation of GLCM
$\hat{P}_s(i)$	Value of index i of the normalized sum-histogram
P_{rd}	Right-diagonal computation of GLCM

$P_x(i)$	ith entry in the marginal-probability matrix obtained by summing the rows of p(i,j), = $\sum_{j=1}^{N_g} P(i,j)$
P_v	Vertical computation of GLCM
$P(w_i \mid x)$	Probability that w_i is the correct class for a pixel at x
$\mathrm{P}(\mathrm{x}\mid w_\mathrm{i})$	Probability of finding a pixel from class w_i at position x
Q_i	Dispersion matrix of the training set i
R	Number of nearest neighbor pairs
R_n	Number of nearest neighbor pairs (alternate definition)
r_i	Reference spectra vector components
t_i	Test spectra vector components
U_i	Mean texture vector (centroid) of training set i
X	Distance from centroid (within Hsu study)
X_{kk}	Sum of the confusion matrix diagonals
X_{ii}	Sum of the main diagonal of the confusion matrix (within Jensen study)
X_{i+}	Individual confusion matrix row totals (within Jensen study)
X_{+I}	Individual confusion matrix column totals (within Jensen study)
$x_{k\Sigma}x_{\Sigma k}$	Sum of the ground truth pixels in a class times the sum of the classified pixels in that class summed over all classes
Y	Spectral response (texture variables) of the unknown object.

a	ENVI designation for SAM threshold angle
w_i	Spectral classes for an image
g^*	Threshold angle for Spectral Angle Mapper classifier
ASM	Angular Second Moment
CON	Contrast
ENVI	Environment for Visualizing Images
ENT	Entropy
ERTS	Earth Resources Technology Satellite
GLCM	Gray Level Co-occurrence Matrix
IADS	Integrated Air Defense System
IDM	Inverse Difference Moment
ML	Maximum Likelihood
MSI	Multi-Spectral Imaging
ND-vis	n-Dimensional Visualizer
SAM	Spectral Angle Mapper
SPOT	French imaging satellite / Système Probatoire d’Observation de la Terre
TERCAT	Terrain Categorization
VAR	Variance
WMD	Weapons of Mass Destruction

THIS PAGE INTENTIONALLY LEFT BLANK

LIST OF FIGURES

Figure 1. Satellite image of The Pentagon (from Digital Globe) 4
Figure 2. Satellite image of one of the Great Pyramids (from Digital Globe) 4
Figure 3. Images from two popular sporting venues: Qualcomm Stadium in San Diego and the Indianapolis Speedway (from Space Imaging and Digital Globe) 5
Figure 4. Davis-Monthan airfield with multiple aircraft types visible including P-3 Orions, C-130 Hercules, and F-14 Tomcats. (from Digital Globe) 6
Figure 5. Aircraft Carrier with an escort ship in contrast with a civilian cruise ship (from Space Imaging) 7
Figure 6. Distinctive pattern of the Champs-Elysees (from Digital Globe) 7
Figure 7. Mixture of plowed, unplowed, and canopied rows exhibiting different patterns (from Space Imaging) 8
Figure 8. Different patterns of an orchard and a section of natural forest (from Space Imaging) 8
Figure 9. Distinctive pattern of multiple Russian SA-2 “Guideline” Surface-to-Air Missile (SAM) launch sites. 9
Figure 10. Images with distinct tonal qualities: The island of Bora Bora and a section of the Spanish coastline (from Digital Globe) 11
Figure 11. One of the most widely used examples of shadow showing structure detail and collection orientation (from Digital Globe) . 12
Figure 12. The distinctive shadowed outline of the Eiffel Tower (from Digital Globe) 12
Figure 13. Example of the impact of shadowing on the overall definition of an image. Notice the greater level of detail in the top image (from Avery and Berlin) 13
Figure 14. Pickleweed, Scrub Brush, and dried salt ponds lining the edge of the Elkhorn Slough. (from Space Imaging) 14

Figure 15. Busherhr Nuclear Plant, Iran (from Space Imaging) 15
Figure 16. Russian SA-10 associated “Flap Lid” target acquisition radar Right: “Flap Lid” with associated SA-10 “Grumble” missile launchers. (from Jane’s Database) 16
Figure 17. Satellite image of central California (from Haralick et al.) 23
Figure 18. Comparison of two subset images (from Haralick et al.) 24
Figure 19. Land cover classification for Jensen study (from Jensen et al.) 35
Figure 20. Pixels changing classification with the addition of texture measures (from Jensen et al.) 35
Figure 21. Texture measures implemented within Marceau study. Notation: $P(i,j)$ is the $(i,j)th$ entry in normalized grey-level co-occurrence matrix and N_g is the number of distinct grey levels in the quantized image (from Marceau et al.) 39
Figure 22. Combinations used within the classifier (from Marceau et al.). 40
Figure 23. LANDSAT and RADARSAT images of Jakarta Indonesia (from Wikantika et al.) 42
Figure 24. Textural bands created within study (from Wikantika et al.) 43
Figure 25. Classification accuracies obtained with spectral values only (from Wikantika et al.) 44
Figure 26. Classification accuracies obtained with the combination of spectral and textural features (from Wikantika et al.) 44
Figure 27. Five test images of the Montreal region, labeled A through E within the study (from Gagnon et al.) 45
Figure 28. Methodology employed with second phase of Gagnon study (from Gagnon et al., 2003) 48
Figure 29. Classification results after post-processing for the 17-2 combination (from Gagnon et al.) 49
Figure 30. Classification results after post-processing for the 35-2 combination (from Gagnon et al.) 49
Figure 31. The Ikonos satellite (from Space Imaging) ... 50
Figure 32. Spectral response of Ikonos sensors 51

Figure 33. Kodak camera telescope system on-board Ikonos (from Kodak) 52
Figure 34. Ikonos image used in this study (from Space Imaging) 53
Figure 35. Average spectra response curves for various materials (from Avery and Berlin) 56
Figure 36. Average spectral response curves for four types of vegetation (from Avery and Berlin) . 56
Figure 37. Comparison of infrared image (top) and panchromatic image (bottom) showing the ability to discriminate different types of vegetation (from Avery and Berlin) 58
Figure 38. Average spectral response curves for different stages of plant leaf health (from Avery and Berlin) 59
Figure 39. Basic leaf structure showing chloroplasts and mesophyll cells responsible for green and infrared reflectivity (from Avery and Berlin) 60
Figure 40. SAM maximum threshold angle - 0.15 radians for this study (from Kruse, 1993) 63
Figure 41. (a) Spectral characteristics of test pixels represented by spectral angle. (b) Segmentation of the multispectral space by angle. (From Richards, 1999) 63
Figure 42. General outline of methodology employed 69
Figure 43. Methodology employed for processing and analysis of full scene imagery data. 70
Figure 44. Three mosaics utilized in this study. Elkhorn Slough mosaic, Fields mosaic, Various mosaic. 72
Figure 45. File output after texture filtering process . 74
Figure 46. Example of n-D Visualizer - Elkhorn Slough spectral class separation obtained using the n-D Visualizer(from ENVI) 76
Figure 47. Example of error matrix and kappa coefficient calculation (from Jensen) 79
Figure 48. N-dimensional Visualizer view of the Elkhorn Slough mosaic, 5x5 textures. The left hand figure is for two elements of the occurrence matrix (mean and variance), the right hand figure shows two elements of the co-occurrence matrix (mean and entropy) 82
Figure 49. Full image - ML classified with 41 element ROI set (key shown in Appendix D) 85

Figure 50. Class separation achieved with green and NIR bands..... 87
Figure 51. Class separation achieved with two texture-filtered bands. 88
Figure 52. 4 band MSI data (ML classified) showing a portion of the Elkhorn Slough and the surrounding area. 89
Figure 53. 12 band (MSI and texture combined – ML classified) data of the same scene..... 90
Figure 54. 4 band MSI and 12 band (MSI and texture combined) images of the Elkhorn Slough displaying greater woodland delineation and removal of urban misclassification. 91
Figure 55. 4 band MSI and 12 band (MSI and texture combined) images of a small residential sub-division displaying greater woodland delineation. 91
Figure 56. Example of fields misidentified as berries covered with plastic 92
Figure 57. n-D Visualizer presentation of various plastics compared to several types of vegetation 93
Figure 58. n-D Visualizer presentation of the misidentified class of field, various plastics, and several types of vegetation ... 93
Figure 59. n-D Visualizer presentation of the misidentified class of field, various plastics, and several types of vegetation ... 94

LIST OF TABLES

Table 1. Resolution cell and eight nearest-neighbor cells (from Haralick et al.) 19
Table 2. An example of a 3X3 image quantized to four gray tone values ranging from 0 to 3. 19
Table 3. Number of nearest neighbor pairs (*R)* per orientation 20
Table 4. General form of a brightness value spatial-dependency matrix 21
Table 5. Land-use categories used in Hsu study 28
Table 6. Variables employed with Models I and II (from Hsu) 29
Table 7. Probability values as defined by Hsu 30
Table 8. Computation of probability values (from Hsu) 31
Table 9. Land use categories used within Jensen study 33
Table 10. Classifiers used in Jensen study (from Jensen et al.) 34
Table 11. Calculation of the impact of the addition of texture features within the Jensen study (from Jensen et al.) 36
Table 12. Improvement of overall classification rates with the addition of texture measures (Marceau et al.). 41
Table 13. The eight Haralick textures used in this study 47
Table 14. Ikonos image geographical data 54
Table 15. Image collection data for Ikonos images used in this study (from Space Imaging) 54
Table 16. Texture filters within ENVI 62
Table 17. Spectral classes identified within Elkhorn Slough mosaic image. 76
Table 18. Change in correct classification rates for various woodland classes due to the addition of texture bands 86
Table 19. Color coding map key for the following ML classified images 89

THIS PAGE INTENTIONALLY LEFT BLANK

LIST OF EQUATIONS

Equation 1. Angular Second Moment feature (f_1) 23
Equation 2. Contrast textural feature (f_2) 25
Equation 3. Correlation textural feature (f_3) 25
Equation 4. Classifier used in Hsu study..... 30
Equation 5. Variance..... 32
Equation 6. Contrast..... 32
Equation 7. High-Frequency 33
Equation 8. ASM..... 33
Equation 9. ENVI computation of spectral angle during SAM classification process (from Kruse, 1993)..... 64
Equation 10. Maximum Likelihood decision rule (from Richards, 1999) 66
Equation 11. ENVI's calculation of the kappa coefficient . 78

THIS PAGE INTENTIONALLY LEFT BLANK

ACKNOWLEDGEMENTS

The author would like to thank Professor Alan A. Ross of the Naval Postgraduate School and Eric Van Dyke of the Elkhorn Slough Foundation for providing valuable ground truth information of the test area. The author would also like to thank Professor Richard C. Olsen of the Naval Postgraduate School for his insight into multispectral imaging and for all of his help with using the ENVI software. Finally, the author would like to thank his wife Jane for her patience and support throughout the entire process.

THIS PAGE INTENTIONALLY LEFT BLANK

I. INTRODUCTION

Terrain classification is a primary goal in much of remote sensing, and is an essential tool in military planning. Recent launches of commercial satellites offering high-resolution imagery have introduced new opportunities in scene classification. The advent of new sources of high-resolution panchromatic imagery has coincided with advances in computational capabilities that enable the application of analysis approaches which were not previously feasible for large images. Texture-based filtering of high-resolution panchromatic imagery is one such analysis tool that bears further investigation.

The first major study of texture as an imagery analysis tool took place in 1973 (Haralick et al.). The addition of textural measures proved to enhance overall classification accuracy rates. The benefits of the additional measures within that study and much of the follow-on research was offset, however, by the additional costs (both money and time) due to the data processing constraints of the time. Today's data processing capabilities combined with commercially available image processing software such as ENVI have provided a tremendous opportunity to take a closer look at the impact and utility of texture filtering.

Texture can be defined as the spatial or statistical distribution of individual gray tones throughout an imagery data set. Several factors affect the textural qualities of an image including the surface material of the object, the angle of illumination during data collection, and the

overall scale of the image. Texture and tone, the most widely utilized element of recognition within image interpretation, are closely linked and the combination of the two can prove to be a powerful tool for achieving greater classification accuracies.

This study attempts to address two major questions concerning the impact of texture filters on image classification. Can the addition of textural measures to panchromatic data provide the same level of spectral class separability as multispectral data and does the addition of textural filters to multispectral data increase the overall accuracy rates obtained?

To attempt to answer those questions, one meter resolution panchromatic and four meter resolution multispectral IKONOS imagery were analyzed using ENVI image processing software. The area examined within this study is a roughly 250 km^2 section of the central California coastal region just north of the city of Monterey that included a small portion of the Monterey Bay, the Elkhorn Slough estuary, numerous agricultural fields, and several small cities.

The development of this study includes a review of texture and the earlier research that forms the foundation for the use of texture in imagery analysis (Chapter II), a description of the tools used within the study and the investigative methodology employed (Chapters III), and the results and conclusions achieved from the study (Chapters IV and V).

II. BACKGROUND

A. ELEMENTS OF RECOGNITION

The general qualities of an image can be broken into several basic characteristics or elements of recognition that will provide extremely important insight into what information can be collected from that image. The individual elements of recognition can vary greatly from image to image but most researchers identify eight standard keys to interpretation. The eight keys include; shape, size, pattern, tone (color or hue), shadows, site, association, and texture. The impact that each element has upon the overall interpretation is also variable, ranging from being the dominant and most easily recognizable feature to being non-existent. The absence of certain qualities can also provide important additional clues for more accurate interpretation.

Shape is often considered to be one of the more defining elements of recognition and many images can be interpreted solely by the shapes of significant objects contained within. Depending upon the scale of the image, the distinct outline of many man-made objects provide invaluable clues to image interpreters. Shape can help determine the purpose or use of a structure or, in some cases, actually provide a definitive identification of what the structure is. Some classic examples of shape as the most dominant feature are shown in Figures 1 and 2, the Pentagon and one of the great pyramids. Figure 3 shows two sports venues which are easily identified, by their shape in a more generic way.

Figure 1. Satellite image of The Pentagon (from Digital Globe)

Figure 2. Satellite image of one of the Great Pyramids (from Digital Globe)

Figure 3. Images from two popular sporting venues: Qualcomm Stadium in San Diego and the Indianapolis Speedway (from Space Imaging and Digital Globe)

From a military viewpoint, shape is one of the most important aspects of image interpretation. Shape can help identify individual ship and aircraft type, airfield location, and defensive positions among many other objects. Figure 4 shows the 'Boneyard' at Davis-Monthan Air Force Base. The aircraft present in the image are identifiable by shape and size.

Figure 4. Davis-Monthan airfield with multiple aircraft types visible including P-3 Orions, C-130 Hercules, and F-14 Tomcats. (from Digital Globe)

Size is the second element that can serve as an aid to interpretation. The relative size of an article within an image can provide useful clues about the nature and utility of the object. Size of an object in photographs must be considered in the context of the photo scale. The size of a naval vessel, for example, when combined with other elements of recognition can help provide a more detailed analysis of ship type and other tactically relevant characteristics. Figure 5 shows how the size of naval vessels can aid in identification.

Figure 5. Aircraft Carrier with an escort ship in contrast with a civilian cruise ship (from Space Imaging)

Pattern is the third element of recognition that can provide useful information for accurate image interpretation. The overall pattern characteristics contained within an image are dependent upon the spatial arrangement or orientation of tone or color within the image. The repetition of certain forms or relationships is characteristic of many objects and gives the object a pattern that aids the photo interpreter in recognition. (Lillesand and Keiffer, 1994) Figure 6 illustrates how the distinctive pattern of an image can aid identification.

Figure 6. Distinctive pattern of the Champs-Elysees (from Digital Globe)

The pattern contained within images of natural phenomena is clearly evident at times. A plowed field will appear markedly different from an unplowed field and an orchard containing organized rows of trees or crops will exhibit significant pattern differences from an image of a forest or wild brush. Figures 7 and 8 show a mixture of patterns associated with vegetation and agricultural industries.

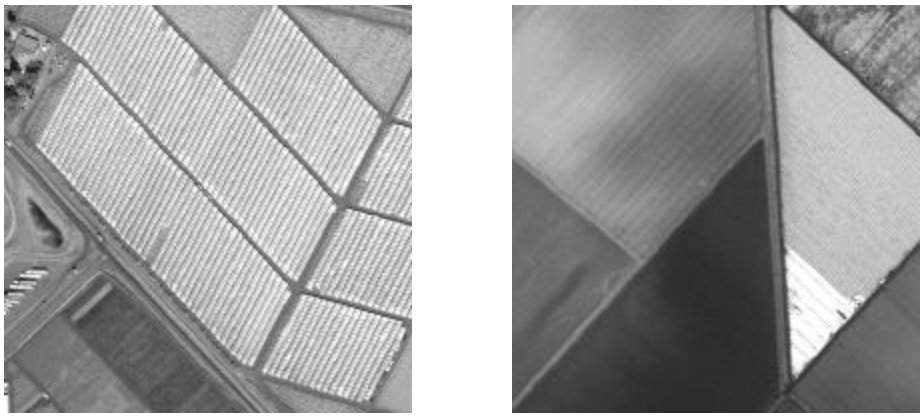

Figure 7. Mixture of plowed, unplowed, and canopied rows exhibiting different patterns (from Space Imaging)

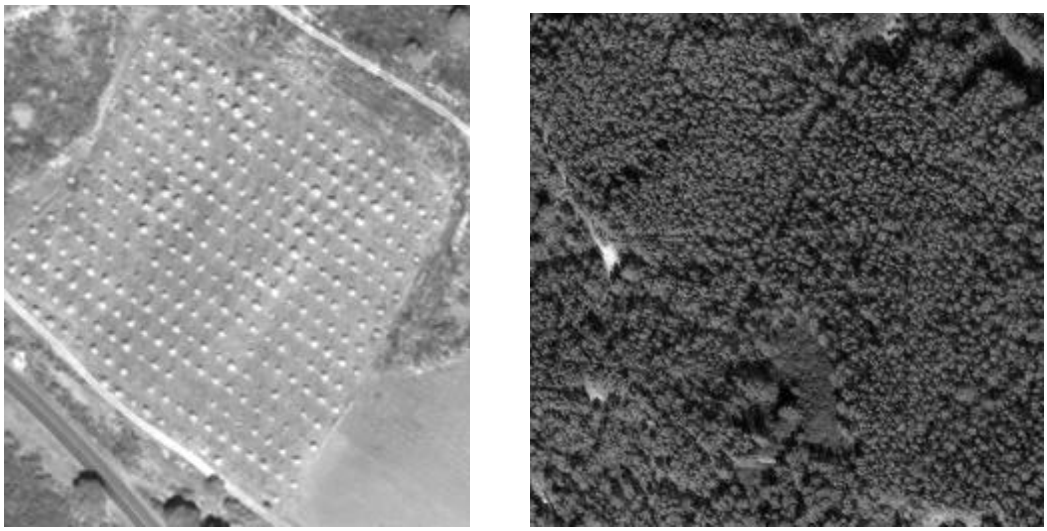

Figure 8. Different patterns of an orchard and a section of natural forest (from Space Imaging)

Pattern also plays a significant role in the interpretation of military-related images. Pattern can provide vital clues to the tactical utility or associated mission of an object. Pattern, for example, can help identify key nodes of an enemy's Integrated Air Defense Systems (IADS) architecture or communication network. These identifying characteristics can play an extremely important role in the attempt to exploit the enemy's command and control networks for intelligence purposes or provide accurate targeting data for offensive attacks (see Figure 9).

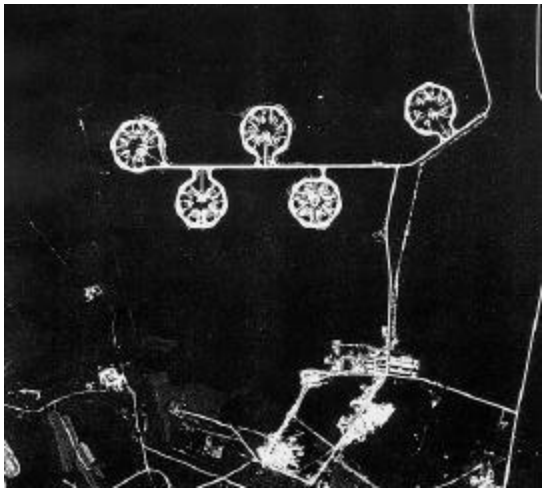

Figure 9. Distinctive pattern of multiple Russian SA-2 "Guideline" Surface-to-Air Missile (SAM) launch sites.

The tone or color characteristics contained within an image are the most widely utilized elements of recognition for most interpretation applications. Tone, or hue, refers to the relative brightness or color of objects within an image and tone can provide the interpreter with valuable information for discerning the pattern and texture of objects (Lillesand and Keifer, 1994). The importance of

tone is reflected in the fact that tone is the most dominant feature within most automated image classifiers. The majority of all digital image analysis appears to be dependent primarily upon just the tone and color of individual pixels contained within the scene (Hardin and Thomson, 1992).

The tonal qualities of individual objects within an image are a function of the reflective qualities of those objects and the illumination present. The reflected radiation, at any given wavelength, coming from an object is dependent upon its surface composition and physical state plus the intensity and angle of illumination. (Avery and Berlin, 1992) Tone can play an important role in distinguishing natural features included within an image and it can also aid in the detection and analysis of man-made objects or regions. The tonal characteristics contained within the following images are clearly evident and present extremely valuable aids to overall image interpretation. Figure 10 highlights the impact that tone has on the overall image and how tone can play a vital role in image interpretation.

Figure 10. Images with distinct tonal qualities: The island of Bora Bora and a section of the Spanish coastline (from Digital Globe)

The size, shape, and orientation of shadows present within an image constitute one more important key to accurate image interpretation. The most obvious use of shadow comes with the examination of man-made objects and the distinctive shadows that they cast. Figures 11 and 12 highlight the effect of shadowing, showing the shadows of the Washington Monument and the Eiffel Tower.

Figure 11. One of the most widely used examples of shadow showing structure detail and collection orientation (from Digital Globe)

Figure 12. The distinctive shadowed outline of the Eiffel Tower (from Digital Globe)

The use of shadows is extremely important for military related imaging where accurate and timely target identification is vital on today's high-tech and highly dynamic battlefield. A building or vehicle, illuminated at an angle, casts a shadow that may reveal characteristics of its size or shape that would not be obvious from the overhead view alone. "Because military photo interpreters

often are primarily interested in identification of individual items of equipment, shadow has been of great significance in distinguishing subtle differences that might not otherwise be available" (Campbell, 1996).

One of the least obvious but more effective uses of shadow for interpretation involves the investigation of natural phenomena including assessing natural topographic variations. Enhancement of subdued topography is one of the most important uses of shadow. Minor surface irregularities, as seen in Figure 13, can be accentuated by taking the image with low sun-angles in the early morning or late afternoon. (Avery and Berlin, 1992)

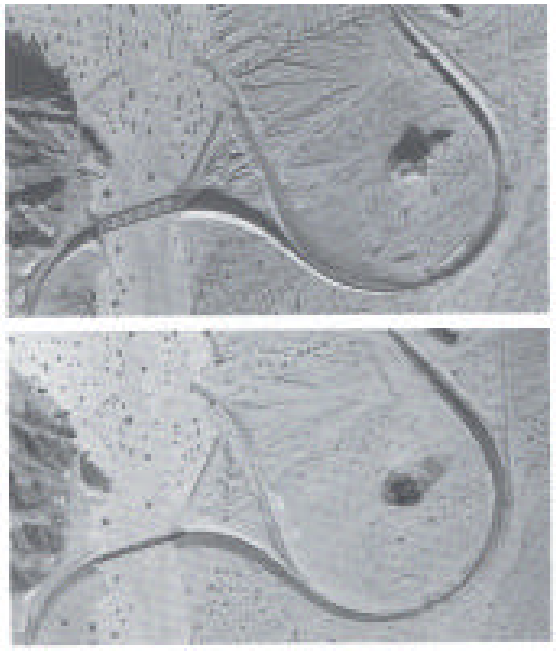

Figure 13. Example of the impact of shadowing on the overall definition of an image. Notice the greater level of detail in the top image (from Avery and Berlin)

The topographical or geographical region associated with an object of interest is an additional key to accurate

image interpretation. Site is considered a contextual element of image interpretation because it is dependent upon the other elements within the surrounding environment. The location of an object in relation to its environment is called the site factor and is important for recognizing many cultural and natural features. Natural vegetation is characteristically confined to specific locales such as swamps, marshes, and stream banks and this fact aids in image interpretation (Avery and Berlin, 1992).

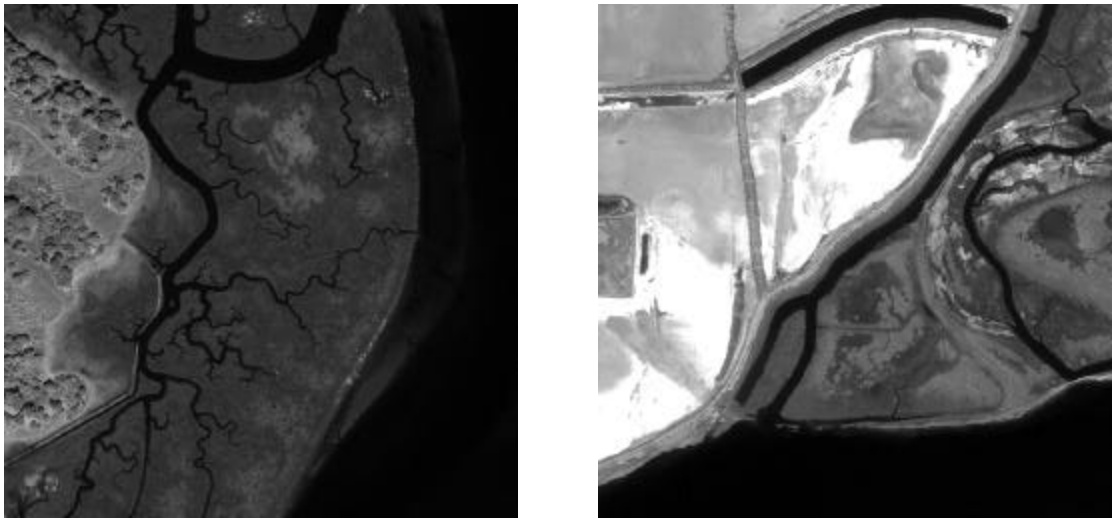

Figure 14. Pickleweed, Scrub Brush, and dried salt ponds lining the edge of the Elkhorn Slough. (from Space Imaging)

The surrounding environment, or site, can also play a role in military and national security-related image interpretation. A recently developed industrial park with security fencing or security-related structures situated within poorly developed portions of countries like Iraq or North Korea could be an indicator of possible weapons of mass destruction (WMD) development programs and may result in further investigation. Site can also play a role in the

discovery of further proliferation of nuclear capabilities by foreign countries. Nuclear power plants need an abundant supply of coolant water nearby and this can aid in identification (Avery and Berlin, 1992). Figure 15 shows an Iranian nuclear power plant and how site can play a role in recognition.

Figure 15. Busherhr Nuclear Plant, Iran (from Space Imaging)

Association is another contextual element of recognition and is closely related to, and sometimes overlaps with, site characteristics. Certain objects are "genetically" linked to other objects, so that identifying one tends to indicate or confirm the other. Association is a key element of image interpretation for military and defense related issues. "In the context of military photo interpretation, association of specific items has great significance, as, for example, when the identification of a

specific class of equipment implies that other, more important items are likely to be found nearby" (Campbell, 1996). One example of how association plays a role in military image processing and interpretation is the identification of a nearby surface-to-air missile (SAM) based upon the distinct types of target acquisition and target tracking radars present in the image. This is evident in Figure 16 below which shows the "Flap Lid" multi-function radar alongside its associated weapon system. Another example of using association for accurate interpretation is identifying key airfield structures like weapons bunkers, aircraft hangars, and control towers that are associated with the easily recognizable runway itself.

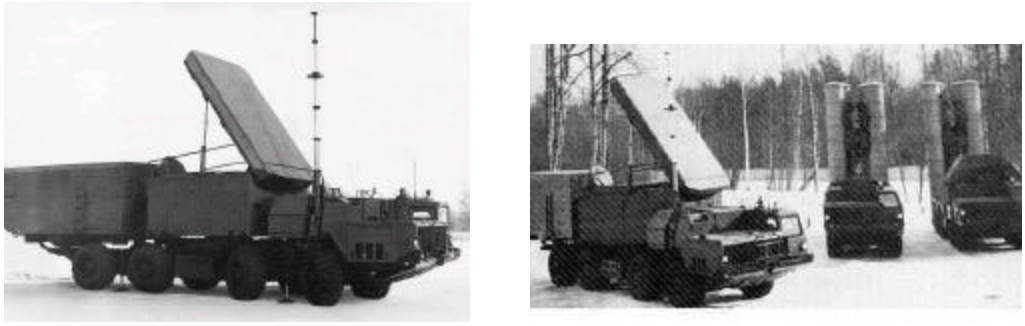

Figure 16. Russian SA-10 associated "Flap Lid" target acquisition radar Right: "Flap Lid" with associated SA-10 "Grumble" missile launchers. (from Jane's Database)

Texture is the last remaining element of recognition and will be discussed in much greater detail in the following sections.

B. USE OF TEXTURE

The accurate interpretation of photographs and other images depends on three major components of the image

itself. The spectral, contextual, and textural characteristics or features of an image provide an underlying basis for the classification and interpretation of imagery data. The spectral features of an image can be described as the variations of tone contained within the image and these tonal or spectral qualities are often the most widely utilized characteristic in image processing. The contextual characteristics of an image can be derived from the relationships between adjacent segments or blocks of data and can be used as an additional aid in the interpretation of imagery. The textural qualities of an image are inherent in the spatial or statistical distribution of individual tones throughout the data set. These three image characteristics; spectral, contextual, and textural, are present in every image, but each will have a varying degree of impact upon the overall image (Haralick et al., 1973).

The greater emphasis placed on spectral qualities, when compared to textural characteristics, within most image classification procedures hides the inter-dependency that the two qualities share. The concept of tone is based on the varying shades of gray of resolution cells in a photographic image, while texture is concerned with the spatial (statistical) distribution of those gray tones (Haralick et al.). The combination of spectral and textural characteristics can result in more accurate image interpretation and classification procedures.

Several factors affect the textural qualities of an image including the surface material of the object, the angle of illumination, and the scale of the image.

Texture, just like object size, is directly correlated with photo scale. “Thus, a given feature may have a coarse texture in a low-altitude photograph and a smooth texture in a high-altitude photograph” (Avery and Berlin, 1992). Texture can be broadly defined by the terms “roughness” and “smoothness” which correspond to the overall change in tone within the picture but Haralick et al. provide additional descriptive categories of fine, coarse, smooth, rippled, molled, irregular, and lineated. (Haralick et al., 1973) The following section will trace the development and evolution of the use of texture for image interpretation and classification.

C. PREVIOUS WORK

1. Textural Features for Image Classification (Haralick, 1973).

Haralick, et al. (1973) laid the foundation for most of the follow-on research concerning texture-based analysis by providing a computational method to extract the textural characteristics of selected blocks of imagery. They then compared and contrasted the utility and efficacy of each filter within the selected data sets. “The approach is based on the assumption that the texture information in an image (I) is contained in the overall or ‘average’ spatial relationship which the gray tones in the image have to one another” (Haralick et al., 1973). The initial procedure in the process is to create a set of angular nearest-neighbor gray-tone spatial-dependence matrices that are eventually used to produce fourteen individual textural characteristics. Definitions of the nearest neighbors are

illustrated in Table 1, and a sample ‘image’ matrix is shown in Table 2.

1	2	3
8	*	4
7	6	5

Table 1. Resolution cell and eight nearest-neighbor cells (from Haralick et al.)

0	1	1
0	1	1
2	3	3

Table 2. An example of a 3X3 image quantized to four gray tone values ranging from 0 to 3.

The gray level co-occurrence matrices (GLCM) are created from the image. This is done using the angular dependence of neighboring gray tonal values which are evaluated at 45 degree increments and at varying distance intervals. The angular subsets are delineated by horizontal (0 degrees), right-diagonal (45 degrees), vertical (90 degrees), and left-diagonal (135 degrees). For ease of computation, a linear separation distance of one cell (d=1) will be used throughout the following examples. The number of gray tones possible for each individual resolution cell is N_g (equal to 4 in this

example) and this value will be limited to 4 gray tonal values of 0, 1, 2,and 3 for the following examples. The total number of nearest neighbor pairs (*R*) will vary for each angular orientation and are summarized in Table 3. In Table 3, N_x=3 and N_y=3 for the 3x3 'image' shown in Table 2.

	Horizontal	Right-Diagonal	Vertical	Left-Diagonal
R	$2\ N_y\ (N_x - 1)$	$2\ (N_y - 1)\ (N_x - 1)$	$2\ N_x\ (N_y - 1)$	$2\ (N_x - 1)\ (N_y - 1)$

Table 3. Number of nearest neighbor pairs (*R)* per orientation

An illustration of the process follows. The nearest neighbor pairs for each (row, column) horizontal nearest neighbor are as follows.

R_h = [(1,1)(1,2)] , [(1,2)(1,1)] , [(1,2)(1,3)]
[(1,3)(1,2)] , [(2,1)(2,2)] , [(2,2)(2,1)]
[(2,2)(2,3)] , [(2,3)(2,2)] , [(3,1)(3,2)]
[(3,2)(3,1)] , [(3,2)(3,3)] , [(3,3)(3,2)]

$R_h = 2\ N_y\ (N_x - 1) = 2 * 3\ (3 - 1) = 12$

We see that there are a total of twelve horizontal nearest neighbor pairs. The Haralick GLCM is then built using an approach illustrated here for horizontal nearest neighbors. Table 5 shows how for each discrete gray level, the co-occurrence is obtained.

	Gray Tone Values				
Gray Tone Values		0	1	2	3
	0	#(0,0)	#(0,1)	#(0,2)	#(0,3)
	1	#(1,0)	#(1,1)	#(1,2)	#(1,3)
	2	#(2,0)	#(2,1)	#(2,2)	#(2,3)
	3	#(3,0)	#(3,1)	#(3,2)	#(3,3)

Table 4. General form of a brightness value spatial-dependency matrix

For example, #(0,0) in the top left corner is the number of times zero occurred with another zero as its nearest horizontal neighbor. Using the example given in Table 2, the computation of the four angular, *d*=1, four possible gray tone, spatial dependent matrices are as follows:

Horizontal $P_h = \begin{pmatrix} 0 & 2 & 0 & 0 \\ 2 & 4 & 0 & 0 \\ 0 & 0 & 0 & 1 \\ 0 & 0 & 1 & 2 \end{pmatrix}$

Right-Diagonal $P_{rd} = \begin{pmatrix} 0 & 1 & 0 & 0 \\ 1 & 2 & 1 & 1 \\ 0 & 1 & 0 & 0 \\ 0 & 1 & 0 & 0 \end{pmatrix}$

Vertical $P_v = \begin{pmatrix} 2 & 0 & 1 & 0 \\ 0 & 4 & 0 & 2 \\ 1 & 0 & 0 & 0 \\ 0 & 2 & 0 & 0 \end{pmatrix}$

Left-Diagonal $P_{ld} = \begin{pmatrix} 0 & 1 & 0 & 1 \\ 1 & 2 & 0 & 1 \\ 0 & 0 & 0 & 0 \\ 1 & 1 & 0 & 0 \end{pmatrix}$

For eight bit data these would be 255x255 matrices and for Quickbird and Ikonos with 11-12 bit data, the matrices would be even larger. Each pixel contained within the image would have one of these GLCM assigned to it during the texture processing. The standard algorithm thus generates a finite number of gray levels.

Haralick et al. proceeded to use these matrices to extract fourteen separate measures of image texture. “The initial assumption is that all the texture information is contained within the gray-tone spatial dependence matrices” (Haralick et al., 1973). For illustrative purposes, 3 of the 14 texture filters were singled out for further exploration. The Angular Second Moment (ASM), contrast, and correlation textural features were highlighted for the separate land-use category images. Computing capabilities at the time of this research (1973) limited the scale of the investigation and two 64 X 64 images of the central California coastline (Figure 17) taken from the LANDSAT 1 satellite (formerly named NASA ERTS) were utilized for the

study. The two samples included a primarily grasslands image and a waterbody image (Figure 18).

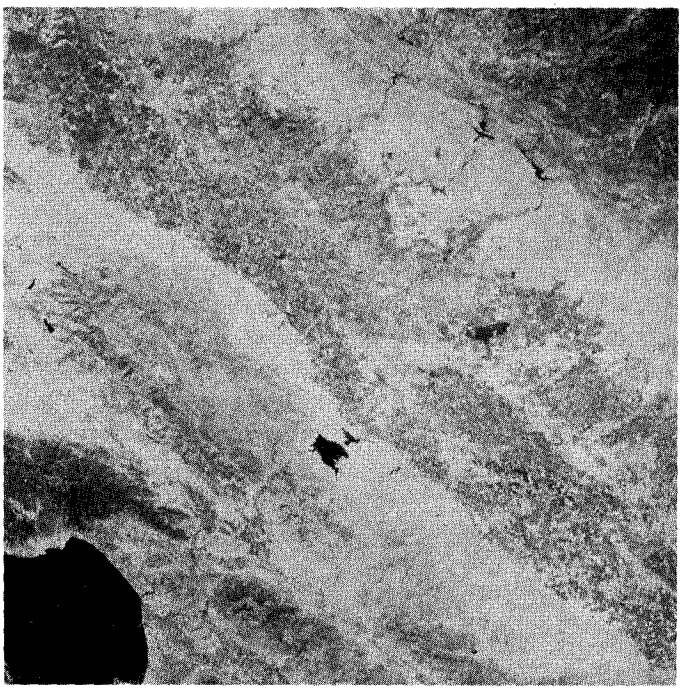

Figure 17. Satellite image of central California (from Haralick et al.)

The Angular Second Moment (ASM) feature is an extremely useful indicator of the overall homogeneity of an image and is easily distinguishable between the two land-use categories.

$$f_1 = \sum_i \sum_j \{p(i,j)\}^2$$

Equation 1. Angular Second Moment feature (f_1)

Notation:

p(i,j) = (i,j)th entry in a normalized gray-tone spatial dependence matrix, = P(i,j) / R.

$P_x(i)$ = ith entry in the marginal-probability matrix obtained by summing the rows of p(i,j), = $\sum_{j=1}^{N_g} P(i,j)$

R = total number of nearest neighbor pairs.

Ng = Number of distinct gray levels in the quantized image.

The largely homogeneous water body image presents much larger ASM across all angles of examination while the less homogenous grassland image provides significantly smaller ASM values. This is evident in Figure 18 below, which displays the corresponding values for each textural feature of the two images.

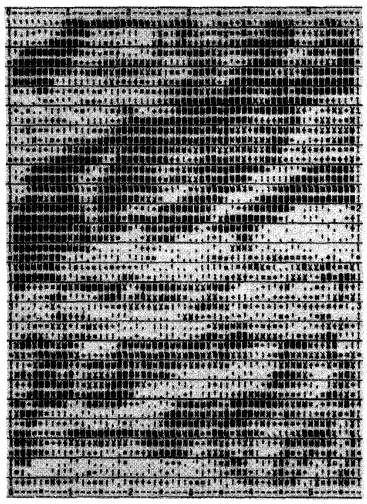

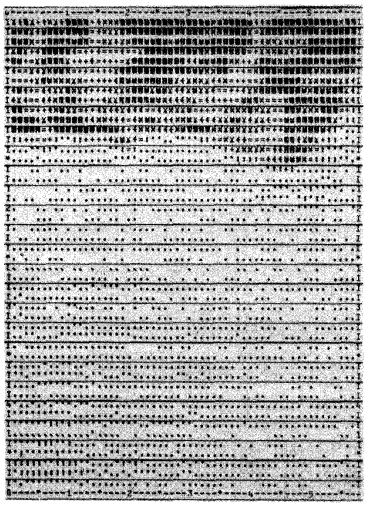

	Grassland			Water Body		
Angle	ASM	Contrast	Correlation	ASM	Contrast	Correlation
0°	.0128	3.048	.8075	.1016	2.153	.7254
45°	.0080	4.011	.6366	.0771	3.057	.4768
90°	.0077	4.014	.5987	.0762	3.113	.4646
135°	.0064	4.709	.4610	.0741	3.129	.4650
Avg.	.0087	3.945	.6259	.0822	2.863	.5327

Figure 18. Comparison of two subset images (from Haralick et al.)

The contrast feature of textural qualities is directly related to the amount of local textural variations contained within a selected image.

$$f_2 = \sum_{n=0}^{N_g-1} n^2 \left\{ \sum_{i=1}^{N_g} \sum_{j=1}^{N_g} p(i, j) \right\}$$

Equation 2. Contrast textural feature (f_2)

The large amount of local variation inherent within the grasslands image, as compared to the waterbody image, accounts for the higher contrast feature values.

The correlation feature of an image is directly related to the image's gray tone linear dependence characteristics.

$$f_3 = \frac{\sum_i \sum_j (i, j) p(i, j) - m_x m_y}{s_x s_y}$$

Equation 3. Correlation textural feature (f_3)

Both images present significantly greater linear dependence in the horizontal (0 degrees) direction and this is evident in the relatively higher zero degree angle correlation values for each image. One additional defining characteristic of the grasslands image is a strong linear dependence along the 45 degree angle and a corresponding large correlation value.

To analyze the impact the textural features had upon image classification, Haralick et al. utilized three separate types of images; photomicrographs, aerial

photographs, and satellite multispectral images. In the interest of brevity, only the results from the satellite multispectral images will be described in this study. A 14,400 mi^2 section of the central California coastline, including Monterey Bay, was examined. The four channel multispectral image was 2340 X 3200 pixels and a subset of 624 image blocks of size 64 X 64 pixels were taken and utilized in the study (Haralick et al., 1973). The image was divided into seven land-use categories; coastal forest, woodlands, annual grasslands, urban areas, small and large irrigated fields, and water bodies. Each individual 64 X 64 block was categorized according to the MSI's color composite image and the MSS band was used for the extraction of the image textural features.

"The classification algorithm utilized for the satellite imagery was a Piecewise Linear Discriminant (PLD) function method where the pattern space is partitioned into a number of regions using a set of hyperplanes (decision boundaries) whose location are determined by sample patterns and each region is dominated by sample patterns of a particular category" (Haralick et al., 1973). Inputs to the classifier included the mean variance of four textural features; the ASM, contrast, correlation, and entropy, in addition to eight spectral features of the image. An overall accuracy rate of 83.5% was attained during classification of the test samples, compared to a 74-77% classification accuracy with spectral characteristics alone. The results show that a significant improvement in the classification accuracy might result if the textural measures are used in combination with multispectral bands as inputs to the classifier (Haralick et al., 1973).

2. Texture-Tone Analysis for Automated Land-Use Mapping (Hsu, 1978).

Utilizing black-and-white aerial photos taken by U.S. Air Force U-2 reconnaissance aircraft, Hsu examined the effect of employing textural filters in combination with spectral qualities on the overall classification accuracy rate. The data set for this study was composed of eight scenes (four low-altitude and four high-altitude) from four different test sites in the state of New York (Hsu, 1978). The low-altitude imaging runs were conducted at altitudes ranging from 15,000 to 16,000 feet and resulted in image resolutions of 8.75 feet while the high-altitude runs were conducted in the 60-62,000 foot range and resulted in image resolution of 56.75 feet. Each resulting image had tonal densities ranging from 0 (black) to 255 (white) and was 256 by 256 pixels. For classification purposes, Hsu defined seven land-use categories or terrain types (Table 5) plus a “rejected” classification which encompassed all terrain types that could not be grouped into one of the seven categories.

	Class	Description
1	Metal	Metal roofs, oil tanks, and light colored cars
2	Pavements	Cement roads, asphalt roads, and tarred surfaces such as paved roofs and parking lots
3	Water	Deep and shallow water bodies
4	Soil	Bare soils and sands
5	Cultivated Fields	Active and inactive farm lands
6	Vegetation	Trees and bushes
7	Composition	A mixture of several categories such as urbanized area

Table 5. Land-use categories used in Hsu study

At the time of this research, the U.S. Air Force's Rome Air Development Center (RADC) was beginning to employ an image data processing system called DICIFER. This system had only a limited capability for texture analysis. The need for a more capable texture filter led to the development of a new textural measure by Hsu. A two model system was developed and implemented to investigate the additional capabilities available with texture analysis. Model I utilized 17 texture tone variables with a 3 by 3 pixel window design while Model II employed 23 variables with a 5 by 5 pixel window design. The variables used are shown in Table 6 below.

Code	Description or Computational Formula
1. MEAN	average
2. STD	standard deviation
3. SKEW	skewness
4. KURT	kurtosis
	(the four central moments)
5. MDEVN	$\Sigma\lvert x_i - \bar{x}\rvert/n$, where x = tone value of individual pixels, $\bar{x}$ = mean
6. MPTCON	$\Sigma\lvert x_i - x_c\rvert/n$, where x_c = tone value of the center point
7. MPTREL	$\Sigma(x_c - x_i)/n$
8. MINCON	$\Sigma\lvert x_i - x_j\rvert/n$, i and j are adjacent pixels
9. MINSQR	$\Sigma(x_i - x_j)^2/n$
10. M2NCON	$\Sigma\lvert x_i - x_k\rvert/n$, x_c and x_k are second nearest neighbors
11. M2NSQR	$\Sigma(x_i - x_k)^2/n$
12. MADAT1	numerical calculation of mean area above datum 1 (50)
13. MADAT2	mean area above datum 2 (100)
14. MADAT3	mean area above datum 1 (50)
15. MBDAT1	mean area below datum 1 (50)
16. MBDAT2	mean area below datum 2 (100)
17. MBDAT3	mean area below datum 3 (150)
	Additional Variables—Model II
18. XCONT	(Distance from peaks to troughs) along x-axis
19. XPEAK	(Peak positions from the origin) along x-axis
20. XPANDT	(Number of peaks and troughs) along x-axis
21. YCONT	(Distance from peaks to troughs) along y-axis
22. YPEAK	(Peak positions from the origin) along y-axis
23. YPANDT	(Number of peaks and troughs) along y-axis

Table 6. Variables employed with Models I and II (from Hsu)

The 3 by 3 and 5 by 5 data matrices were chosen over larger data windows because individual pixels, rather than larger regions or subsets, were being classified. Additionally, using the larger windows resulted in greater edge effects where more pixels situated between two adjacent categories were being rejected. Even with the 5 by 5 design, the edge effect was still substantial. This resulted in the utilization of the 3 by 3 system for generating the final decision maps and hit-rate analyses (Hsu, 1978).

In this study, the linear discriminant analysis approach was employed and the maximum likelihood solution

leads to a Mahalanobis classifier with equation 4 as a classification rule (Hsu, 1978).

$$D_i^2 = (Y - U_i)^T (Q_i)^{-1} (Y - U_i)$$

Equation 4. Classifier used in Hsu study.

Notation:

Y = spectral response (texture variables) of the unknown object.

U_i = mean texture vector (centroid) of training set i.

Q_i = dispersion matrix of the training set i.

To solve the problem of "rejects' within the classification process, two probability functions were implemented. The two probability functions are shown in Table 7. .

	Value	Description
1	P (G / x)	Probability that the pixel with score x is a member of group G
2	P (x / G)	Probability that a member of group G would have a distance from G's centroid of x or more

Table 7. Probability values as defined by Hsu

The computational formulas for the two probability values are shown in Table 8.

	Value	Description
1	P (G / x)	$P(G/x) = \frac{e^{L}}{\sum e^{-x_i}}$ where L is the largest x_i
2	P (x / G)	Is equal to the probability of D^2 obtained from the chi-square table with the degree of freedom given by the rank of Q_i in Equation 4

Table 8. Computation of probability values (from Hsu)

Following the step-wise discriminant analysis procedures it was determined that 13 of 17 Model I (3x3) variables and 19 of the 23 Model II (5x5) variables were statistically significant. Other results obtained from the research included the observation that the hit-rate difference between the two models was insignificant and that Model I was very effective in classifying general land use types. As stated earlier, an additional observation concluded that significant edge effects were evident when using the 5 by 5 data matrix while edge effects were negligible when using the 3 by 3 matrix.

3. Spectral and Textural Features to Classify Elusive Land Cover at the Urban Fringe (Jensen, 1979).

Jensen focused on the impact and utility of combining four texture measures with available spectral features to evaluate the improvement in overall land-cover classification accuracy. This research focused on a 16 square mile LANDSAT image centered on the Central Californian town of Goleta. At the time of this research (1979), the LANDSAT sensor was only capable of providing a

spatial resolution of 59 by 79 meters and this low resolution rate resulted in numerous misclassifications of different land-use types. There is often significant overlap of spectral signatures of residential developments and natural vegetation in the urban-rural transition zone (Jensen, 1979). This overlap in spectral signature limited the utility of LANDSAT and comparable systems for analyzing and classifying land cover within the urban fringe.

To overcome this limitation Jensen implemented several texture measures to increase the accuracy rate attained by the image classification algorithms. "By incorporating textural data in conjunction with the traditional spectral data in the pattern recognition algorithm, it was hypothesized that improvement in Level II and III residential land-use classification might be attained relative to classifications based solely on spectral features" (Jensen, 1979). Four texture measures were chosen based on their potential for improving the classification of suburban and rural land-cover within the urban fringe. The four measures used are listed below.

$$s = \sqrt{\frac{\sum_{i=1}^{n}\sum_{j=1}^{n}\{p(i,j)-m\}^2}{n^2-1}}$$

Equation 5. Variance

$$c = \frac{\sum_{i=1}^{n}\sum_{j=1}^{n} p(i,j) - p_c}{n^2}$$

Equation 6. Contrast

$$L_c = \frac{\sum_{i=1}^{n}\sum_{j=1}^{n} p(i,j) - p_c}{n^2 - 1} \qquad H_c = \left| p_c - L_c \right|$$

Equation 7. High-Frequency

$$f_1 = \sum_i \sum_j \left\{ p(i,j) \right\}^2$$

Equation 8. ASM

Where *n* is the number of rows and columns in the moving average, *p(i,j)* is the tonal value of the a pixel adjacent to the central control point p_c.

The study area of Goleta is located to the north of the mainly urban area extending from Los Angeles north to Santa Barbara. Jensen identified six land-use categories that are present within the study area and these are summarized in Table 9.

	Land Use Category
1	Natural vegetation (primarily Chapparral)
2	Agriculture (dominated by mature citrus and avacado orchards)
3	Single-family residences
4	Multiple-family residences
5	Commercial complexes and barren regions
6	Water surfaces

Table 9. Land use categories used within Jensen study

The image chosen for examination was a May 4, 1974 LANDSAT image made up of four spectral channels ranging from 0.5 to 1.1 mm and quantized to 64 levels. The four LANDSAT channels available for the study were channel 4 (green 0.5-0.6 mm), channel 5 (red 0.6-0.7 mm), and channels 6 and 7 (two separate infrared bands 0.7-0.8 mm and 0.8-1.1 mm). Channel 7 was considered redundant with channel 6 and was not used for the classifiers developed by Jensen.

Jensen et al. ran the classifiers with five variations in the input bands to analyze the improvement yielded with the addition of textural data to the classifier. The five classifiers are labeled A through E and are listed below in Table 10.

	Classifier
A	Spectral (channels 4,5,6) alone
B	Spectral (channels 4,5,6) + textural (variance coding)
C	Spectral (channels 4,5,6) + textural (contrast)
D	Spectral (channels 4,5,6) + textural (high frequency)
E	Spectral (channels 4,5,6) + textural (angular second moment)

Table 10. Classifiers used in Jensen study (from Jensen et al.)

The resulting classifications (B to E) were individually compared with the land cover classification map (Figure 19) and pixels changing categories were evaluated using ground truth information (Jensen, 1979).

The impact of including the four additional texture measures is shown in Figure 20 which shows the number of pixels that changed category with each texture measure.

Figure 19. Land cover classification for Jensen study (from Jensen et al.)

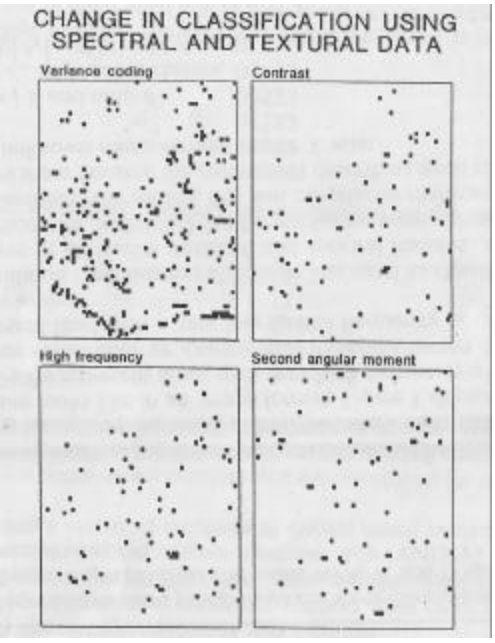

Figure 20. Pixels changing classification with the addition of texture measures (from Jensen et al.)

Based on this analysis, contingency tables for classification B, C, D, and E reflect deviations from the purely spectral classification and identify whether these deviations improve or deter classification of land-use categories at the urban fringe. These contingency tables and an accompanying example are shown in Table 11 below.

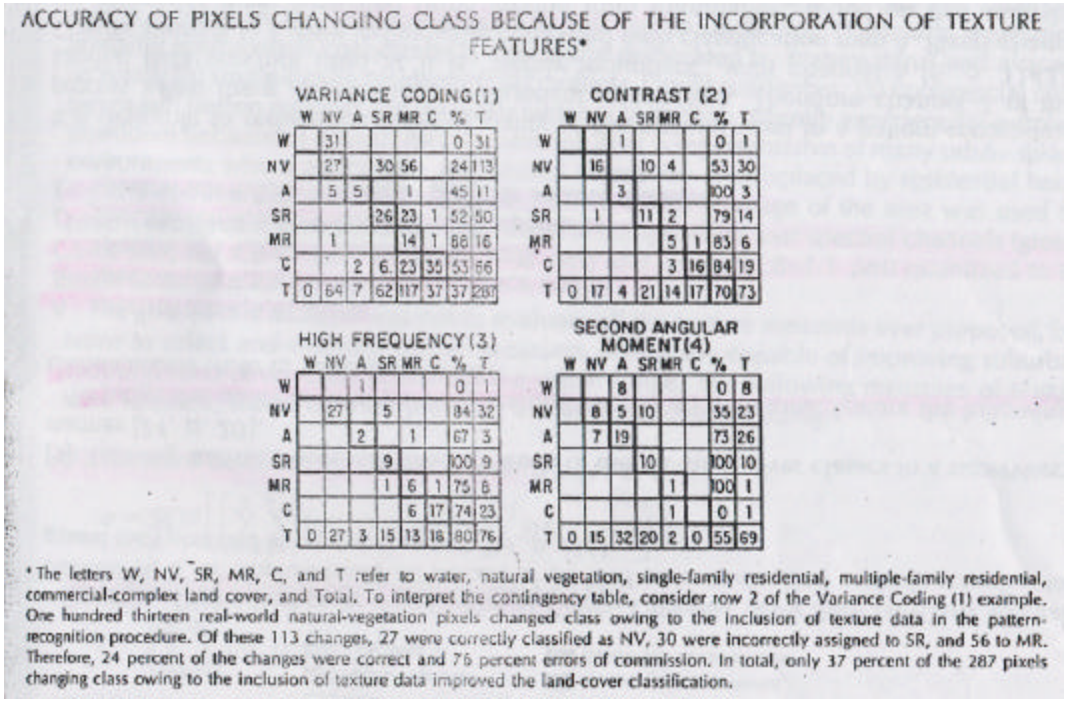

ACCURACY OF PIXELS CHANGING CLASS BECAUSE OF THE INCORPORATION OF TEXTURE FEATURES*

VARIANCE CODING (1)

	W	NV	A	SR	MR	C	%	T
W		31					0	31
NV		27		30	56		24	113
A		5	5		1		45	11
SR				26	23	1	52	50
MR		1			14	1	88	16
C			2	6	23	35	53	66
T	0	64	7	62	117	37	37	287

CONTRAST (2)

	W	NV	A	SR	MR	C	%	T
W			1				0	1
NV		16		10	4		53	30
A			3				100	3
SR		1		11	2		79	14
MR					5	1	83	6
C					3	16	84	19
T	0	17	4	21	14	17	70	73

HIGH FREQUENCY (3)

	W	NV	A	SR	MR	C	%	T
W			1				0	1
NV		27		5			84	32
A			2		1		67	3
SR				9			100	9
MR				1	6	1	75	8
C					6	17	74	23
T	0	27	3	15	13	18	80	76

SECOND ANGULAR MOMENT (4)

	W	NV	A	SR	MR	C	%	T
W			8				0	8
NV		8	5	10			35	23
A		7	19				73	26
SR				10			100	10
MR					1		100	1
C					1		0	1
T	0	15	32	20	2	0	55	69

* The letters W, NV, SR, MR, C, and T refer to water, natural vegetation, single-family residential, multiple-family residential, commercial-complex land cover, and Total. To interpret the contingency table, consider row 2 of the Variance Coding (1) example. One hundred thirteen real-world natural-vegetation pixels changed class owing to the inclusion of texture data in the pattern-recognition procedure. Of these 113 changes, 27 were correctly classified as NV, 30 were incorrectly assigned to SR, and 56 to MR. Therefore, 24 percent of the changes were correct and 76 percent errors of commission. In total, only 37 percent of the 287 pixels changing class owing to the inclusion of texture data improved the land-cover classification.

Table 11. Calculation of the impact of the addition of texture features within the Jensen study (from Jensen et al.)

As can be expected and as is evident in Table 11, the impact of adding the texture was variable and depended largely on the texture filter being utilized. The variance coding texture measure showed the least improvement overall with only 37% of the 287 pixels changing class being assigned to a more correct land-cover class. The contrast measure and high-frequency measure showed more promise with

70% and 80% improvement respectively. The angular second moment filter showed mixed results that Jensen thought merited more attention in later studies. Jensen used a moving 3 by 3 data window instead of a larger window and he believed the smaller window may have accounted for the lower improvement percentage. “Such a small sub-region does not appear to have enough textural information to separate all the categories of interest and of the 69 pixels changing class (with the ASM measure) only 55% were improvements over the conventional spectral classification” (Jensen, 1979). Jensen advocated examining larger data windows, using 5x5 and 10x10 matrices as examples, to take a closer look at the impact of the additional ASM filter.

4. Evaluation of the Grey-Level Co-Occurrence Matrix Method for Land-Cover Classification Using SPOT Imagery (Marceau et al., 1990)

Building on the earlier research concerning textural filters, this study focused on three principal elements of classification accuracy. The contribution and influence of window size, texture filter, and quantization level on land-use category classification accuracy were examined within the study.

Using the French-made and operated Système Probatoire d’Observation de la Terre (SPOT) imaging satellite, the study uses a 1986 image of the area surrounding the Bay of Chaleur within Quebec, Canada for analysis. At the time of this research, SPOT was capable of 10x10 meter spatial resolution in the panchromatic mode and 20x20 meter resolution in the multispectral mode. A 248 by 248 pixel subscene of the larger image was highlighted and the

sensor's near-infrared band (0.79-0.89 mm), with 20 meter resolution, was chosen for further investigation. Land cover categories contained within the image included residential areas, agricultural fields, fallow land, three forest types (deciduous, mixed, and coniferous), bare soil, a peat bog, disused quarries, and water surfaces (Marceau et al., 1990).

The first issues examined by this study are the variables associated with the Haralick Grey-Level Co-occurrence Matrix (GLCM). Marceau et al. identify six variables that are directly associated with the GLCM; the spatial resolution, the spectral band, the quantization level of the image, the size of the moving window, the interpixel distance and angle during the co-occurrence computation, and the statistics used as texture measures. The three variables identified earlier were then singled out for further development.

Fifty-six separate texture measures were then created using quantization levels of 16 and 32, seven moving windows from 5x5 to 49x49 pixels, an average interpixel distance of one, and the average of the four main interpixel angles (0, 45, 90, and 135 degrees). The Angular Second Moment (ASM), Contrast (CON), Inverse Difference Moment (IDM), and the Entropy (ENT) were calculated for each of the available combinations.

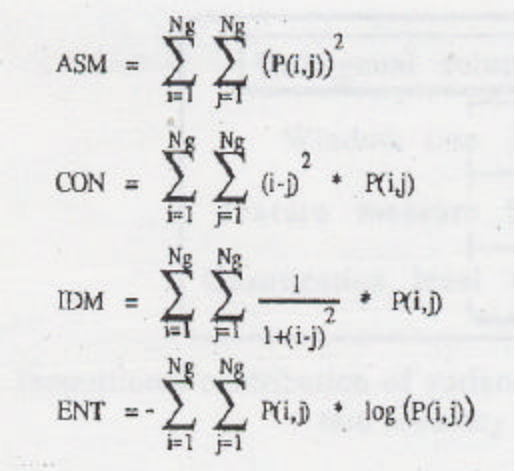

Figure 21. Texture measures implemented within Marceau study. Notation: *P(i,j)* is the *(i,j)th* entry in normalized grey-level co-occurrence matrix and N_g is the number of distinct grey levels in the quantized image (from Marceau et al.).

For classification purposes, a total of 70 band combinations were created. A supervised classification based on the maximum-likelihood algorithm was applied to the three SPOT multispectral bands combined with each texture image individually and to the three spectral bands combined with all four texture images together. These maximum likelihood classifications were repeated for each individual window size and quantization level to give a total of 70 classifications (Marceau et al., 1990).

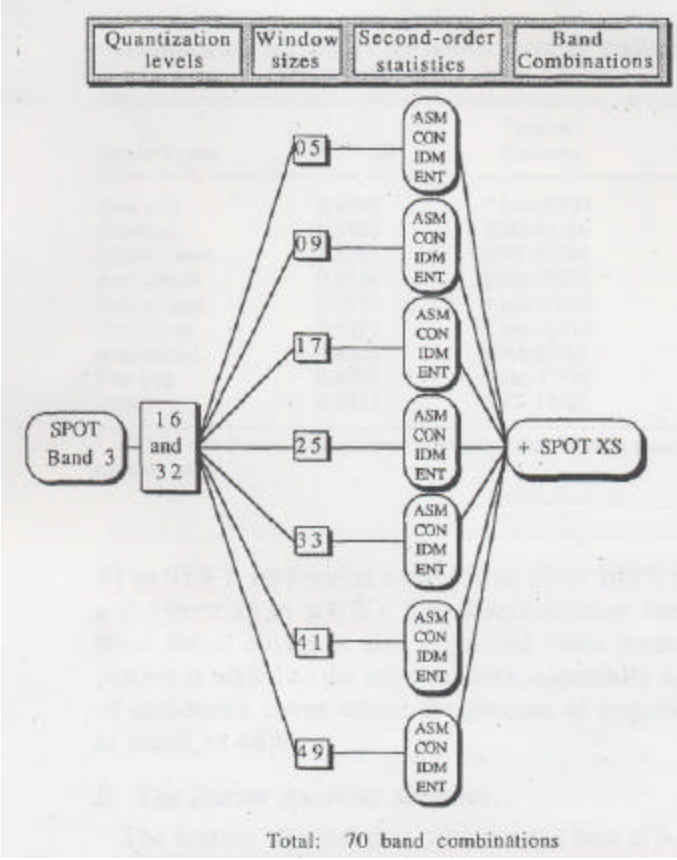

Figure 22. Combinations used within the classifier (from Marceau et al.).

From this study, it was determined that the accuracy of the multispectral classification process was significantly improved with the addition of texture features to the spectral image itself. The most significant improvements are obtained in the classification of fallow land (from 9 to 40%), agricultural fields (from 61 to 93%), residential areas (from 63 to 100%), and bare soil (from 45 to 100%) (Marceau et al., 1990).

CLASSIFICATION ACCURACY COMPARISON: SPOT XS VERSUS DIFFERENT SPECTRAL/TEXTURAL COMBINATIONS

Cover Types	SPOT XS	Texture[a] Features	SPOT Plus Texture
Bare soil	0.4546	7 bds-25/16	1.0000
Conifers	0.1805	IDM-41/16	0.4001
Mixed forest	0.1757	ENT-17/16	0.3790
Agriculture	0.6116	CON-05/32	0.9322
Fallow land	0.0927	7 bds-25/16	0.4012
Deciduous	0.3521	7 bds-41/16	0.8351
Residential	0.6325	IDM-25/16	1.0000
Peat bog	0.8096	ASM-17/16	1.0000
Quarry	0.8377	ENT-17/16	1.0000

[a]7 bds = 7 bands, first number is window size, second number is quantization level

Table 12. Improvement of overall classification rates with the addition of texture measures (Marceau et al.).

Each of the three principle variables being investigated provided a different level of contribution to the overall accuracy of the classifier. Of the three, it was determined that the size of the moving window provided the greatest impact with the texture measure being implemented and the quantization level providing much smaller contributions. The contribution of each factor to the total variance derived from an orthogonal solution is 90% for window size, 7% for the texture measure employed, and 3% for the quantization level.

The optimal sizes for the moving window were identified as 17x17 and 25x25 pixels. “Small window sizes do not capture the particular pattern of most classes, while the large ones can include pixels from more than one class and this results in poorer classifications” (Marceau et al., 1990). The texture measure used provided a much smaller overall impact on the classification results but it was determined that the ASM measure was the least effective

of the four measures for separating agricultural fields from residential areas and the CON measure was the least effective for discriminating forest cover. The effect of varying the quantization level was considered negligible.

5. Spectral and Textural Information of Multisensor Data for Land Use Classification in Metropolitan Area (Wikantika et al., 2000)

Like some of the earlier research, this study focused on the impact upon classification accuracy when textural features are combined with spectral features. The geographic area utilized for this study centers on the metropolitan area of Jakarta, Indonesia and the terrain within the study area was divided into nine main components: ocean, water, cultivated areas, grassland, deciduous vegetation, residential areas, commercial and service areas, and main roads and transportation related areas. RADARSAT and LANDSAT TM images (Figure 23) were utilized and Band 4 (NIR) of the LANDSAT sensor was selected due to its display characteristics.

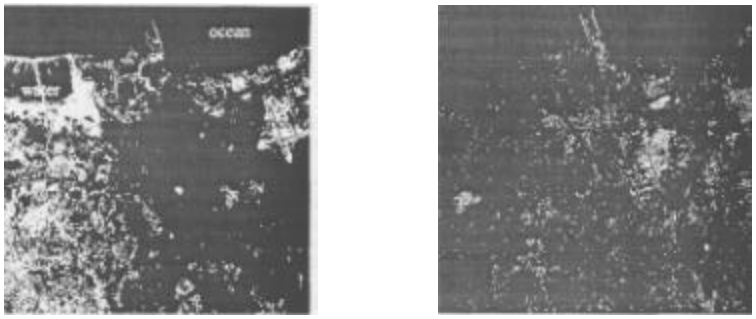

Figure 23. LANDSAT and RADARSAT images of Jakarta Indonesia (from Wikantika et al.)

A 512 by 512 pixel subscene of each image was used for the processing and the pixel size within the subscene was 30 meters. Four textural features utilizing the gray-level-co-occurrence matrix (GLCM) discussed earlier were then used; variance (VAR), entropy (ENT), angular second moment (ASM), and contrast (CON). Wikantika et al. analyzed the effect of using three different window sizes when processing the subscenes. The window sizes used were 3x3, 5x5, and 7x7. The angular distance used when creating the GLCM was kept constant at one, as with the Marceau et al. study, and the average of the four main interpixel angles (0, 45, 90, and 135 degrees) was used. A 256 gray level scale was also utilized for this study. More than 40 textural bands were then created using the varying images, window sizes, and filters (Figure 24).

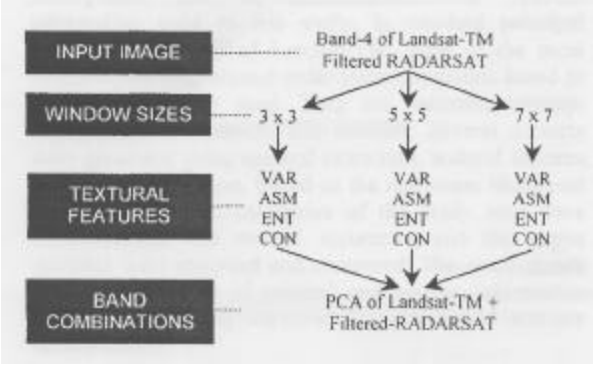

Figure 24. Textural bands created within study (from Wikantika et al.)

Wikantika et al. then examined the classification accuracies obtained from using only spectral values and then the accuracies obtained when the textural features were combined with the spectral data.

No.	Spectral information	Overall acc.	Kappa
1	PC-1, PC-2, PC-3	73.27 %	0.693
2	Haar + DBC	51.95 %	0.462
3	(1) + (2)	80.66 %	0.776

Notes : PC-1, PC-2, and PC-3 are principal component of Landsat-TM
Haar and DBC are original of RADARSAT image filtered by
Haar and Daubechies wavelet, respectively

Figure 25. Classification accuracies obtained with spectral values only (from Wikantika et al.)

No.	Spectral and texture*	Overall acc.	Kappa
1	PC + TM (3x3)	75.36 %	0.714
2	PC + TM (5x5)	78.10 %	0.745
3	PC + TM (7x7)	79.32 %	0.759
4	PC + TM (3x3)(5x5)(7x7)	80.04 %	0.767
5	(1) – ASM	74.50 %	0.706
6	(2) – ASM	79.03 %	0.756
7	(3) – ASM	80.76 %	0.776
8	(4) + Haar + DBC	88.40 %	0.863
9	(5) + Haar + Haar (3x3)	82.56 %	0.796
10	(6) + Haar + Haar (5x5)	83.61 %	0.808
11	(7) + Haar + Haar (7x7)	85.01 %	0.824
12	(5) + DBC + DBC (3x3)	81.45 %	0.782
13	(6) + DBC + DBC (5x5)	86.96 %	0.846
14	(7) + DBC + DBC (7x7)	88.40 %	0.863
15	(3) + Haar + Haar (7x7) + DBC + DBC (7x7)	90.38 %	0.887

Notes : PC = principal component 1, 2, 3 of Landsat-TM ; TM (3x3) = textural features (variance, angular second moment, entropy and contrast) Band-4 of Landsat-TM with window size of 3x3 ; ASM = angular second moment ; Haar = original of RADARSAT filtered by Haar wavelet ; DBC = original of RADARSAT filtered by Daubechies wavelet ; Haar (3x3) = textural features of RADARSAT image with window size of 3x3

Figure 26. Classification accuracies obtained with the combination of spectral and textural features (from Wikantika et al.)

This study presented similar results to the research discussed earlier. The addition of textural features to the classification effort resulted in greater overall accuracies for land use categorization within an urban area. Wikantika et al. identified one data window size that provided greater accuracies during the classification process. The window size identified as the most capable of

achieving satisfactory classification results was the 7x7 window (Wikantika et al.). This study also identified the ASM texture feature as the least useful of the four texture features for providing additional impact to the classification process.

6. Texture-Based Segmentation of Temperate-Zone Woodland in Panchromatic IKONOS Imagery (Gagnon et al., 2003)

In one of the most recent examinations of the use of texture for terrain classification, Gagnon et al. utilized high-resolution panchromatic imagery from Ikonos in an attempt to delineate woodlands in an urban area. Focusing on a 12km by 12km section of suburban Montreal, five subset areas were selected for further investigation. The five 512 by 512 pixel sub-images are shown below in Figure 27.

Figure 27. Five test images of the Montreal region, labeled A through E within the study (from Gagnon et al.)

The methodology employed within the study included 1) creation of texture images, 2) selection of the optimal texture measures, 3) maximum likelihood (ML) classification, and 4) post-classification analysis. Instead of using the gray level co-occurrence matrices (GLCM) discussed earlier, a sum and a difference histogram were employed to calculate the texture measures. "The sum histogram represents the numbers of time each sum of two pixel value pairs is present in the window and the difference histogram is the same but for differences between pixels" (Gagnon et al., 2003). Similar to the GLCM, but with different notation, three parameters characterize the creation of the texture measures, the window size (*f*), the step size (*p*), and the angular orientation of the sampling (*d).*

Gagnon et al. proceeded to calculate eight separate texture measures as shown in table 13, where $\hat{P}_s(i)$ is the value of index *I* of the normalized sum-histogram and $\hat{P}_d(j)$ is the value of index *j* of the normalized difference-histogram (Gagnon et al., 2003).

Mean	$\mu = \frac{1}{2}\sum_i i.\hat{P}_x(i)$
Contrast	$\sum_j \left(j^2 \cdot \hat{P}_d(j)\right)$
Correlation	$\frac{1}{2}\left(\sum_i (i-2\mu)^2.\hat{P}_x(i) - \sum_j j^2.\hat{P}_d(j)\right)$
Energy	$\sum_i \left(\hat{P}_x(i)^2\right) \cdot \sum_j \left(\hat{P}_d(j)^2\right)$
Entropy	$-\sum_i \left(\hat{P}_x(i) \cdot \log\left(\hat{P}_x(i)\right)\right) - \sum_j \left(\hat{P}_d(j).\log\left(\hat{P}_d(j)\right)\right)$
Homogeneity	$\sum_i \sum_j \left(\frac{1}{1+j^2} \cdot \hat{P}_d(j)\right)$
Maximal Probability	$Max\left\{\hat{P}_x(i)\right\}$
Standard Deviation	$\sqrt{\frac{1}{2}\left(\sum_i \left((i-2\mu)^2 \cdot \hat{P}_x(i)\right) + \sum_j \left(j^2 \cdot \hat{P}_d(j)\right)\right)}$

Table 13. The eight Haralick textures used in this study

Four of these texture measures; mean, contrast, correlation, and standard deviation, were determined to be optimum. In order to find the ideal combination of window and step size, a second optimization procedure was performed. The block diagram of the methodology employed during the second optimization procedure is shown below in Figure 28.

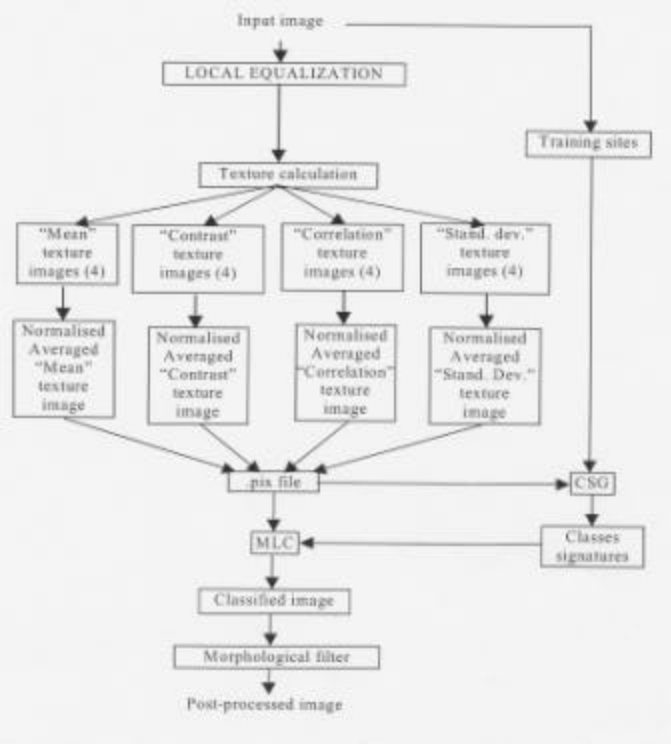

Figure 28. Methodology employed with second phase of Gagnon study (from Gagnon et al., 2003)

During the post-classification analysis, Gagnon et al. determined that large step sizes (p = 7, 11, and 16) were unacceptable due to the resulting high false alarm rates generated. It was also determined that the optimal window size must be equal or greater than the diameter of a tree and could possibly fall in the range of f = 17 to 35. This study showed that woodland segmentation within an urban environment is possible and that texture is a viable method for discriminating between general spectral classes such as woodland and urban areas (Gagnon et al., 2003). Two of the resulting woodland-segmented images are shown below in Figures 29 and 30.

Figure 29. Classification results after post-processing for the 17-2 combination (from Gagnon et al.)

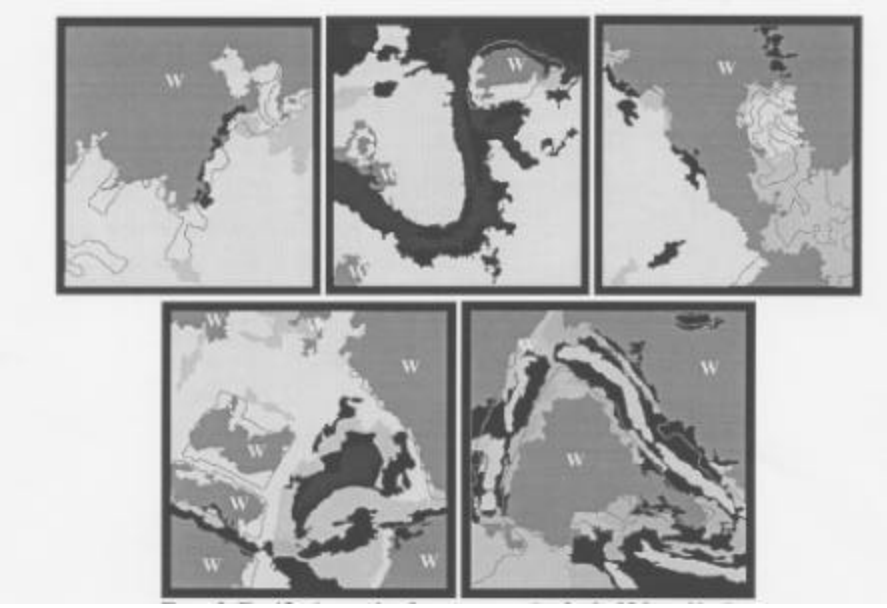

Figure 30. Classification results after post-processing for the 35-2 combination (from Gagnon et al.)

The earlier work cited throughout this chapter has effectively laid the foundation for the textural analysis

being presented in this study. The tools initially presented by Haralick et al. were refined and expanded upon by the follow-on studies. We attempt to use those tools in our analysis of the test image and the impact that textural features have upon the panchromatic imagery data. Chapters 3 through 5 will highlight the investigative tools utilized within this study to accomplish those goals.

D. IKONOS REMOTE SENSING PLATFORM

Ikonos, launched on September 24th 1999 and owned and operated by the Space Imaging Corporation, is the first high-resolution commercial imaging satellite. Collecting one meter panchromatic and four meter multi-spectral imagery through its high resolution Kodak camera telescope, Ikonos supplies the commercial user with detailed imaging capabilities that were only previously available through classified military systems.

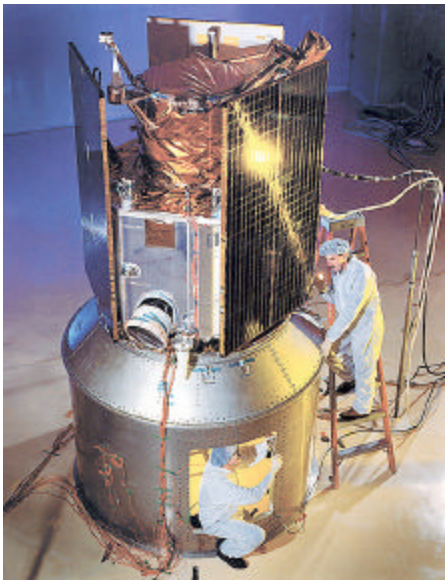

Figure 31. The Ikonos satellite (from Space Imaging)

Ikonos is deployed in a sun-synchronous Low Earth Orbit (LEO) at an altitude of 681 km and an orbital inclination of 98 degrees. The sensor's orbit provides an orbital period of 98 minutes with a one meter resolution revisit time of 2.9 days.

The sensors on-board Ikonos are capable of providing one meter resolution panchromatic data in the 0.45 to 0.9 um range and multispectral data in four bands also covering the 0.45 to 0.9 micron range. The individual bands are broken down as follows: band #1 (blue) 0.45-0.52 mm, band #2 (green) 0.52-0.6 mm, band #3 (red) 0.63-0.69 mm, and band #4 (Near IR) 0.76-0.9 mm. The spectral response of the Ikonos sensors are shown in Figure 32.

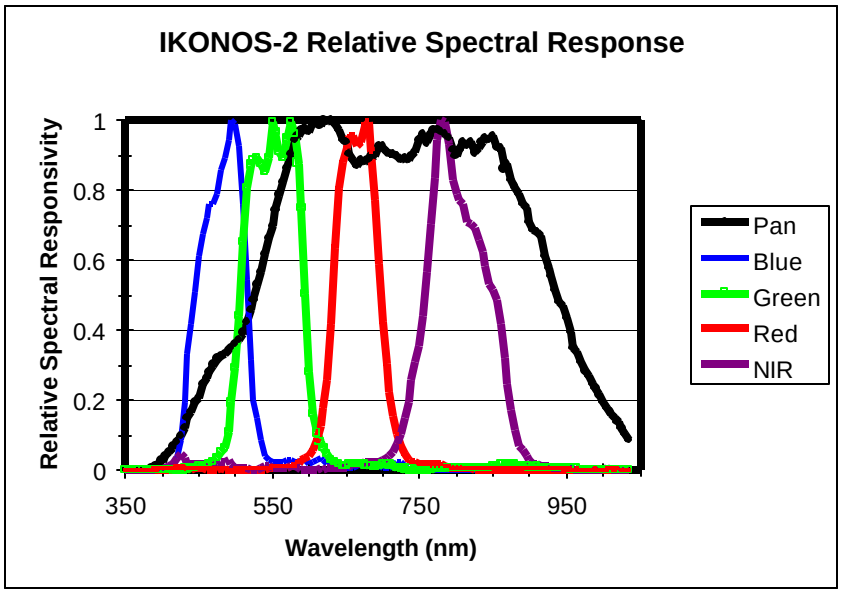

Figure 32. Spectral response of Ikonos sensors

The Kodak camera system associated with Ikonos is a three mirror system including a 0.7 meter primary mirror. The Ikonos telescope has the equivalent resolving power of

a 10,000 mm telephoto lens (Olsen, 2002). 13,500 12-micron large pixels form the panchromatic sensor within the focal plane unit and 3375 48-micron sized pixels make up the satellite's multispectral sensor (Olsen, 2002).

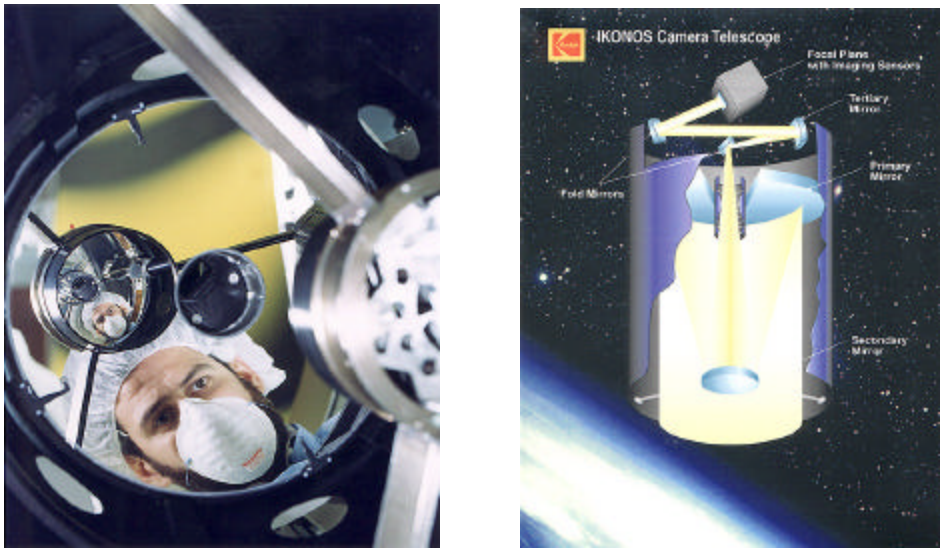

Figure 33. Kodak camera telescope system on-board Ikonos (from Kodak)

The high-resolution imagery available from sensors like Ikonos provide a tremendous opportunity for a detailed analysis of the impact of adding texture-filtered imagery data to the panchromatic imagery data. For this study, the Ikonos platform was tasked to take both panchromatic and MSI data for a portion of the central Californian coastline. The coverage area, collection parameters, and terrain included within the Ikonos image are covered in greater detail in the following section.

E. AREA OF INVESTIGATION

1. Coverage area

Ikonos images of the central California coastal region were utilized for this study. The region of interest for this study covered the area just north of Monterey to north of the city of Watsonville and extended from the Monterey Bay in the west to just east of Highway 101. Significant geographical regions included within the subject area included the Monterey Bay, the Elkhorn Slough and its surrounding wetlands, and the cities of Watsonville, Prunedale, and Castroville.

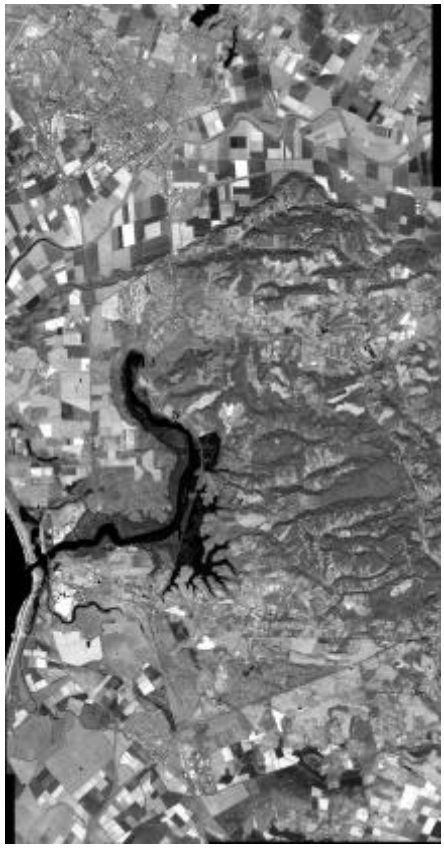

Figure 34. Ikonos image used in this study (from Space Imaging)

The detailed image positional data for the IKONOS image is shown in table 14 below.

Location	Latitude	Longitude
Southwest	36.7407 N	121.7981 W
Northwest	36.9420 N	121.7949 W
Northeast	36.9406 N	121.6658 W
Southeast	36.7393 N	121.6693 W

Table 14. Ikonos image geographical data

The image was acquired on the 1st of October, 2002 at 19:00 GMT and the imagery data was collected in the panchromatic and four spectral bands; blue, green, red, and NIR. The panchromatic data was collected at one meter resolution and the image was 11,504 by 22,340 pixels large. The source image metadata is shown below in Table 15.

Acquisition Date / Time	2002-10-01 / 19:00 GMT
Scan Azimuth	180.04 degrees
Normal Collection Azimuth	132.2669 degrees
Normal Collection Elevation	70.32868 degrees
Sun Angle Azimuth	158.7623 degrees
Sun Angle Elevation	47.88973 degrees

Table 15. Image collection data for Ikonos images used in this study (from Space Imaging)

2. Terrain Within the Study Area

The region of interest for this study encompassed a fairly diverse group of land use types or categories. Much of the area is devoted to agricultural industries and the crops and fields within the image include strawberries, squash, artichokes, brussel sprouts, cabbage, broccoli, and celery. Many unplowed and plowed fields in between growing seasons were also imaged. The Elkhorn Slough and its surrounding wetlands, including its large mudflats, provided a wide range of soils and vegetation. Pickleweed dominates the lower marsh area of the slough but several other types of vegetation thrive in the immediate area including salt grass, saltbush, wild mustard, coyote bush, oak trees, and several types of chaparral plants (Silberstein and Campbell, 1989). The urban areas contained within the study area include several small to medium sized towns and the build-up along the two major roads in the region, highway one to the west and highway 101 to the east.

F. SPECTRAL CHARACTERISTICS OF VEGETATION

A major portion of this study is devoted to investigating the ability to discriminate between several different classes of vegetation using only panchromatic and texture filtered panchromatic data when compared with equivalent multispectral data. The ability to distinguish different species of vegetation is a direct function of which region of the electromagnetic spectrum is utilized during the analysis. The spectral responsivity of vegetation in general is easily distinguishable when compared to a diverse range of materials (Figure 35) but

the average spectral response curves are much more difficult to distinguish when comparing individual types of vegetation (Figure 36).

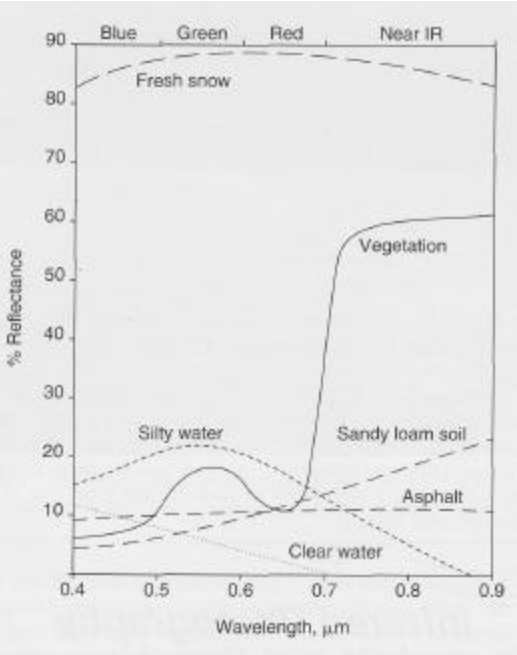

Figure 35. Average spectra response curves for various materials (from Avery and Berlin)

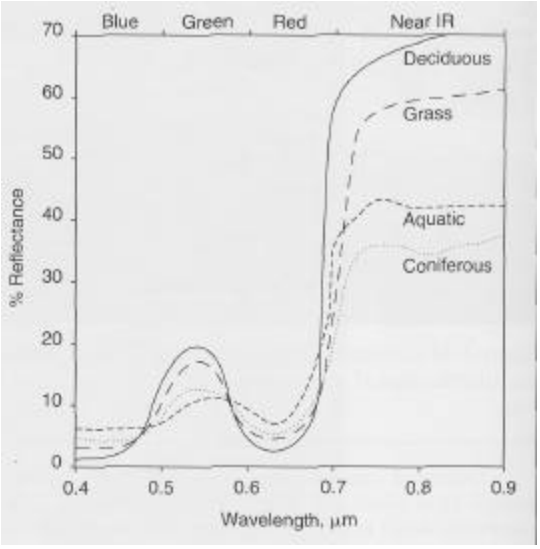

Figure 36. Average spectral response curves for four types of vegetation (from Avery and Berlin)

The difficulty in discerning individual vegetation can be overcome by using sensors in the near-infrared (NIR) and infrared (IR) regions of the EM spectrum. “It is seen that the most appropriate region for differentiating between most of the materials would be the photographic IR region because it is here where the greatest differences in reflectance generally occur” (Avery and Berlin, 1992). This effect can be clearly seen in Figure 37 which shows the contrast between an infrared image and a panchromatic image of a mixture of natural vegetation. The infrared photo enables the observer to distinguish not only the different species of trees contained in the image but also provides a clear separation of the small stream running down the right side of the image.

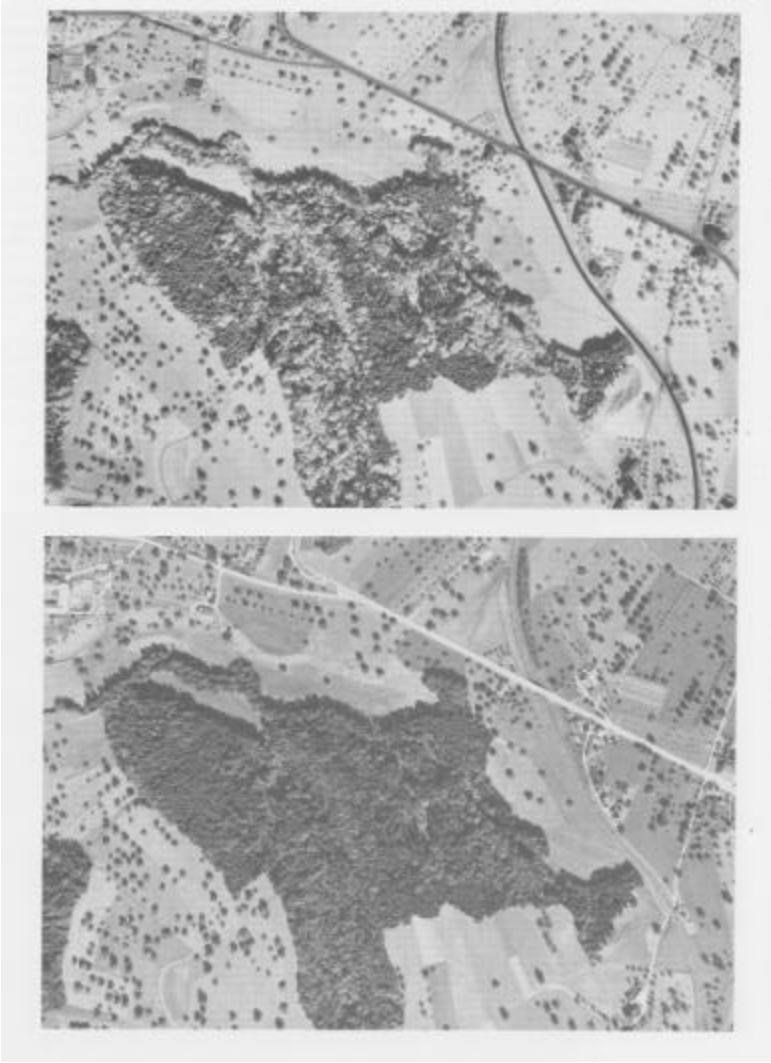

Figure 37. Comparison of infrared image (top) and panchromatic image (bottom) showing the ability to discriminate different types of vegetation (from Avery and Berlin)

Several factors affect the spectral responsivity of vegetation including the species of vegetation, the overall health of the vegetation, the age of the vegetation, the water content, the time of year, and the topographic location. The effect of damage to a plant leaf can be seen in Figure 38 which shows the reflectance curves for several stages of leaf damage.

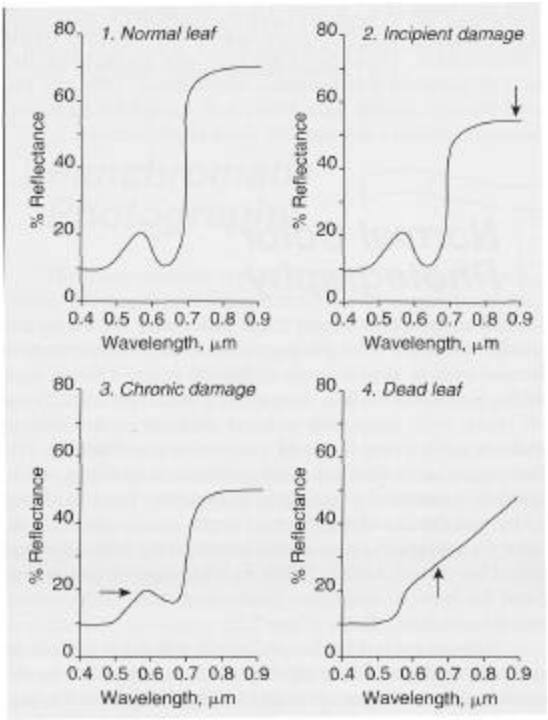

Figure 38. Average spectral response curves for different stages of plant leaf health (from Avery and Berlin)

The general spectral response curve is characterized by two important regions; the local maximum in reflectivity in the green region (approximately 0.55 *mm*) and the IR ledge, or "red shift" by another name, occurring at approximately 0.7 *mm*. "There are large reflectance differences in the near IR region but, by comparison, the differences in reflectance in the green region are negligible and distinct tonal or color separations would be associated with the infrared region" (Avery and Berlin, 1992).

The reflectance of vegetation in the green and infrared regions are directly linked to two major groups of cells found in all vegetation. Closer to the leaf surface,

Palisade cells and the chloroplasts they contain are responsible for the peak in reflectance within the green region. Up to 20 percent of incident green light is reflected by the chloroplasts, and the chlorophyll they contain, in the normal functioning of a plant and this results in the green color of leaves (Avery and Berlin, 1992). Deeper within the leaf structure are mesophyll cells which are responsible for the large spike in reflectance in the NIR and IR regions. Near IR radiation is unaffected by the upper layer chloroplasts, but is strongly reflected by the mid-layer mesophyll and it is not uncommon for more than 50 percent of incident near IR radiation to be reflected upward through the leaf. (Avery and Berlin, 1992). A generalized diagram of a leaf structure is shown in Figure 39 but the actual structure will vary from species to species and the size, orientation, and health of the individual cells will have a great effect on overall reflectance characteristics.

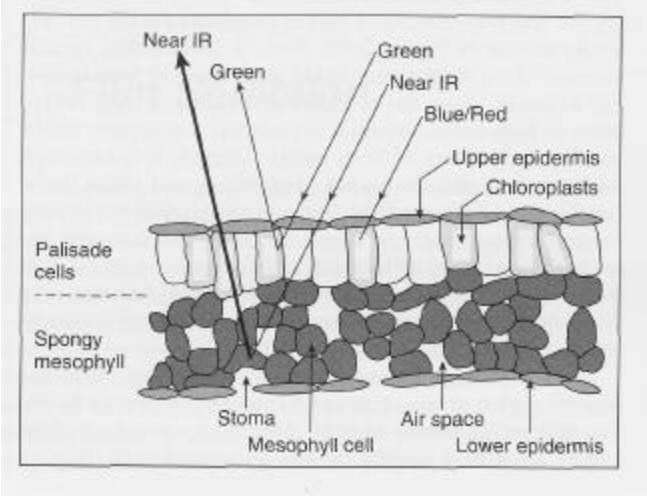

Figure 39. Basic leaf structure showing chloroplasts and mesophyll cells responsible for green and infrared reflectivity (from Avery and Berlin)

The spectral response of vegetation has a considerable impact upon the execution and outcome of this study. The question of spectral class separation using only texture-filtered panchromatic data is driven by the characteristics described above. The methodology employed during the course of this study will be discussed in greater detail in Chapter 3 and the spectral response of vegetation will have a major effect upon all phases of the research. Chapters 3 through 5 will highlight the investigative tools and procedures employed during the analysis of texture-based filtering.

G. ENVI SOFTWARE

The computational tool used in the development of this research was the Environment for Visualizing Images (ENVI) software created by Research Systems Incorporated (RSI), of the Kodak Company. ENVI is an Interactive Data Language (IDL) based image processing package that enables users to access and work with images in multiple formats and sources. For this study, only a small subset of ENVI functions were utilized including basic image manipulation tools, the 13 embedded texture filters within the software, the Spectral Angle Mapping (SAM) and Maximum Likelihood (ML) classifiers, and several post-classification functions.

1. Texture Filters

The texture filters within ENVI are based upon the work by Haralick and are separated into two categories; occurrence-based filters and co-occurrence-based filters. Occurrence measures use the number of occurrences of each gray level within the processing window for texture

calculations while the co-occurrence measures use a gray-tone spatial dependence matrix to calculate texture values (ENVI User's Guide, 2001). There are five occurrence filters and eight co-occurrence filters available to the user (Table 16).

OCCURRENCE	
1	Data Range
2	Mean
3	Variance
4	Entropy
5	Skewness

CO-OCCURRENCE	
6	Mean
7	Variance
8	Homogeneity
9	Contrast
10	Dissimilarity
11	Entropy
12	Second Moment
13	Correlation

Table 16. Texture filters within ENVI

2. Classifiers

Two of ENVI's classification algorithms were utilized for this study. The first classifier employed was the Spectral Angle Mapper (SAM). In n-dimensional multi-spectral space a pixel vector X has both magnitude (length) and an angle measured with respect to the set of axes that define the coordinate system of the space (Richards, 1999). SAM uses only the angular characteristics of the pixel spectrum for identification and classification purposes. The SAM algorithm determines the spectral similarity between two spectra by calculating the angle between the spectra, treating them as vectors in n-space with n equal to the number of bands (ENV User's Guide, 2001). The angle between the test spectrum and the reference spectrum

(Figures 35 and 36) is a direct function of the spectral similarity between the pixels being investigated. Small angles indicate a closer match between test and reference spectrum.

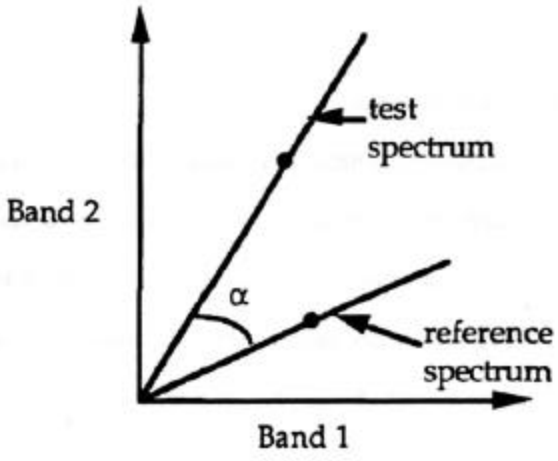

Figure 40. SAM maximum threshold angle - 0.15 radians for this study (from Kruse, 1993)

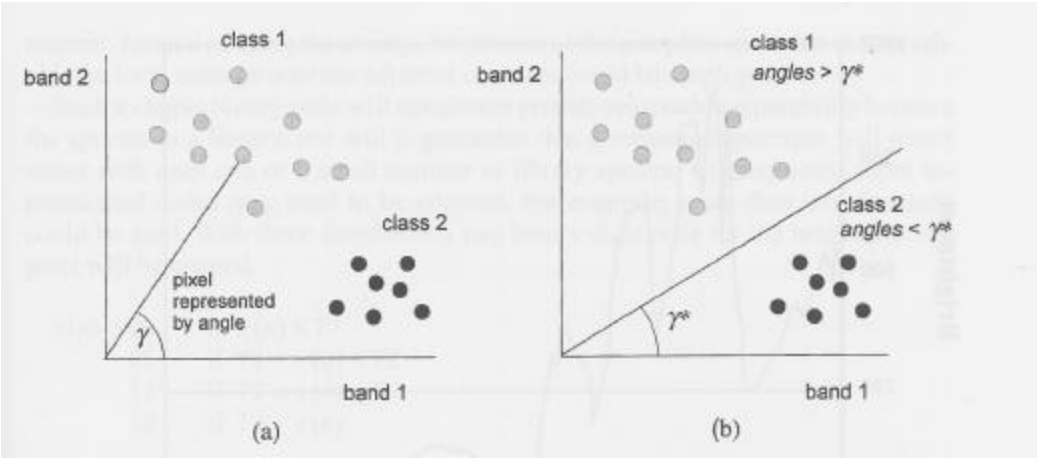

Figure 41. (a) Spectral characteristics of test pixels represented by spectral angle. (b) Segmentation of the multispectral space by threshold angle (g^*). (From Richards, 1999)

a. Spectral Angle Mapper

Operator inputs within the ENVI SAM functions include a specified maximum angle threshold in radians and if the test spectrum falls outside of this angle it will not be classified as the reference material. For this study, a maximum angle threshold of 0.15 radians was used during the SAM classification process. The spectral angle is computed by ENVI using the following equation where N = the number of bands, r_i = the reference spectra vector components, and t_i = the test spectra vector components:

$$a = \cos^{-1}\left[\frac{\sum_{i=1}^{N} t_i r_i}{\left(\sum_{i=1}^{N} {t_i}^2\right)^{1/2}\left(\sum_{i=1}^{N} {r^2}_i\right)^{1/2}}\right]$$

Equation 9. ENVI computation of spectral angle during SAM classification process (from Kruse, 1993)

During SAM classification, a set of rule images is also created, one for each input ROI used in the classifier. The rule image that has the highest probability for a pixel is the class that pixel is assigned to. The probability values themselves are only retained in the rule image, not in the classified image (ENVI User's Guide, 2001).

b. Maximum Likelihood Classifier

The second classification algorithm employed within this study was the maximum likelihood classifier. The Maximum Likelihood classifier is the most widely used

supervised classification method associated with remote sensing applications (Richards, 1999). The ML algorithm is computationally intensive and was not widely utilized in the earlier studies cited due to the lack of adequate computing power at the time. Today's processing speeds have allowed greater use of the ML algorithm and this has resulted in improved classification accuracies. "This approach to classification is extremely useful and flexible and, under certain conditions, provides what is probably the most effective means of classification given the constraints of supervised classification" (Richards, 1999).

The ROI's previously processed through the n-D Visualizer were imported into the ML classifier and serve as the training set of spectral classes for the classification process. ML classification assumes that the statistics for each class in each band are normally distributed and calculates the probability that a given pixel belongs to a specific class and each pixel is assigned to the class with the highest probability (ENVI User's Guide, 2001).

The Maximum Likelihood decision rule is developed using Bayes theorem and an excellent development of the rule is found in Richards, 1999. A summary of the development of the decision rule is found below.

w_i = thespectral classes for an image

$w_i, i = 1,...M$ (whereM=the totalnumber of classes)

$p(w_i \mid x)$ where x is a column vector of brightness valuesfor thepixel)

[$p(w_i \mid x)$istheprobability that w_i isthecorrectclass for a pixelat x.]

$x \in w_i$ *if* $p(w_i / x) > p(w_j / x)$ *for all* $j \neq 1$

[the pixel at x belongs to w_i if $p(w_i \mid x)$ is larger than the probability that it belongs to another class $p(w_j \mid x)$]

$p(x|w_i)$ is the probability of finding a pixel from class w_i at position x and there are as many $p(x|w_i)$ as there are training classes.

Using Bayes' Theorem: $p(w_i \mid x) = \dfrac{p(x \mid w_i)p(w_i)}{p(x)}$ where $p(w_i)$ is the probability that class w_i occurrs in the image, $p(x)$ is the probability of finding a pixel from class at position x, and $p(x) = \left[\sum_{i=1}^{M} p(x \mid w_i)\, p(w_i)\right]$

This leads to the Maximum Likelihood classification rule:

$$x \in w_i \text{ if } p(x \mid w_i)p(w_i) > p(x \mid w_j)p(w_j) \text{ for all } j \neq 1$$

Equation 10. Maximum Likelihood decision rule (from Richards, 1999)

ENVI operator inputs associated with the ML classifier include the ability to designate a probability threshold. This means that if the probability that the test pixel is below the operator input value then the pixel will remain unclassified. No probability threshold was designated during this study and this meant that all pixels would be

classified into one of the reference classes and that no pixel would remain unclassified.

As with the SAM classification process, a set of rule images are also created, one for each input ROI used in the classifier. The rule image that has the highest probability for a pixel is the class that pixel is assigned to. The probability value themselves are only retained in the rule image, not in the classified image (RSI, 2001).

THIS PAGE INTENTIONALLY LEFT BLANK

III. METHODOLOGY

A. GENERAL PROCEDURES

A general outline of the investigative methodology used within this study is shown below in Figure 40. Each individual step within the larger process will be examined in greater detail in the following section but the methodology incorporated the following steps: 1) Creation of a mosaic image containing four to six sub-images 2) Texture filtering of the mosaics 3) Histogram creation to examine the filtered outputs 4) Creation of Region-of-Interests (ROI's) for follow-on image classification purposes 5) Utilization of Spectral Angle Mapper (SAM) and Maximum Likelihood (ML) classification algorithms 6) Post-classification analysis to evaluate the impact of textural filters upon overall classification accuracy.

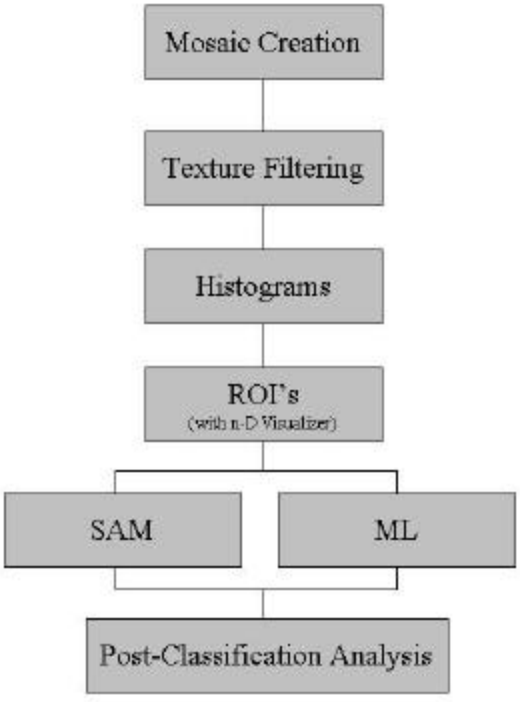

Figure 42. General outline of methodology employed

Following the analysis of the mosaic images, the general methodology was repeated, with some minor changes, for the full scene Ikonos panchromatic imagery data. The methodology employed for the full image analysis and classification can be seen below in Figure 41.

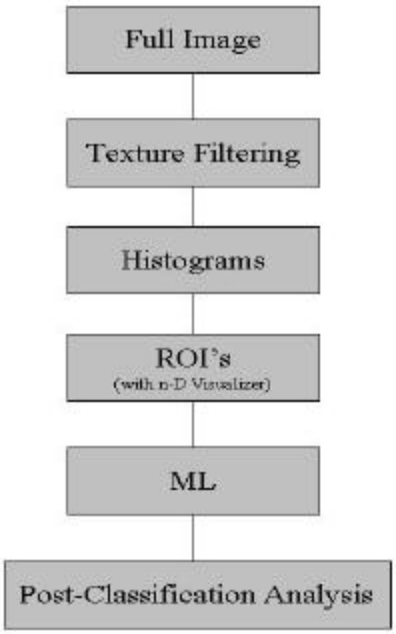

Figure 43. Methodology employed for processing and analysis of full scene imagery data.

B. MOSAIC IMAGES

The mosaic function within ENVI was used to reduce the workload associated with the texture filtering of the test images because all the sub-images contained within the mosaic could be filtered at the same time. Two of the three mosaic images evaluated within this study were created using ENVI's mosaic functions and fused four 512 by 512 pixel sub-images into a 512 by 2048 pixel mosaic image. The two mosaics included a Elkhorn Slough mosaic made up of

four different sub-images of the terrain and vegetation within the Elkhorn Slough region and a Fields mosaic that incorporated four sub-images of agricultural related fields within the study area. The resulting mosaic images are shown below in Figures 44.

A third mosaic image was created from six 512 by 512 pixel sub-images and incorporated a mixture of terrain and land-use categories that were available within the IKONOS image. This mosaic included residential, industrial, agricultural, and wetland regions in effort to evaluate the impact of the texture filters on a wider variety of subjects prior to employing the texture filters on the entire image. The new mosaic, labeled the Various mosaic, is also shown below in Figure 44.

Figure 44. Three mosaics utilized in this study. Elkhorn Slough mosaic, Fields mosaic, Various mosaic.

C. TEXTURE FILTERS

The three mosaic images were texture filtered using both the occurrence and co-occurrence filters contained within ENVI resulting in the creation of two separate files for each mosaic, an occurrence filtered file and a co-occurrence filtered file. Three separate moving data

windows were used during the texture filtering process: 5x5, 17x17, and 35x35. The co-occurrence filtering process also utilized an angular distance (*d*) of one, and a gray level quantization of 64. These two separate files for each data window size were then combined to incorporate both subsets of texture filters for further examination during the supervised classification process (Figure 47). Histograms of each texture-filtered image were then created in order to evaluate the output and utility of the filtering process.

Several anomalies of unknown origin were discovered within the skewness texture images and we chose to remove the skewness data prior to the implementation of image classification algorithms within the follow-on procedures. Several of the texture measures appeared to offer redundant information with slight differences in noise level. Eight texture bands were selected for the final image processing. Mean and variance from the occurrence matrix were included and entropy, homogeneity, dissimilarity, contrast, angular second moment, and correlation were included from the co-occurrence matrix. The final texture filtered images are shown in Appendix A.

Several interesting qualities of the various texture measures can be easily seen in the texture-filtered images. The variance measure was very capable of distinguishing the paved and dirt roads that line the edge of the Elkhorn Slough. The variance measure was also able to distinguish the small stream running through the third sub-image of the Fields mosaic. This performance was not matched by the other co-occurrence measures for the Fields mosaic. The

variance measure did perform poorly, however, in comparison to the homogeneity, entropy, and angular second moment measures in distinguishing the runways of the Watsonville Airport.

Overall, most of the texture measures performed very well at distinguishing the larger water body of the Elkhorn Slough and most were capable of delineating the boundaries between the different types of fields within the Fields mosaic. The variance measure appears to provide the most useable texture information while the correlation measure appears to provide the least.

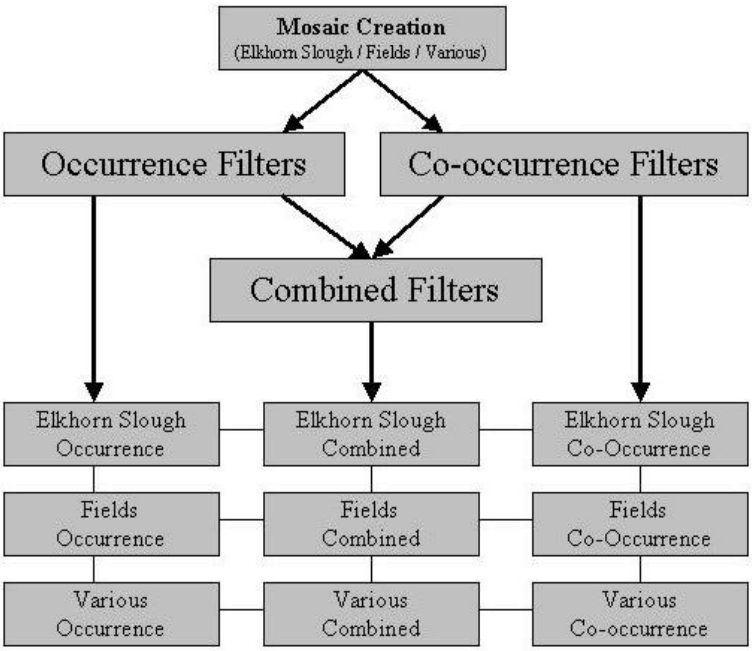

Figure 45. File output after texture filtering process

D. REGIONS-OF-INTEREST CREATION

In order to continue with the supervised classification process on the mosaic images, several regions-of-interest had to be identified and extracted from the imagery data. ROI's are portions of images, either selected graphically or selected by other means and are typically used to extract statistics for classification, masking, and other purposes (ENVI User's Guide, 2001). ROI's are designated based upon their spectral characteristics and are used to develop accurate training sets for the classification process. The initial ROI's were then imported into ENVI's n-Dimensional Visualizer (ND-vis) for further refinement and additional separation into more accurately defined spectral classes. A more detailed description of the ND-vis is contained within the ENVI User's Guide:

> The n-D Visualizer is an interactive tool that is used for selecting the endmembers in n-space. Spectra can be thought of as points in an n-dimensional scatterplot, where n is the number of bands. The coordinates of the points in n-space consist of "n" values that are simply the spectral radiance or reflectance values in each band for a given pixel. The distribution of these points in n-space can be used to estimate the number of spectral endmembers and their pure spectral signatures. (RSI, 2001)

An example of the n-D Visualizer is shown below in Figure 48 with each of the spectral classes separated by color and labeled accordingly.

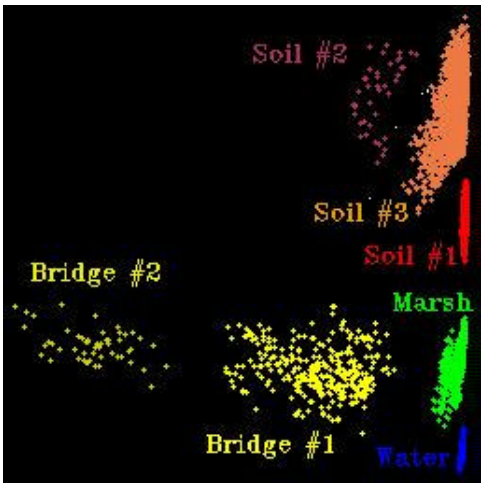

Figure 46. Example of n-D Visualizer - Elkhorn Slough spectral class separation obtained using the n-D Visualizer(from ENVI)

The following ROI's (Table 17) were created using this process and were established for the manipulation of the Elkhorn Slough mosaic image.

Spectral Class	Color
Soil #1 (Plowed Fields)	Red
Soil #2 (Unidentified)	Maroon
Soil #3 (Drainage Pond)	Sienna
Bridge #1	Yellow
Bridge #2	Yellow 2
Water	Blue
Marsh (Pickleweed)	Green

Table 17. Spectral classes identified within Elkhorn Slough mosaic image.

E. SPECTRAL ANGLE MAPPER (SAM) AND MAXIMUM LIKELIHOOD (ML) CLASSIFICATION PROCESS

The ND-vis processed ROI's were then imported into two separate supervised classification algorithms for further processing of the image. "Supervised classification is an analyst-controlled process where pixels that represent patterns or land cover features are recognized and identified with help from collateral sources, such as ground truth, aerial photography, and maps" (Multispectral Users Guide, 1995). As described previously, ENVI has multiple algorithms available for image classification, both supervised and unsupervised, but the SAM and ML classifiers were chosen for their performance characteristics and widespread use within the remote sensing field.

F. POST-CLASSIFICATION PROCEDURES

Several ENVI post-classification functions were employed following the SAM and ML classifications. First a confusion matrix, or error matrix, was created using a comparison between ground truth regions-of-interest (ROI's) and the SAM and ML classified images. ENVI's confusion matrix function reports an overall accuracy, producer and user accuracies, kappa coefficient, confusion matrix, and errors of commission and omission (ENVI User's Guide, 2001). The overall accuracy rates for the classified images are calculated by summing the number of pixels classified correctly and dividing by the total number of pixels present in the image. The ground truth ROI's define the true class of the pixels (ENVI User's Guide, 2001). Several examples of confusion matrices obtained from

evaluating the full image classification efforts are shown in Appendix D.

The kappa coefficient is another accuracy measurement generated by ENVI's post-classification confusion matrix function. The ENVI User's Guide contains the following description of the calculation of the kappa coefficient: The kappa coefficient (k) is calculated by multiplying the total number of pixels in all ground truth classes (N) by the sum of the confusion matrix diagonals (x_{kk}), subtracting the sum of the ground truth pixels in a class times the sum of the classified pixels in that class summed over all classes ($x_{k\Sigma}x_{\Sigma k}$), and dividing by the total number of pixels squared minus the sum of the ground truth pixels in that class times the sum of the classified pixels in that class summed over all classes (ENVI User's Guide, 2001). The calculation of the kappa coefficient is shown below in Equation 11. The kappa coefficients calculated during the execution of this study are shown in Appendix D along with the corresponding confusion matrix.

$$k = \frac{N\sum_{k} x_{kk} - \sum_{k} x_{k\Sigma}x_{\Sigma k}}{N^2 - \sum_{k} x_{k\Sigma}x_{\Sigma k}}$$

Equation 11. ENVI's calculation of the kappa coefficient

An excellent example of both an error matrix and the calculation of the kappa coefficient can be seen in Jensen (1996) and is summarized below in Figure 51.

	Reference Data					
Classification	**Residential**	**Commercial**	**Wetland**	**Forest**	**Water**	**Row Total**
Residential	70	5	0	13	0	88
Commercial	3	55	0	0	0	58
Wetland	0	0	99	0	0	99
Forest	0	0	4	37	0	41
Water	0	0	0	0	121	121
Column Total	73	60	103	50	121	407

Overall Accuracy = 382/407 = 93.86%

Producer's Accuracy (measure of omission error)

Residential = 70/73 =	96%	4% omission error
Commercial = 55/60 =	92%	8% omission error
Wetland = 99/103 =	96%	4% omission error
Forest = 37/50 =	74%	26% omission error
Water = 121/121 =	100%	0% omission error

User's Accuracy (measure of commission error)

Residential = 70/88 =	80%	20% commission error
Commercial = 55/58 =	95%	5% commission error
Wetland = 99/99 =	100%	0% commission error
Forest = 37/41 =	90%	10% commision error
Water = 121/121 =	100%	0% commission error

Computation of K_{hat} Coefficient

$$K_{\text{hat}} = \frac{N\sum_{i=1}^{r} x_{ii} - \sum_{i=1}^{r}\left(x_{i+} \times x_{+i}\right)}{N^2 - \sum_{i=1}^{r}\left(x_{i+} \times x_{+i}\right)}$$

where $N = 407$

$$\sum_{i=1}^{r} x_{ii} = (70 + 55 + 99 + 37 + 121) = 382$$

$$\sum_{i=1}^{r}\left(x_{i+} \times x_{+i}\right) = (88 \times 73) + (58 \times 60) + (99 \times 103) + (41 \times 50) + (121 \times 121) = 36{,}792$$

$$\text{therefore } K_{\text{hat}} = \frac{407(382) - 36{,}792}{407^2 - 36{,}792} = \frac{155{,}474 - 36{,}792}{165{,}649 - 36{,}792} = \frac{118{,}682}{128{,}857} = 92.1\%$$

Figure 47. Example of error matrix and kappa coefficient calculation (from Jensen)

THIS PAGE INTENTIONALLY LEFT BLANK

IV. RESULTS

The analysis process described to this point was conducted in two phases – the analysis of some relatively small mosaics, followed by analysis of the full scene. The first phase was conducted primarily to gain experience with texture analysis, and lead to some useful insights. The primary goal was in the second phase.

A. MOSAIC ANALYSIS

The processing of the image chips showed how different texture elements could be used to discriminate the various elements of the Elkhorn Slough image. The mean texture measure provided the greatest impact to classification effort overall but several other measures displayed superior performance in certain areas. Figure 48 below illustrates how the simple classes in the Elkhorn Slough mosaic (Figures B-1 and B-2) vary in a few dimensions. Water (blue in the figures, here) is low in mean, variance, and entropy, but shows a fair scatter in the last measure.

The main water channel of the slough was easily distinguishable within all the filtered images and it appears that no single texture measure was more capable than the others in this regard. The co-occurrence variance and dissimilarity measures provided the best woodland segmentation capabilities with the correlation measure providing the poorest results. Several measures performed relatively well in discriminating the different types of fields present in the image. Variance, dissimilarity, entropy, and the angular second moment measures all provided impressive definition of the outlines of the

various fields and the transition between the different regions.

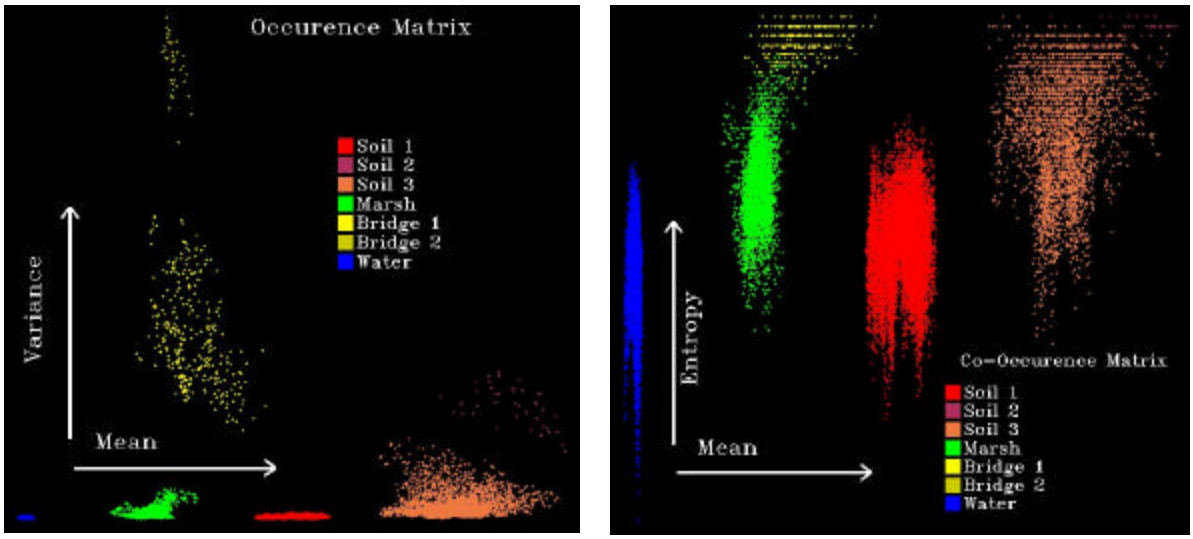

Figure 48. N-dimensional Visualizer view of the Elkhorn Slough mosaic, 5x5 textures. The left hand figure is for two elements of the occurrence matrix (mean and variance), the right hand figure shows two elements of the co-occurrence matrix (mean and entropy)

Application of SAM and ML classifiers to the mosaics illustrated some important capabilities and differences in this new approach to image analysis. SAM classification of the mosaics, as illustrated in B1, shows that water, soil and marsh could be distinguished in the 4 bands of the occurrence matrix, the 8 bands of the co-occurrence matrix, or the 12 bands of a combined texture set to varying extents. The classifier does a poor job on the marsh area in the occurrence measures, and that seems to carry over into the combined analysis, apparently reflecting the low separation in variance for that class in spectral angle.

The ML classifier does a better job of exploiting the statistics of these large training sets. Figure C1 shows the ML classifier for the Elkhorn Slough mosaic set, processed with the 5x5 texture filter. The classification is much cleaner, and does not have nearly as much clutter as the SAM output. Classes are more accurately determined. Application at larger texture patterns leads to somewhat different results, which are not understood at this point, but seem to indicate some of the expected dependence on the spatial scale of the textures in the scene.

Application of the ML classifier to a different mosaic, the 'combined' mosaic, is illustrated in Figure C4, which shows very similar results from the three approaches with a 5x5 window. The most noticeable difference is in the second panel from the top, which is a 512x512 slough chip. The occurrence classifier correctly identifies the marsh area (green) and distinguishes it from the cultivated soil nearby. The addition of the co-occurrence bands leads to false classification of some of the marsh area as soil.

It quickly became clear that the SAM classifier was not particularly useful for our purposes.

B. FULL IMAGE

After the texture-filtered images were analyzed, the Maximum Likelihood classifier was applied to the full Elkhorn Slough image. An initial training set was defined by Eric Van Dyke, an expert on the Elkhorn Slough area. Application of the ML classifier identified a number of regions that were mis-classified, mostly cultivated fields in various states of harvest. Regions-of-Interest (ROI's)

were added for those areas, ultimately resulting in a 41 element training set. The classification results for this process are illustrated in Figure 49 below.

Immediately following the processing of the post-classification analysis several results became apparent. On initial comparison to similar work covering the same geographical area (Olsen, 2002), it became clear that a more narrowly defined training set improved overall classification results. In the Olsen study, thirteen elements were utilized in the training set based initially on a land-use map for the Elkhorn Slough area. Analysis resulted in classification accuracies in the 50-55% range. For the current study, a 41 element training set was utilized and resulted in an 81% accuracy measure as obtained by the confusion matrix.

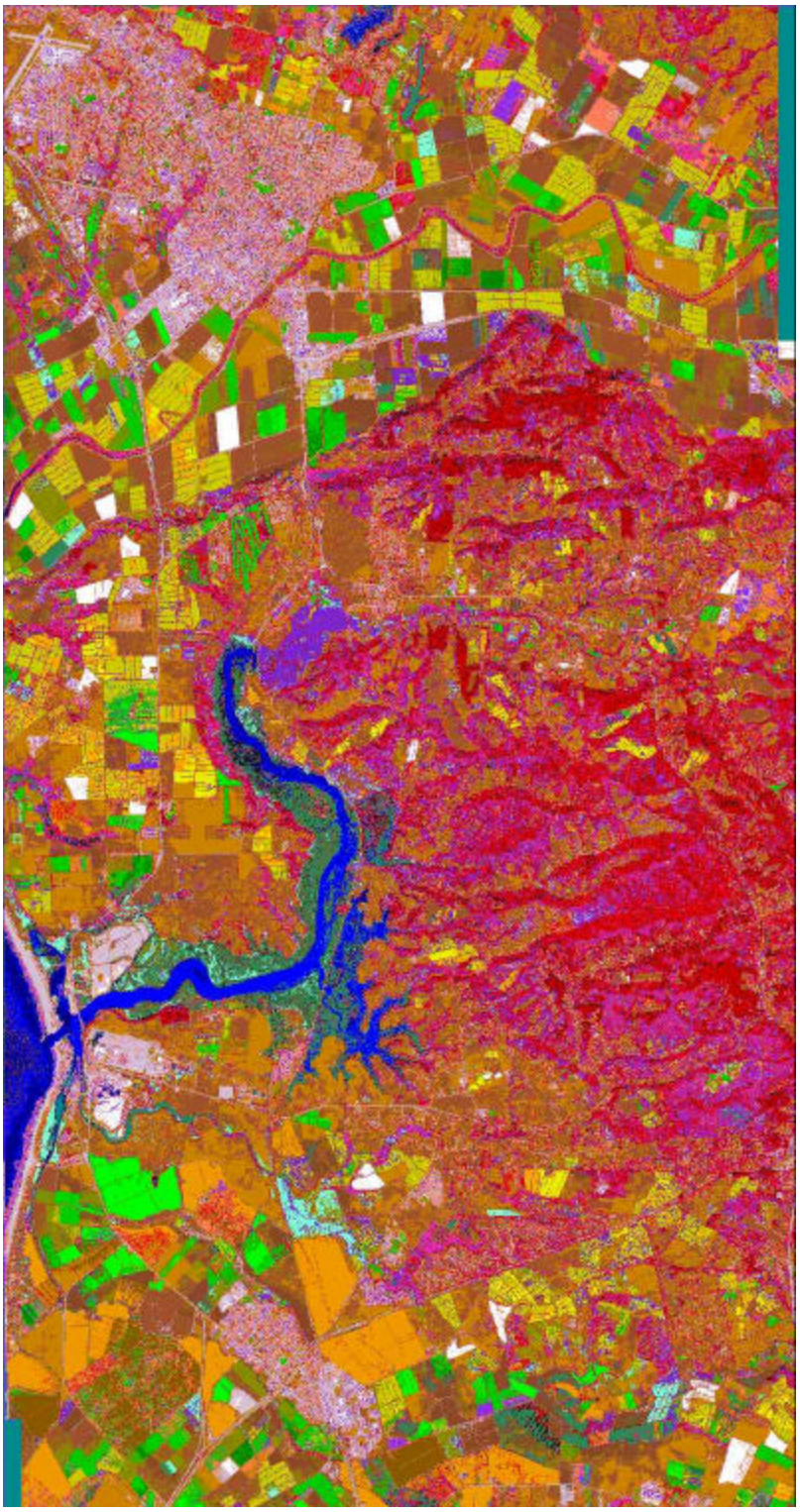

Figure 49. Full image - ML classified with 41 element ROI set (key shown in Appendix D)

The results from the classification efforts for the combined MSI and texture data were modest but improvement in overall classification accuracy was obtained, with an increase to 84%. Using only texture an accuracy of 55% could be obtained. The rates for texture only classification were impressive by themselves and could signal a higher level of effectiveness for the underutilized classification tool than previously thought.

Many intriguing issues became evident as the study progressed. Noticeable improvement in classification accuracy was noted for most of the individual classes of trees. The change in correct classification rates for these various woodland classes are shown below in Table 18 which compares the 4 band MSI classified data and the 12 band (MSI and texture combined) classified data. The class consisting of Willow trees was the only class to not show improvement with the addition of the texture measures.

Class	MSI	MSI and Texture
Oak	36 %	44 %
Eucalyptus	49 %	56 %
Conifer	57 %	76 %
Willow	83 %	80 %
Chapparal	82 %	87 %

Table 18. Change in correct classification rates for various woodland classes due to the addition of texture bands

Another result from the study showed that it is possible to achieve “spectral” separation between several general classes of woodlands, vegetation, and soils using only texture-filtered panchromatic imagery data. The degree of separation achieved depended heavily upon the texture measures being analyzed, with the occurrence-mean filter providing the greatest impact. This can be seen in Figures 50 and 51 below which show the n-D Visualizer output for two separate examples. As expected, the green band versus NIR band display (Figure 50) shows clear separation between the individual categories with some overlap between the two woodlands classes. Figure 51 highlights the effects of texture filtering, showing mean versus variance output. Class separation is also achieved with these two texture-filtered bands.

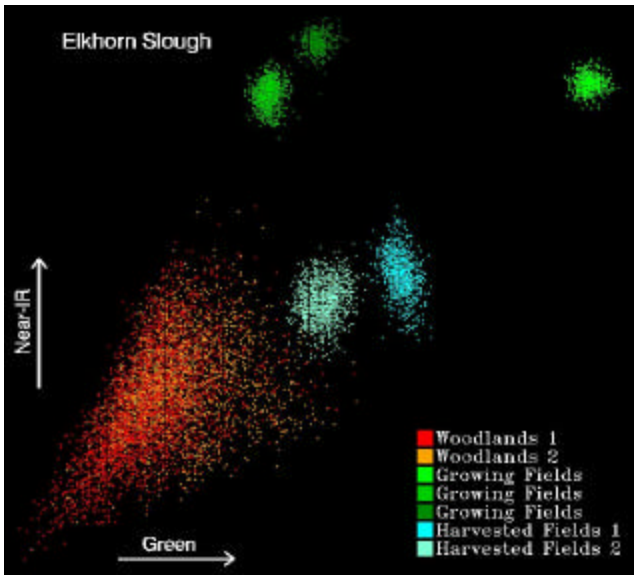

Figure 50. Class separation achieved with green and NIR bands.

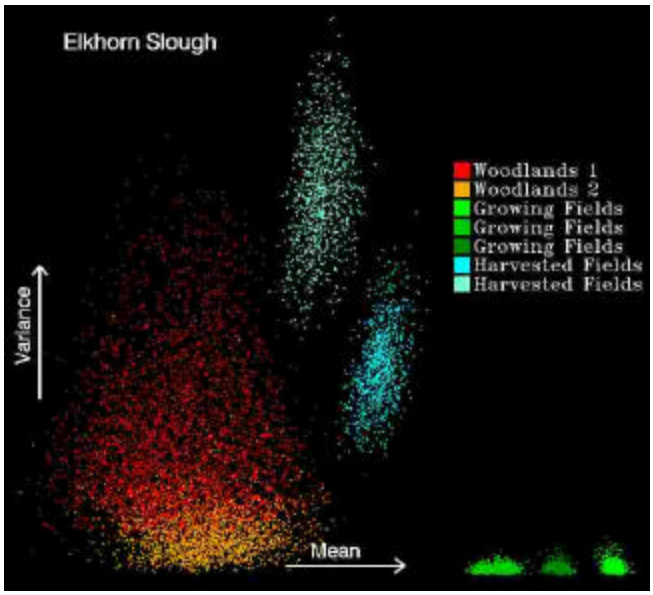

Figure 51. Class separation achieved with two texture-filtered bands.

The output of our Maximum Likelihood (ML) classification efforts also presented some unexpected results which indicated additional benefit from the texture processing. When comparing 4 band MSI (Maximum Likelihood classified) data and 12 band, MSI and texture combined (Maximum Likelihood classified) data it became apparent that several dirt roads and paths in the area immediately adjacent to the Elkhorn Slough became more noticeable. This effect can be seen in Figures 54 and 55 which highlight the dramatic effects that texture filtering had on those sub-images. Table 19 shows the color key for the following images.

Color	Object
Thistle	Urban
Blue	Water
Green	Growing Field 1
Green 2	Growing Field 2
Sienna	Soil 1
Orange 3	Soil 2
Sienna 2	Soil 3
Red	Woodlands 1
Orange 1	Woodlands 2
Aquamarine	Harvested Field 1
Cyan	Harvested Field 2

Table 19. Color coding map key for the following ML classified images

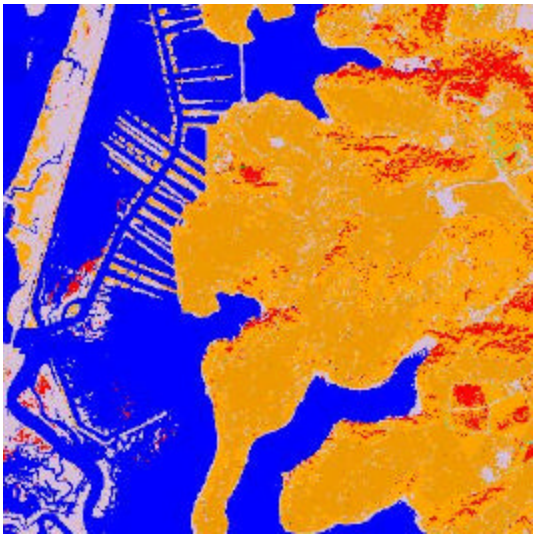

Figure 52. 4 band MSI data (ML classified) showing a portion of the Elkhorn Slough and the surrounding area.

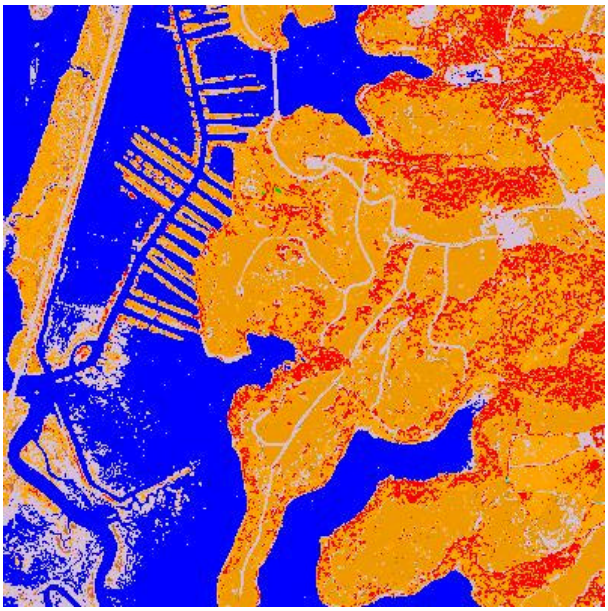

Figure 53. 12 band (MSI and texture combined – ML classified) data of the same scene

Two additional benefits were discovered within the ML classified images. A more distinctive separation of the two woodland classes was achieved and much of the urban misclassification contained within the MSI imagery data was rectified. These effects can be seen in Figures 56 and 57 below which highlight the changes in a section of the Elkhorn Slough and a small residential sub-division.

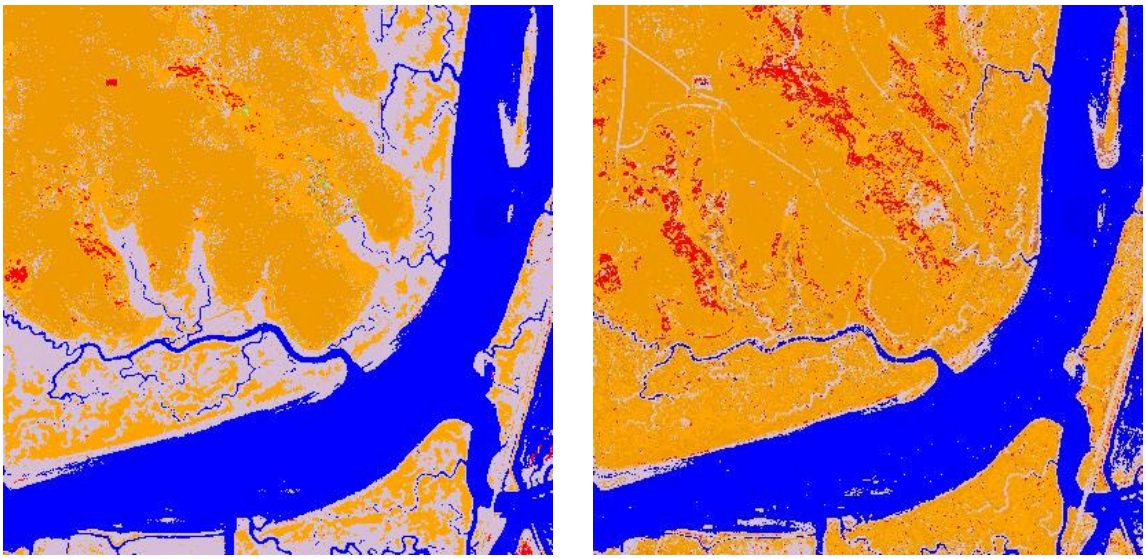

Figure 54. 4 band MSI and 12 band (MSI and texture combined) images of the Elkhorn Slough displaying greater woodland delineation and removal of urban misclassification.

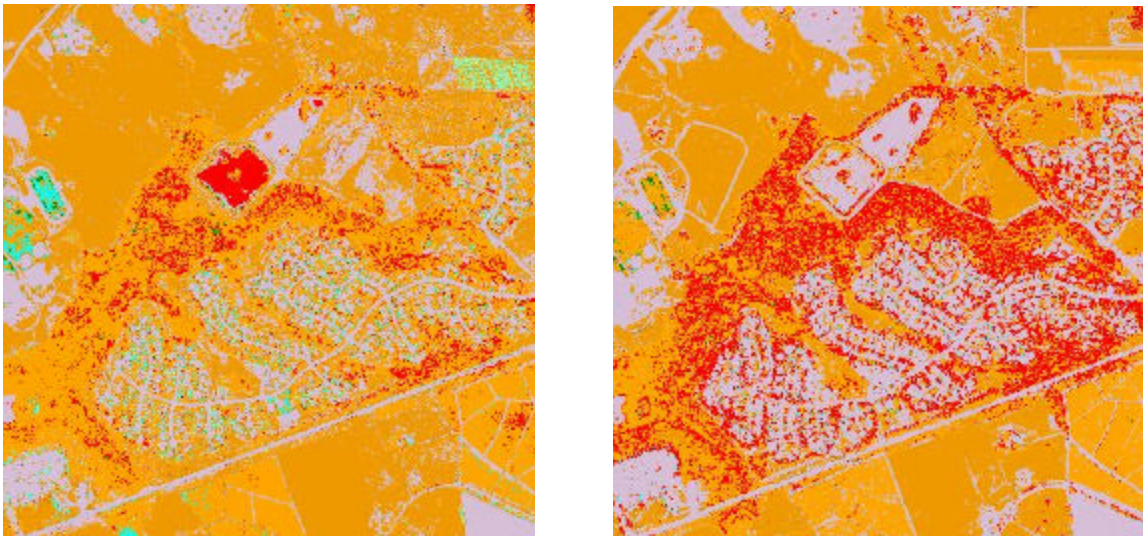

Figure 55. 4 band MSI and 12 band (MSI and texture combined) images of a small residential sub-division displaying greater woodland delineation.

Two significant areas of difficulty were encountered during the classification and analysis process. As expected, the maximum likelihood classifier encountered problems when trying to define areas of mixed spectral

classes such as the sage scrub areas of our image. Another interesting classification error that arose was the misclassification of a small group of recently harvested fields exhibiting significant textural qualities. The classifier misidentified these fields as rows of berries covered with a white plastic. The two separate regions exhibited significant spectral differences but very similar textural characteristics. This effect can be seen in Figures 58 through 61 which show the NIR composite image of on of the misidentified fields and three n-D Visualizer presentations of the misidentified class in three separate band combinations. This latter problem was resolved by adding additional ROI's for the highly textured fields.

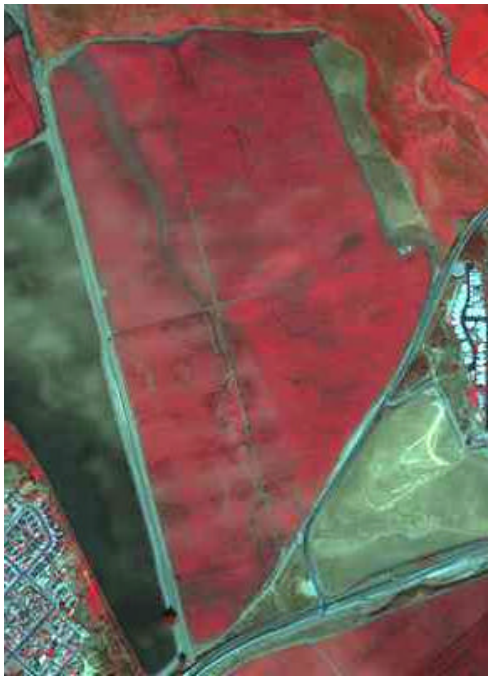

Figure 56. Example of fields misidentified as berries covered with plastic

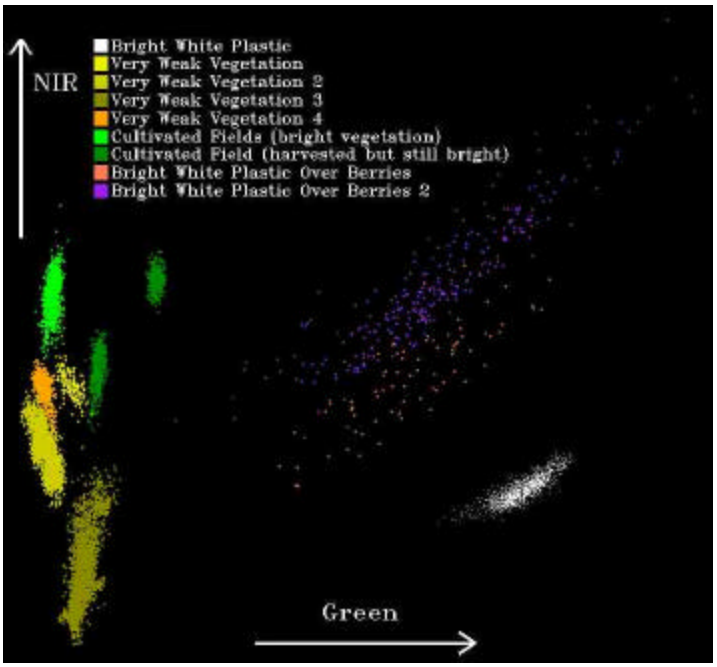

Figure 57. n-D Visualizer presentation of various plastics compared to several types of vegetation

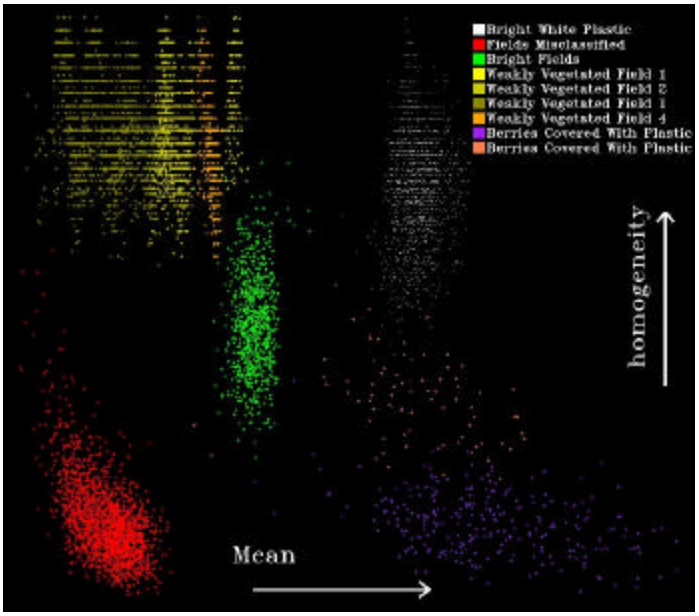

Figure 58. n-D Visualizer presentation of the misidentified class of field, various plastics, and several types of vegetation

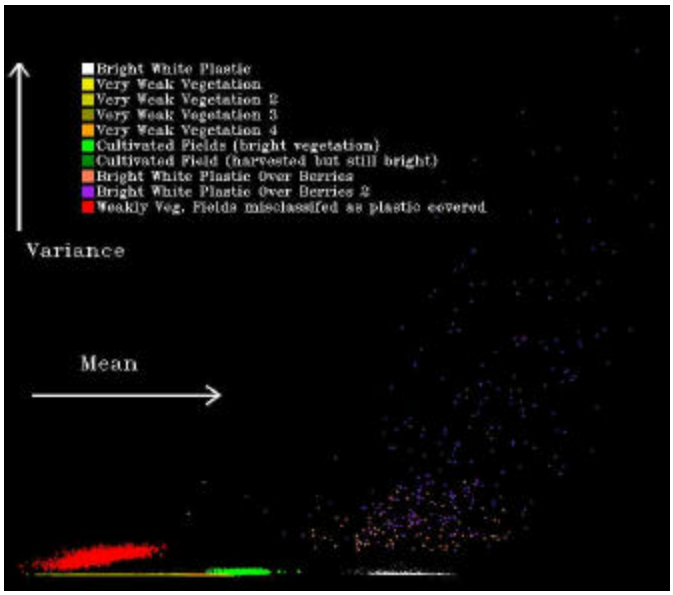

Figure 59. n-D Visualizer presentation of the misidentified class of field, various plastics, and several types of vegetation

V. SUMMARY AND CONCLUSIONS

Ikonos imagery data of a portion of the central California coastal region was utilized in the analysis of texture as an additional aid for image classification. This study focuses on two major questions concerning the impact and effectiveness of using texture for classification efforts. Does the texture-filtered panchromatic imagery data provide the same level of spectral class separation as MSI imagery data and does the addition of texture data to MSI data improve overall classification accuracy rates?

Imagery data consisting of only texture-filtered bands does provide a surprisingly effective method of achieving spectral class separation for certain general classes of vegetation. This is evident in Figures 52 and 53 which highlight the separation achieved when employing only texture-filtered imagery data. This fact indicates that there may be significant capabilities associated with using texture filters that bear further investigation and exploitation.

The addition of texture-based imagery data to multispectral imagery data does provide a modest level of improvement in overall classification accuracies. For this study, the data from eight separate texture-filtered bands were combined with four band multispectral data to evaluate the impact of the texture analysis process. Overall accuracy rates rose from 81.0% for MSI data to 83.9% for the combined MSI and texture data. The overall accuracy rate for the eight band texture data by itself was

impressive. An accuracy rate of 55.1% was obtained using only the texture-filtered data and this would indicate that the textural qualities of objects can play a significant role throughout the classification process.

The necessary computing resources are available today to begin to fully exploit the power and utility of using texture in remote sensing terrain categorization (TERCAT) efforts. Texture provides valuable input to the classification process and should not be underestimated in its impact and effectiveness.

APPENDIX A. TEXTURE FILTERED IMAGES

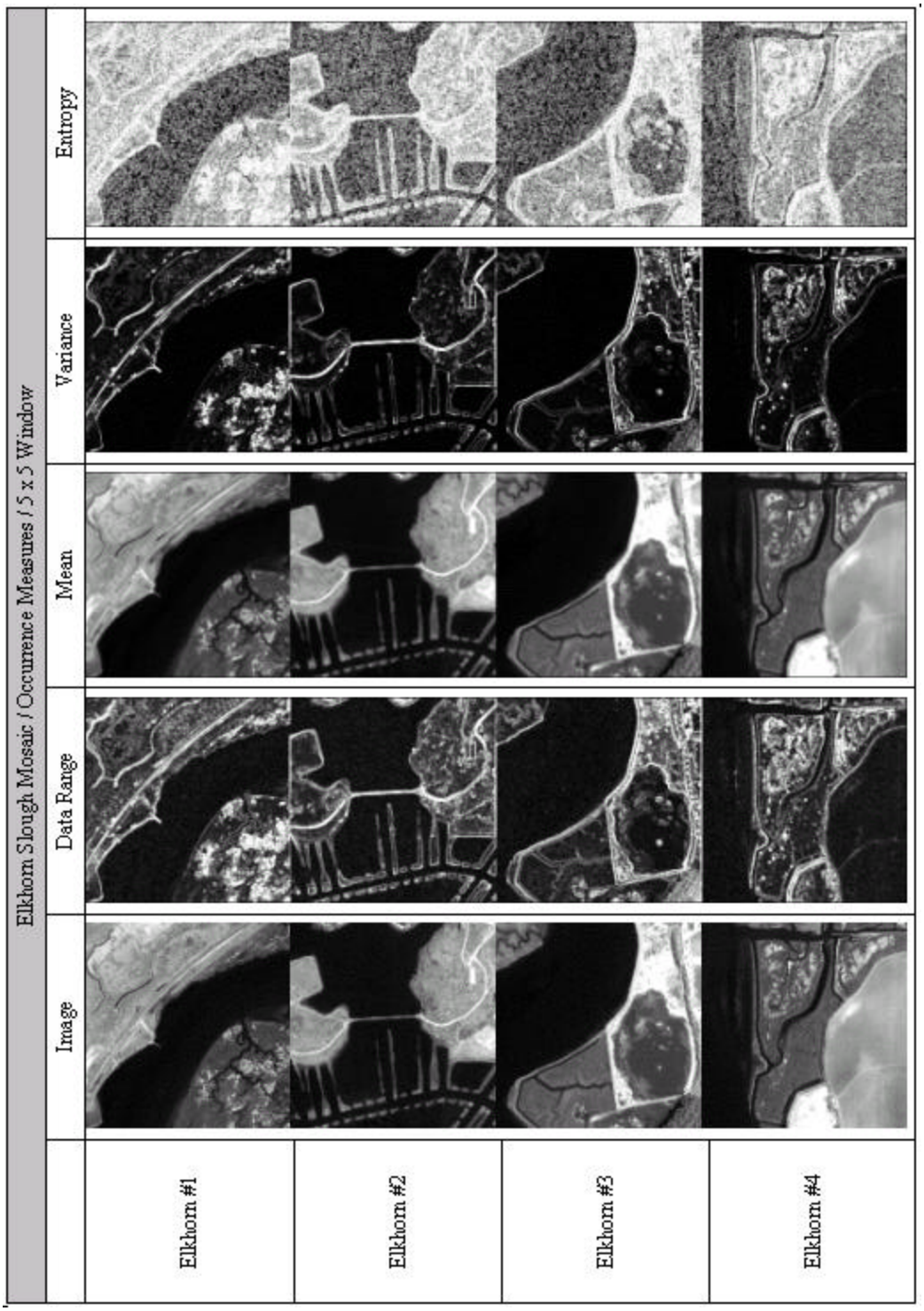

Figure A-1

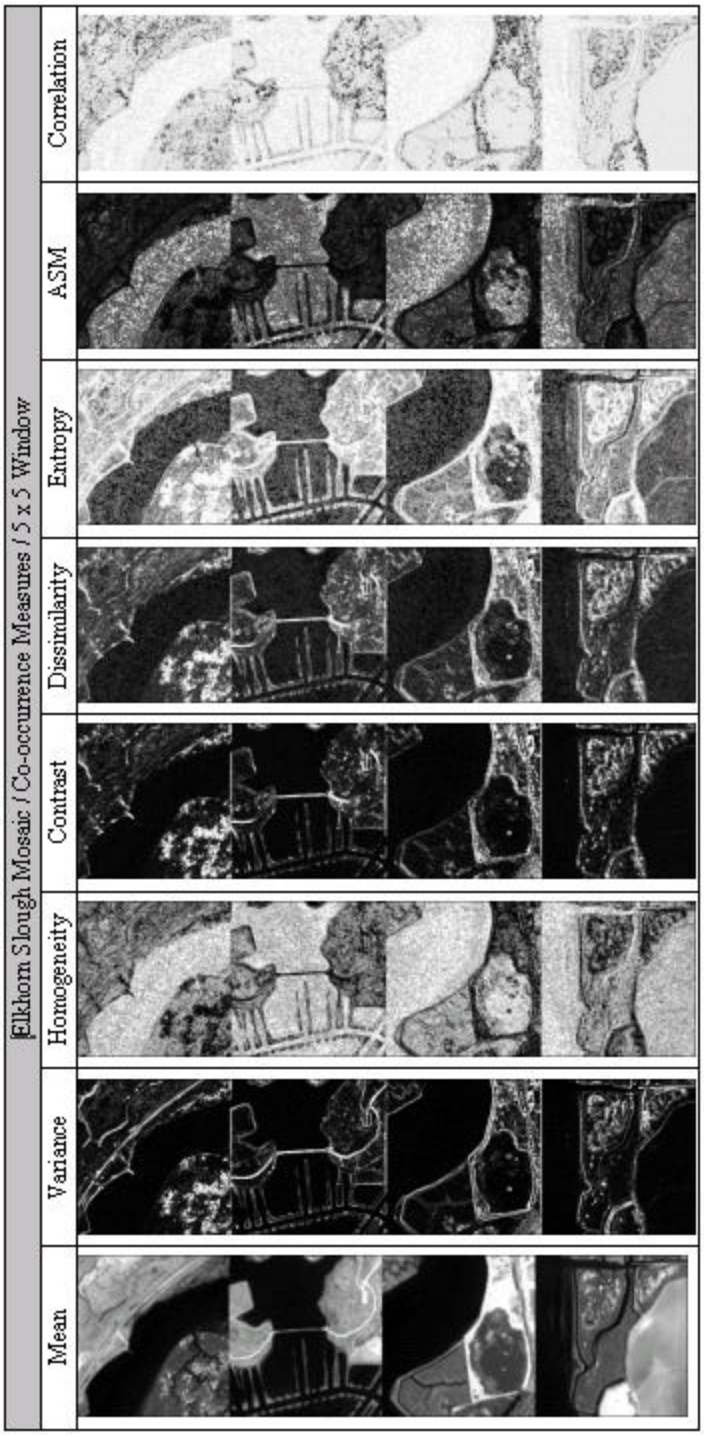
Elkhorn Slough Mosaic / Co-occurrence Measures / 5 x 5 Window
Mean
Variance
Homogeneity
Contrast
Dissimilarity
Entropy
ASM
Correlation

Figure A-2

Elkhorn Slough Mosaic / Occurrence Measures / 17 x 17 Window
Image
Data Range
Mean
Variance
Entropy
Elkhorn #1
Elkhorn #2
Elkhorn #3
Elkhorn #4

Figure A-3

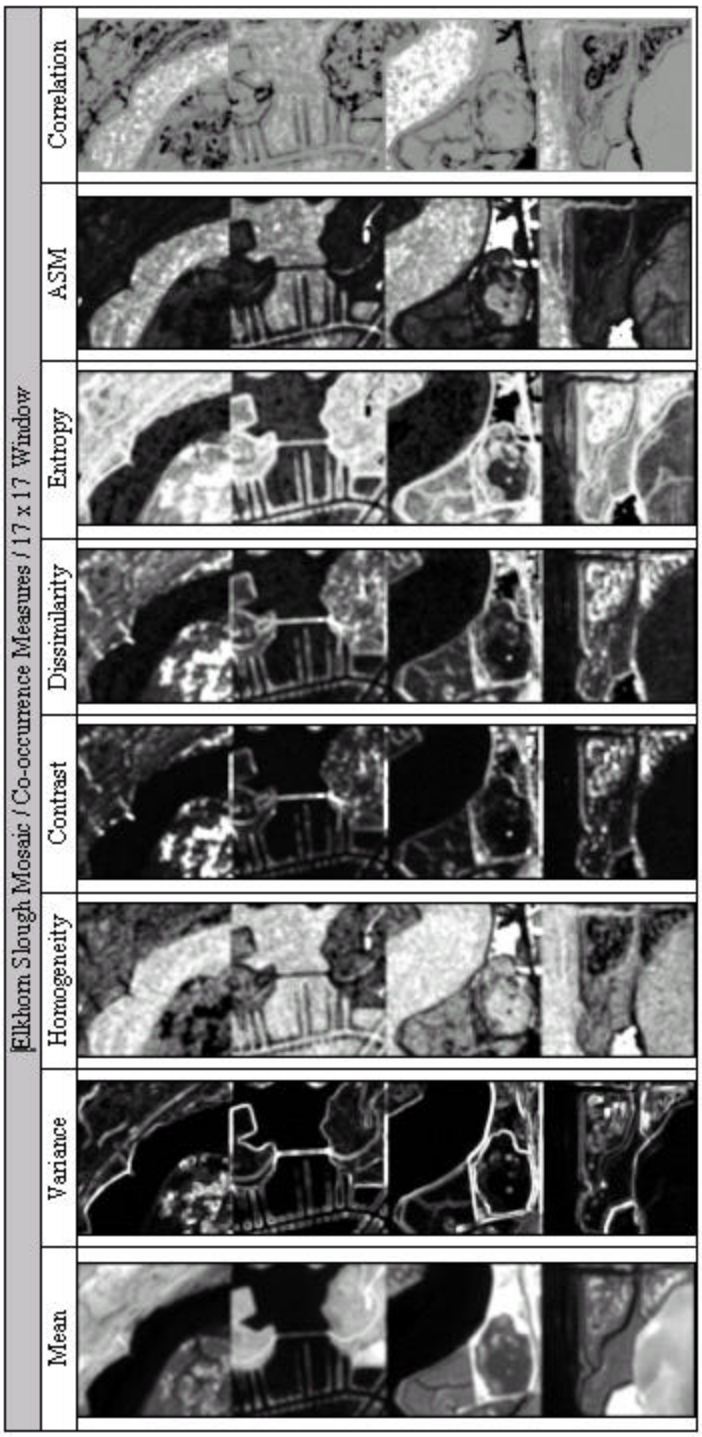
Elkhorn Slough Mosaic / Co-occurrence Measures / 17 x 17 Window
Mean
Variance
Homogeneity
Contrast
Dissimilarity
Entropy
ASM
Correlation

Figure A-4

Elkhorn Slough Mosaic / Occurrence Measures / 35 x 35 Window
Image
Data Range
Mean
Variance
Entropy
Elkhorn #1
Elkhorn #2
Elkhorn #3
Elkhorn #4

Figure A-5

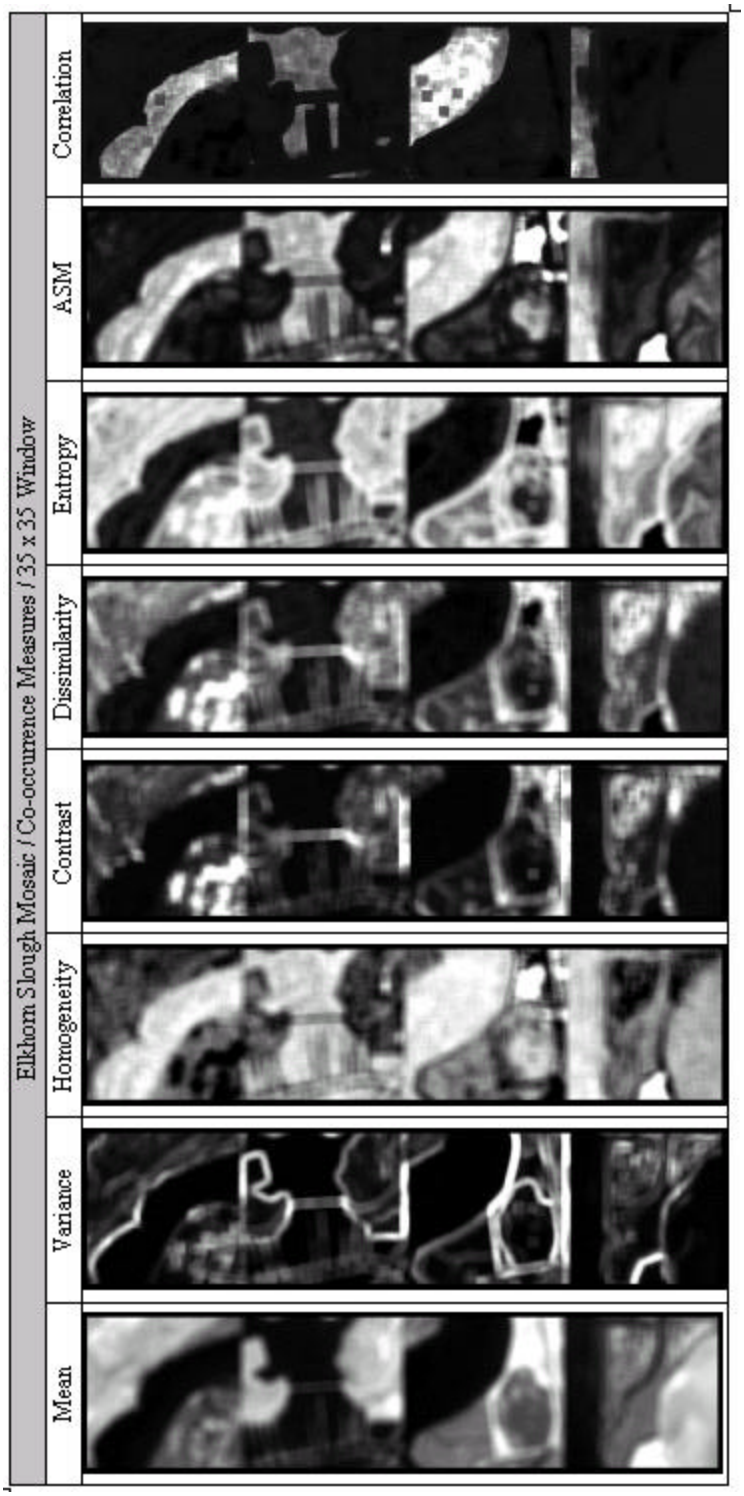
Elkhorn Slough Mosaic / Co-occurrence Measures / 35 x 35 Window
Mean
Variance
Homogeneity
Contrast
Dissimilarity
Entropy
ASM
Correlation

Figure A-6

Fields Mosaic / Occurrence Measures / 5 x 5 Window
Image
Data Range
Mean
Variance
Entropy
Fields #1
Fields #2
Fields #3
Fields #4

Figure A-7

Fields Mosaic / Co-occurrence Measures / 5 x 5 Window
Mean
Variance
Homogeneity
Contrast
Dissimilarity
Entropy
ASM
Correlation

Figure A-8

Fields Mosaic / Occurrence Measures / 17x17 Window
Image
Data Range
Mean
Variance
Entropy
Fields #1
Fields #2
Fields #3
Fields #4

Figure A-9

Fields Mosaic / Co-occurrence Measures / 17x17 Window
Mean
Variance
Homogeneity
Contrast
Dissimilarity
Entropy
ASM
Correlation

Figure A-10

Fields Mosaic / Occurrence Measures / 35x35 Window
Image
Data Range
Mean
Variance
Entropy
Fields #1
Fields #2
Fields #3
Fields #4

Figure A-11

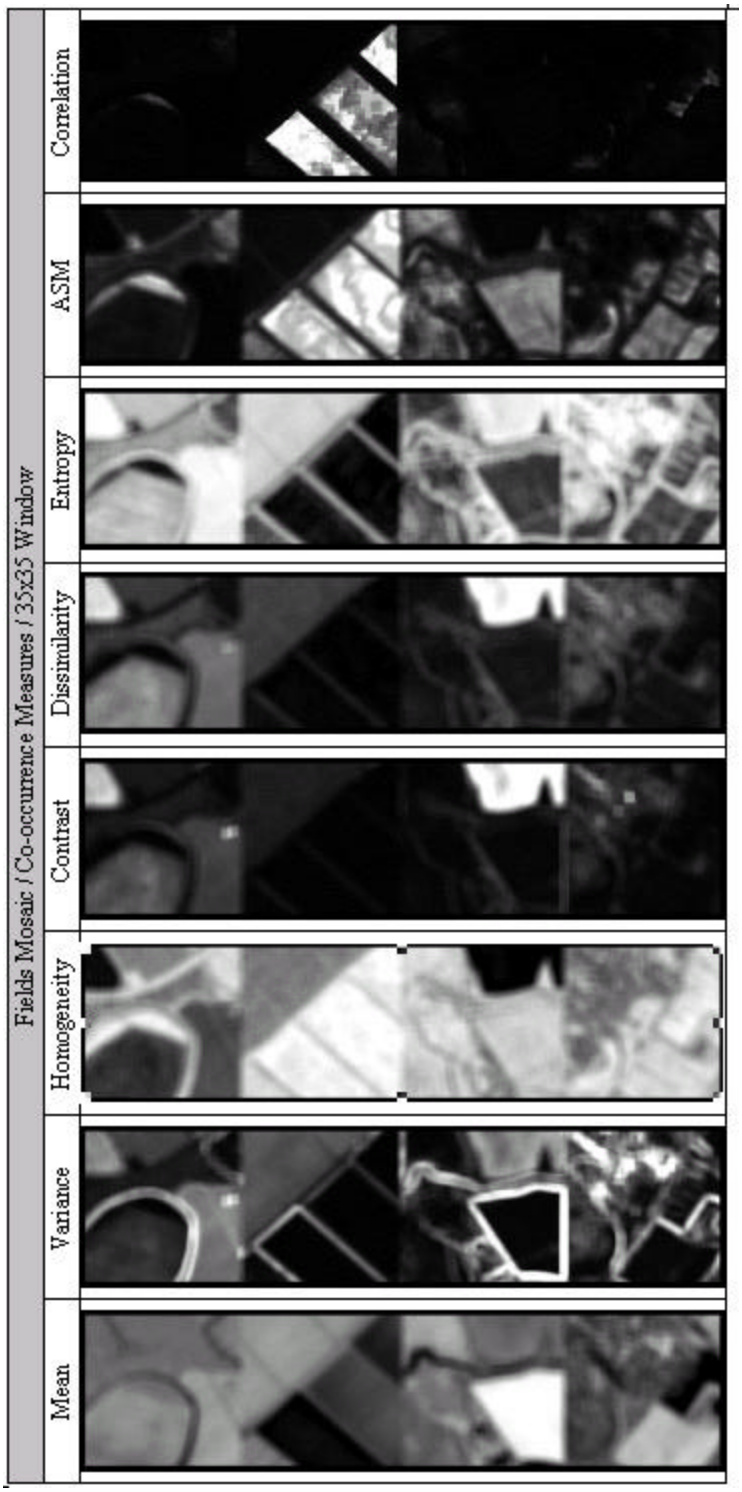
Fields Mosaic / Co-occurrence Measures / 35x35 Window
Mean
Variance
Homogeneity
Contrast
Dissimilarity
Entropy
ASM
Correlation

Figure A-12

Combined Mosaic / Occurrence Measures / 5x5 Window
Image
Data Range
Mean
Variance
Entropy
Residential
Elkhorn Slough
Woodland
Fields #1
Fields #2
Airport

Figure A-13

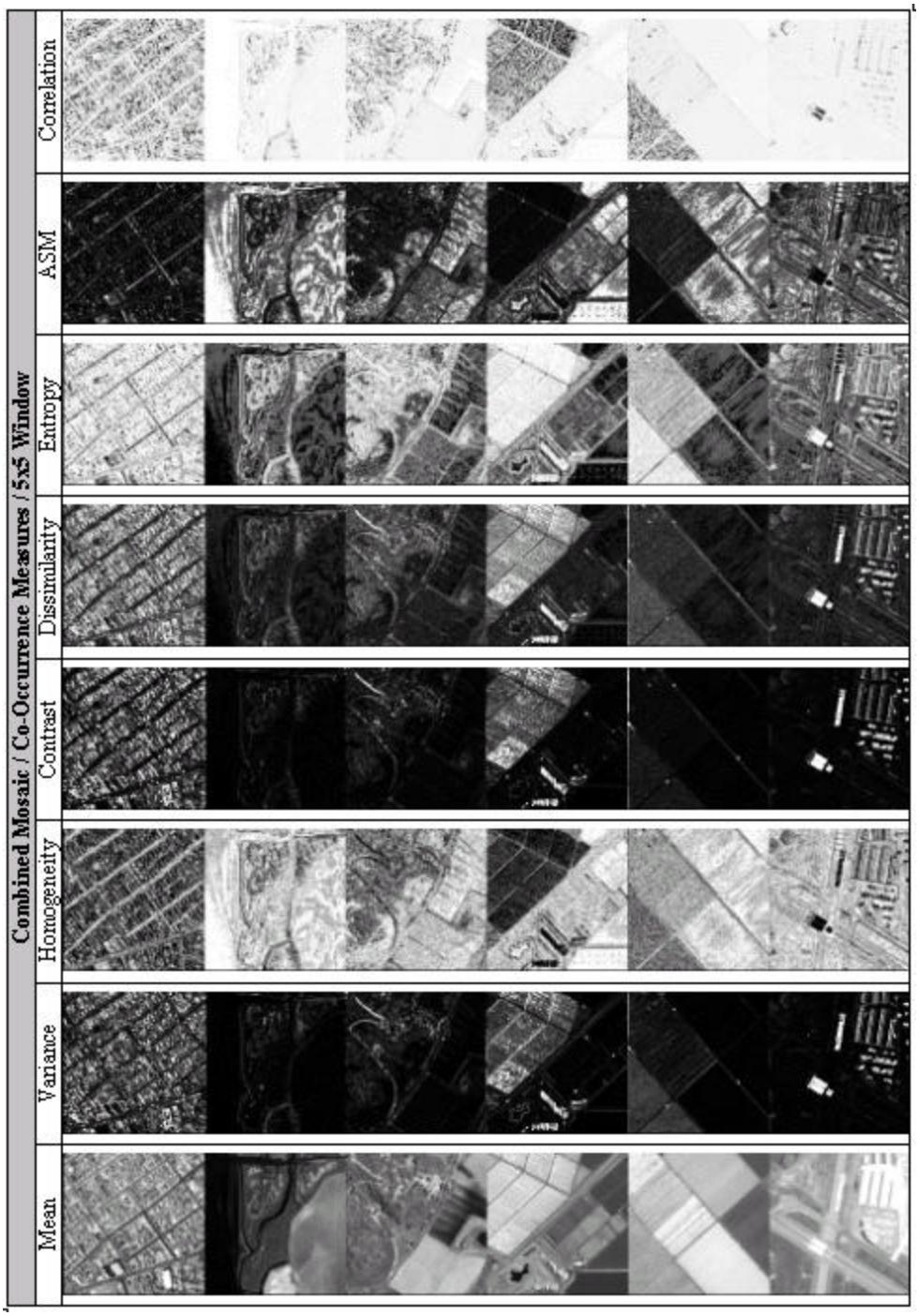
Combined Mosaic / Co-Occurrence Measures / 5x5 Window
Mean
Variance
Homogeneity
Contrast
Dissimilarity
Entropy
ASM
Correlation

Figure A-14

Combined Mosaic / Occurrence Measures / 17x17 Window
Image
Data Range
Mean
Variance
Entropy
Residential
Elkhorn Slough
Woodland
Fields #1
Fields #2
Airport

Figure A-15

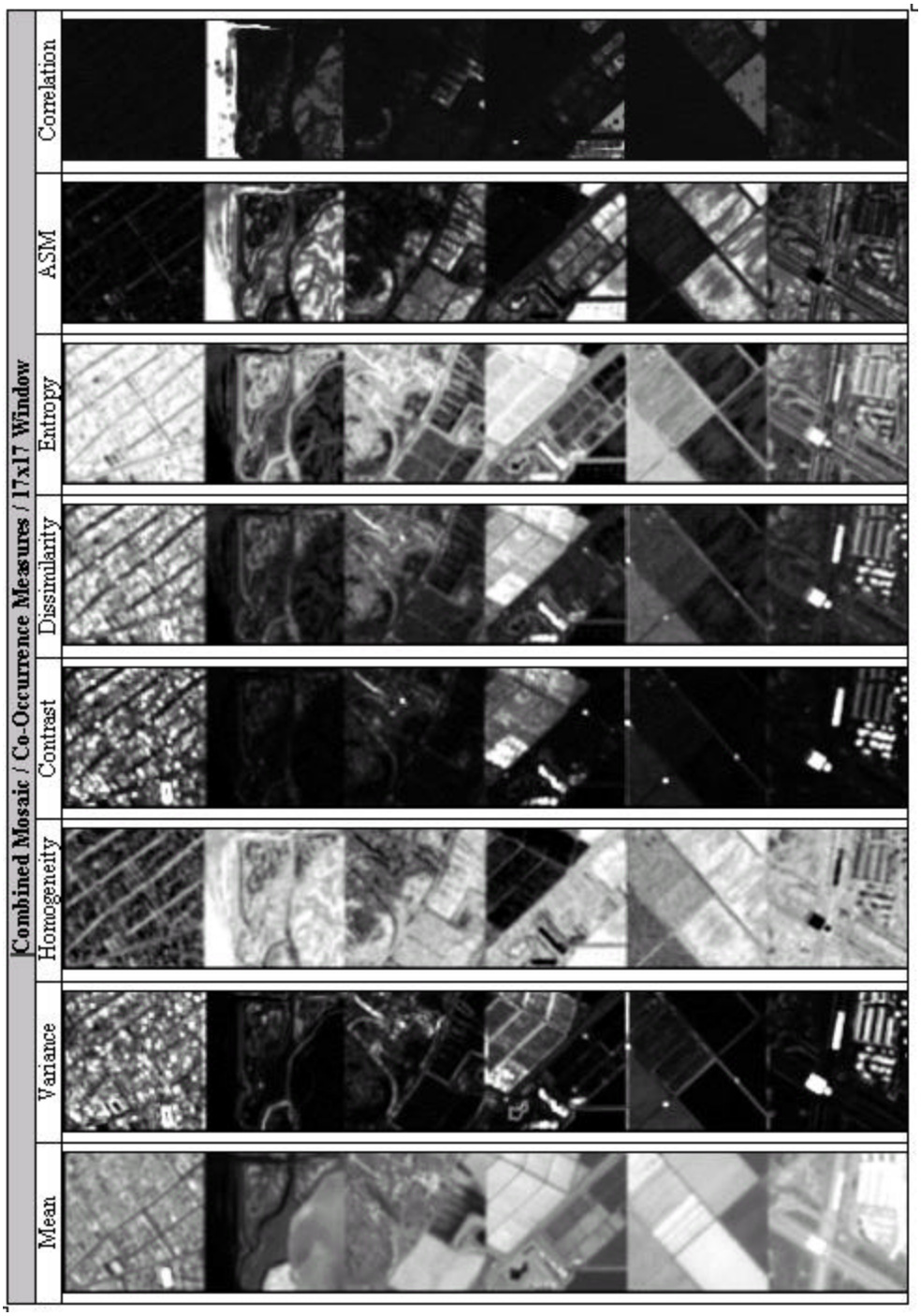
Combined Mosaic / Co-Occurrence Measures / 17x17 Window
Mean
Variance
Homogeneity
Contrast
Dissimilarity
Entropy
ASM
Correlation

Figure A-16

Combined Mosaic / Occurrence Measures / 35x35 Window
Image
Data Range
Mean
Variance
Entropy
Residential
Elkhorn Slough
Woodland
Fields #1
Fields #2
Airport

Figure A-17

Combined Mosaic / Co-Occurrence Measures / 35x35 Window
Mean
Variance
Homogeneity
Contrast
Dissimilarity
Entropy
ASM
Correlation

Figure A-18

APPENDIX B. SAM CLASSIFIED IMAGES

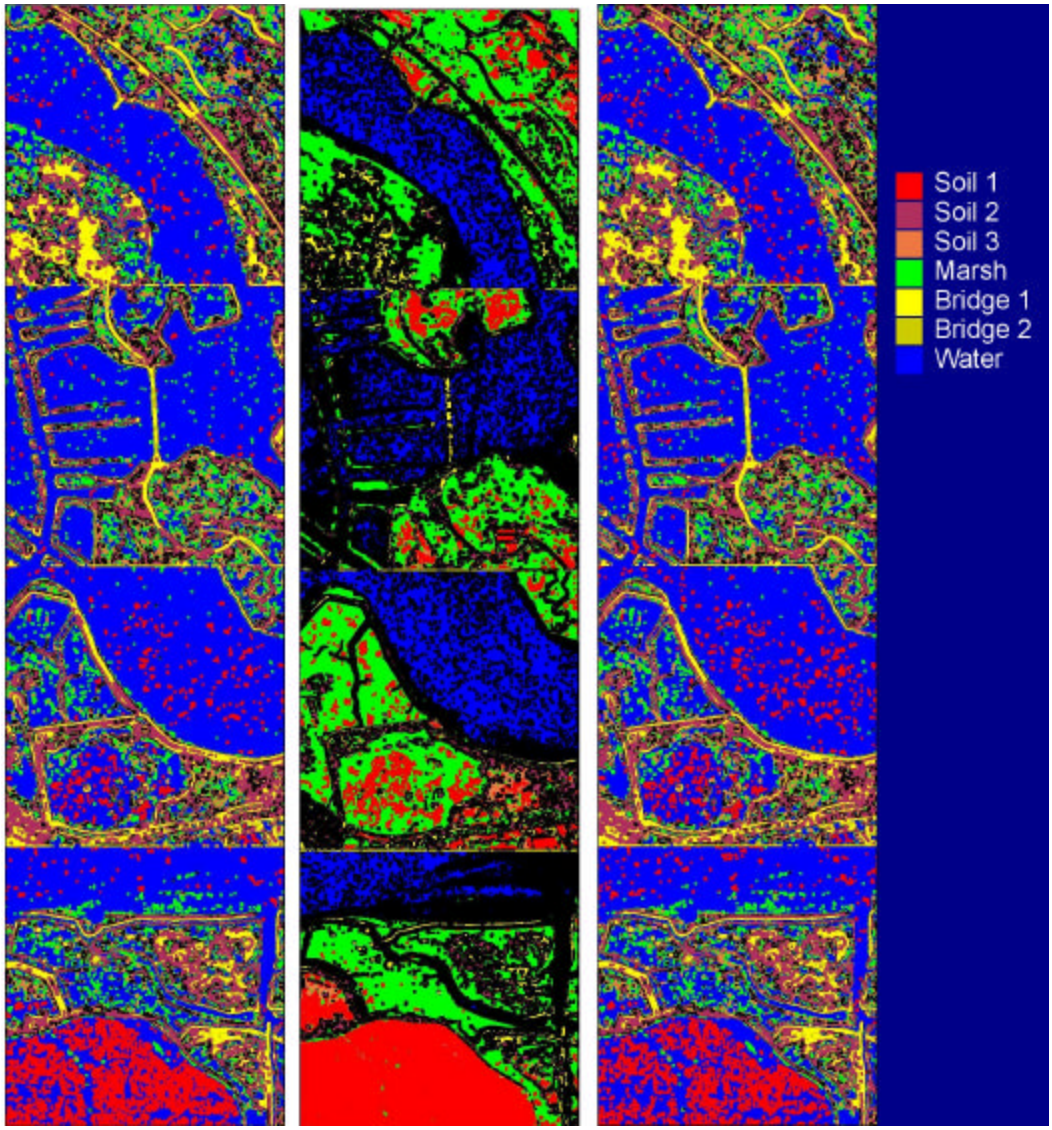

Figure B1. Elkhorn Slough mosaic – SAM classified - 5x5 Window Occurrence (Data Range, Mean, Variance, Entropy)/ Co-occurrence (Mean, Variance, Homogeneity, Contrast, Dissimilarity, Entropy, Second Moment, Correlation) / Combined (Mean, Variance, Homogeneity, Contrast, Dissimilarity, Entropy, Second Moment, Correlation). Spectral angle criteria: 0.15 radians, post classification 'clump' 5x5.

THIS PAGE INTENTIONALLY LEFT BLANK

APPENDIX C. ML CLASSIFIED IMAGES

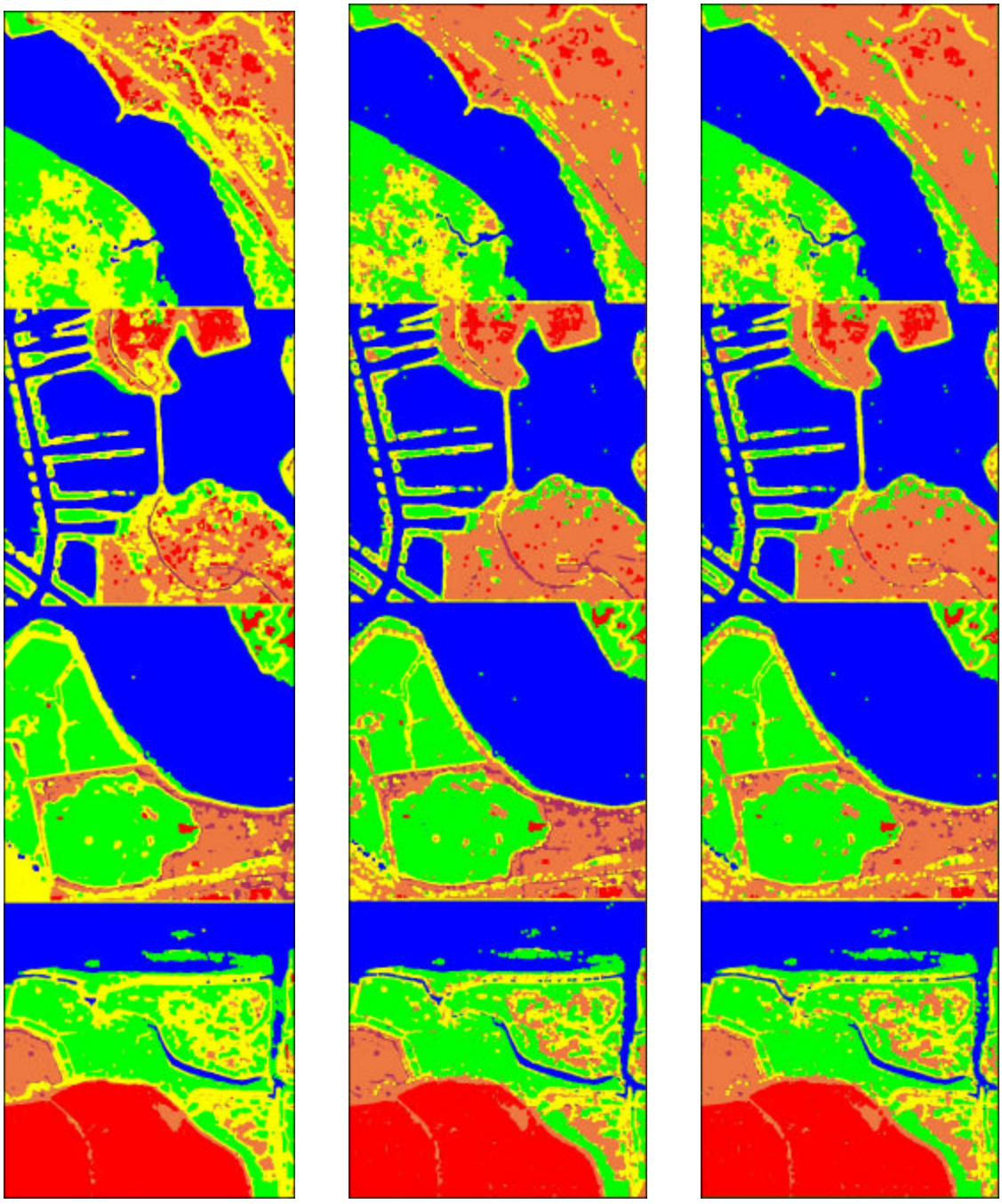

Figure C1. Elkhorn Slough mosaic – ML classified – 5x5 Window Occurrence (4 bands) / Co-occurrence (8 bands) / Combined (12 bands). Red, maroon, and sienna are soil, blue is water, green is marsh, and yellow is the bridge.

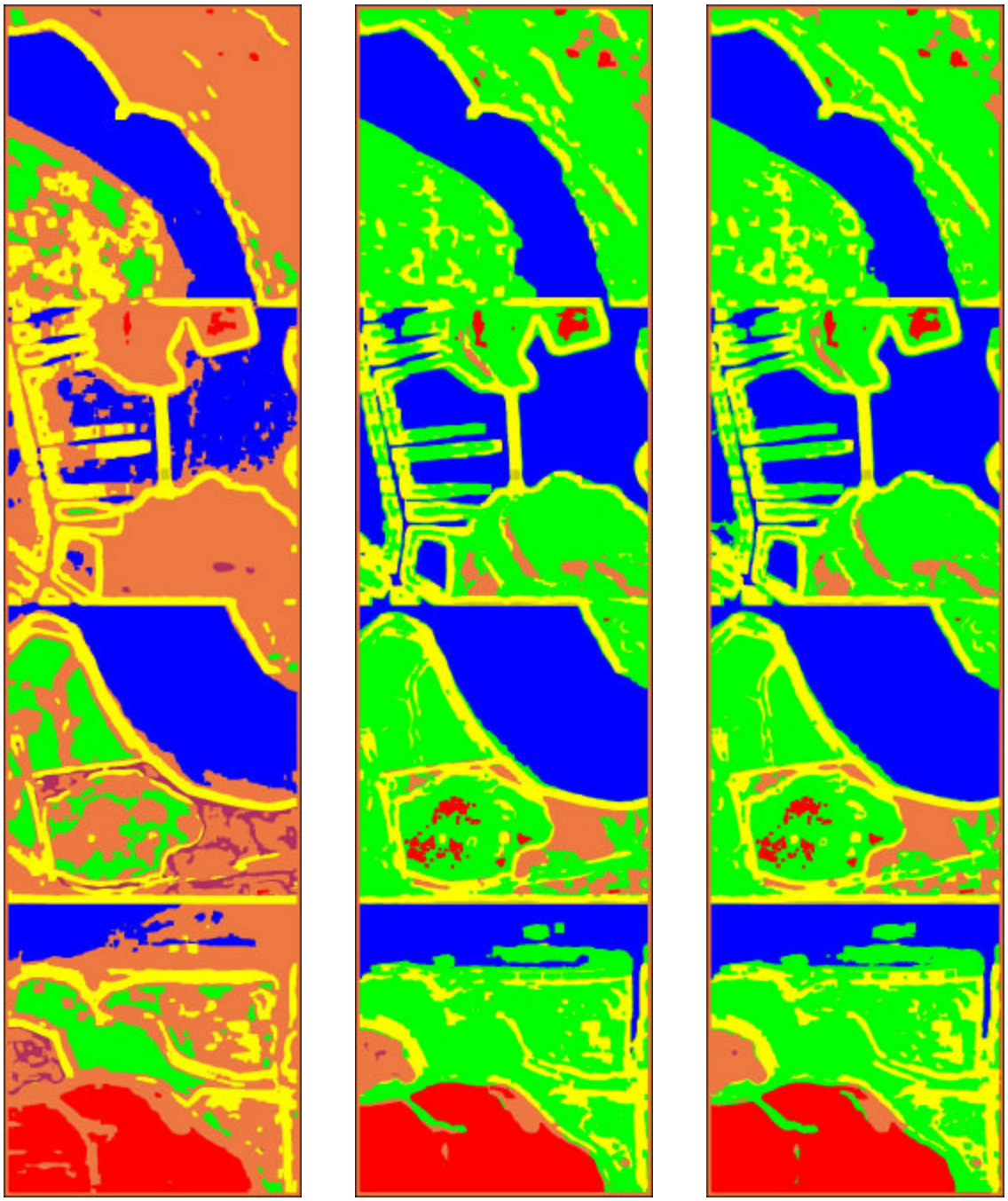

Figure C2. Elkhorn Slough mosaic – ML classified – 17x17 Window Occurrence / Co-occurrence / Combined

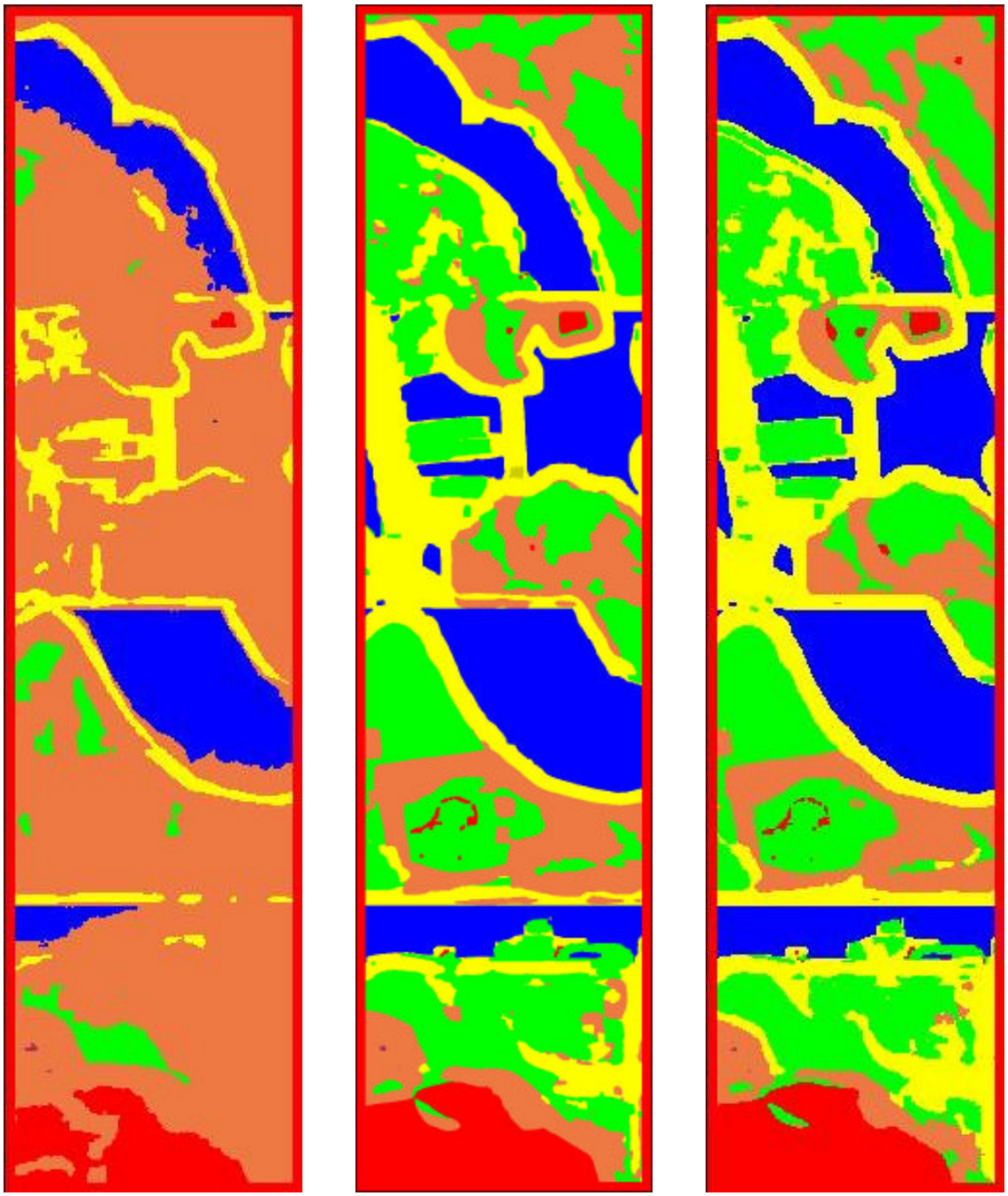

Figure C3. Elkhorn Slough mosaic – ML classified – 35x35 Window Occurrence / Co-occurrence / Combined

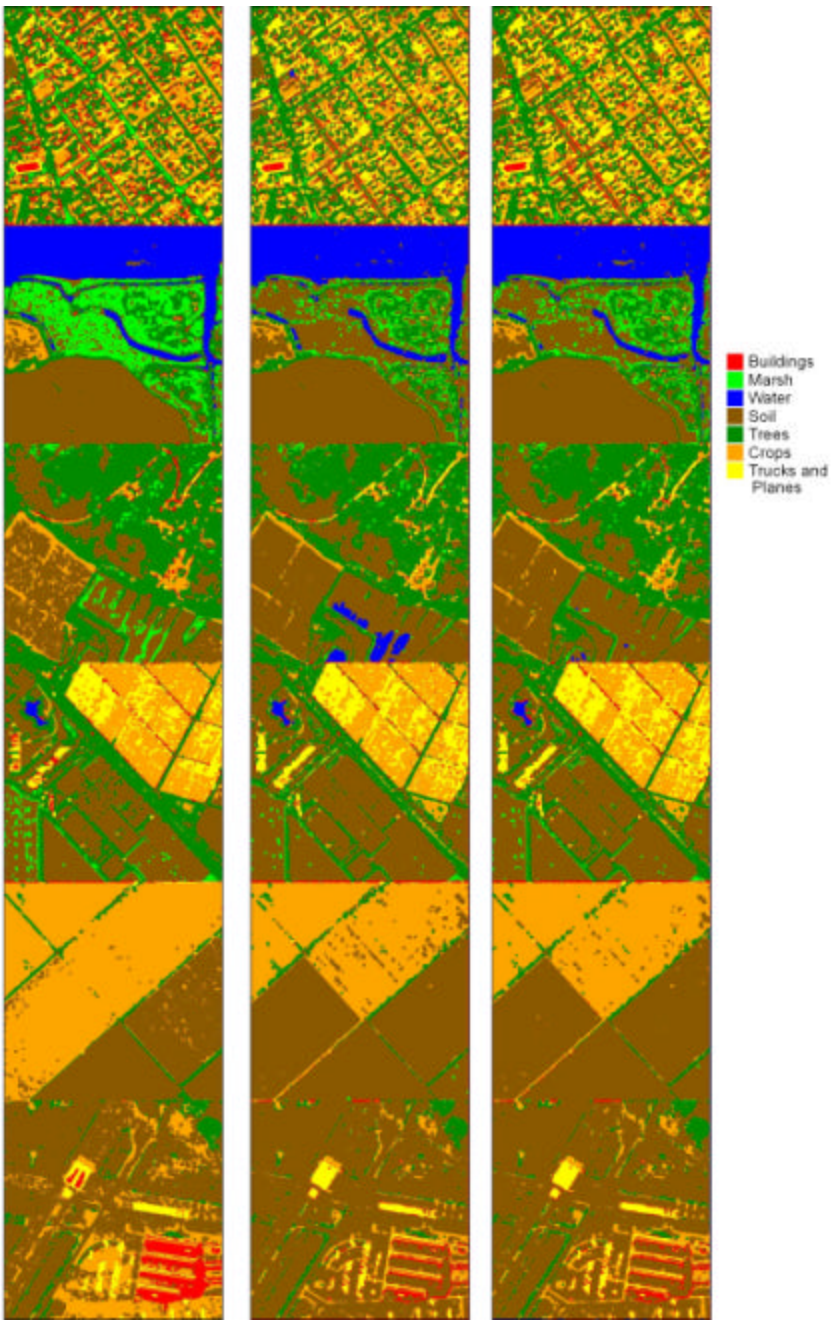

Figure C4. Combined mosaic – ML classified - 5x5 Window Occurrence / Co-occurrence / Combined

APPENDIX D. CLASSIF ICATION RESULTS

color	material
sienna	grassland
sienna 2	fallow
sienna 3	dark soil
red 1	oak
red 2	eucalyptus
red 3	conifer
red	riparian
red 4	sage scrub
maroon	chapparal
black	shadows of trees
sea green	salt marsh
aquamarine	salt marsh, fw
green cstom	salt marsh -porter
green	cult field 3 *****
green	cult field 4 ***
green	cult field 2
green	cult field
green c1	turf
green c2	cult field 2(harvested but still red 2) 421 - was green 2
yellow	vw weak veg 4 - was orange
yellow 1	harvested field - 3761 - was orange 4
yellow 2	very weak veg 1 - was yellow 1
yellow 3	cult field 3 (harvested) 668- was green 3
yellow 4	vw veg 2 - was yellow 2
yellow 5	harvested field - misc 2052 - was orange 2 - first of the misclass
yellow 6	vw veg 3 - was yellow 3
yellow 7	harvested field misc 4 - 866 - was orange 3
thistle	urban roads
thistle 2	urban roads 2
white	white tank
grey	salt flats
grey	cright white plastic
coral	bw plastic over berries
coral 2	bwp over berries
cyan	elk slough water
blue	slough water 1
blue b	slough water 2
blue c	dark water 1
blue d	dark water 2
blue e	water - edge of surf
cyan 3	river water near coast

Figure D2. Map key for full Elkhorn Slough ML image

12 band (MSI and texture combined) classification results:

Overall Accuracy = (98937/117893) 83.9210%

Kappa Coefficient = 0.8260

Class	Commission (Percent)	Omission (Percent)
Grassland (dr	3.73	27.36
Turf (golf co	3.45	7.49
Oak	25.45	56.49
Eucalyptus	21.99	43.63
Conifer	86.82	23.67
Riparian (Wil	21.09	20.55
Sage Scrub	46.66	50.15
Chapparal	30.57	13.23
Fallow	61.99	20.61
Salt Marsh	50.92	31.90
Salt Marsh- f	34.82	0.34
Salt Marsh -	53.62	11.85
Cultivated Fi	1.47	1.72
Cultivated Fi	8.31	1.89
Cultivated Fi	0.11	0.55
Cultivated Fi	1.78	0.30
Urban Roads 1	0.00	0.99
Urban Roads 2	26.70	0.00
White Tank	0.00	0.00
Salt Flats	0.00	0.00
Bright White	0.00	0.14
Bright White	38.98	2.70
Bright White	2.59	0.00
Very Weak Veg	2.92	0.60
Very Weak Veg	1.48	0.77
Very Weak Veg	3.55	0.00
Very Weak Veg	1.47	2.58
Harveted fiel	0.49	0.15
Cultivated Fi	0.00	0.00
Cultivated Fi	0.00	0.60
Shadows of tr	5.63	1.29
Dark soil	3.65	0.39
Harveted fiel	0.46	0.69
Harveted fiel	0.29	0.24
Elk Slough Wa	0.00	0.00

Slough Water	0.04	0.36
Slough Water	0.00	0.27
Dark Water 1	4.66	2.79
Dark Water 2	8.99	14.85
Water - right	1.76	0.00
River water n	0.00	0.00

4 band (MSI only) classification results:

Overall Accuracy = (95506/117893) 81.0107%
Kappa Coefficient = 0.7942

Class	Commission (Percent)	Omission (Percent)
Grassland (dr	5.68	19.04
Turf (golf co	15.97	19.34
Oak	23.87	64.35
Eucalyptus	35.69	51.29
Conifer	86.91	42.63
Riparian (Wil	40.12	16.72
Sage Scrub	43.96	24.91
Chapparal	56.76	18.49
Fallow	55.86	31.67
Salt Marsh	49.47	11.06
Salt Marsh- f	14.28	2.82
Salt Marsh -	34.07	13.49
Cultivated Fi	8.18	3.68
Cultivated Fi	6.92	2.16
Cultivated Fi	0.00	0.33
Cultivated Fi	1.19	0.00
Urban Roads 1	0.00	0.00
Urban Roads 2	10.42	0.00
White Tank	0.90	0.00
Salt Flats	0.00	0.00
Bright White	0.00	0.14
Bright White	21.74	2.70
Bright White	1.92	3.04
Very Weak Veg	2.34	0.00
Very Weak Veg	1.15	0.77
Very Weak Veg	4.02	0.12
Very Weak Veg	1.30	2.26
Harveted fiel	12.91	10.58

Cultivated Fi	0.00	0.00
Cultivated Fi	0.15	0.00
Shadows of tr	9.73	3.77
Dark soil	1.20	5.59
Harveted fiel	5.38	0.58
Harveted fiel	3.88	8.43
Elk Slough Wa	2.02	0.00
Slough Water	4.53	3.05
Slough Water	1.62	0.00
Dark Water 1	9.95	21.72
Dark Water 2	49.41	30.03
Water - right	0.00	0.00
River water n	0.62	0.00

8 band (texture only) classification results:Overall Accuracy = (64993/117893) 55.1288%
Kappa Coefficient = 0.5299

Class	Commission (Percent)	Omission (Percent)
Grassland (dr	25.69	99.31
Turf (golf co	25.41	84.15
Oak	44.41	78.40
Eucalyptus	35.03	72.76
Conifer	92.13	43.10
Riparian (Wil	41.87	57.82
Sage Scrub	85.84	78.32
Chapparal	90.08	99.33
Fallow	74.00	95.58
Salt Marsh	80.75	64.64
Salt Marsh- f	92.99	1.10
Salt Marsh -	93.98	93.06
Cultivated Fi	4.63	6.62
Cultivated Fi	18.43	2.16
Cultivated Fi	22.99	9.15
Cultivated Fi	35.12	41.57
Urban Roads 1	56.00	84.75
Urban Roads 2	95.10	62.02
White Tank	83.27	3.64
Salt Flats	0.00	0.53
Bright White	2.10	74.08

Bright White	37.93	2.70
Bright White	2.23	0.00
Very Weak Veg	76.37	4.19
Very Weak Veg	25.96	2.01
Very Weak Veg	87.77	43.65
Very Weak Veg	33.82	4.35
Harveted fiel	1.83	0.83
Cultivated Fi	3.23	0.48
Cultivated Fi	37.15	72.90
Shadows of tr	7.84	7.63
Dark soil	8.13	1.29
Harveted fiel	6.55	1.15
Harveted fiel	1.01	1.38
Elk Slough Wa	4.95	1.03
Slough Water	2.41	14.22
Slough Water	29.97	5.86
Dark Water 1	5.26	3.00
Dark Water 2	7.23	18.92
Water - right	66.83	34.59
River water n	14.89	0.00

LIST OF REFERENCES

Anys, H., Bannari, A., He, D.C., and Morin, D. "Texture Analysis for the Mapping of Urban Areas Using Airborne MEIS-II Images." Paper presented at the Airborne Remote Sensing Conference and Exhibition. Strasbourg, France, 11-15 September 1994.

Avery, Thomas E., and Berlin, Graydon L. Fundamentals of Remote Sensing and Airphoto Interpretation, Fifth Edition. Macmillan Publishing Company, 1992.

Bhattacharya, A.K., Srivastava, P.K., and Bhagat, A. "A Modified Texture Filtering Technique for Satellite Images." Paper presented at the 22nd Asian Conference on Remote Sensing, Singapore, 5-9 November 2001.

Campbell, James B. Introduction to Remote Sensing, Second Edition. The Guilford Press, 1996.

Gagnon, L., Bugnet P., and Cavayas, F. "Texture-based Segmentation of Temperate-zone Woodland in Panchromatic IKONOS Imagery." Paper presented at SPIE's 17th Annual International Symposium on Aerospace/Defense Sensing, Simulation, and Contols. Orlando, FL. April 2003.

Garner, Jamada Jerael. *Scene Classification Using High Spatial Resolution Multispectral Data*. Master's Thesis. Naval Postgraduate School, Monterey, CA. June 2002.

Haralick, Robert M., Shanmugam, K., and Dinstein, Its'hak. "Textural Features for Image Classification." *IEEE Transactions on Systems, Man, and Cybernetics*. Volume SMC-3, Number 6, pp 610-621, November 1973.

Hsu, Shin-Yi. "Texture-Tone Analysis for Automated Land-Use Mapping." *Photogrammetric Engineering and Remote Sensing*. Volume 44, Number 11, pp 1393-1404, November 1978.

Jensen, John R. Introductory Digital Image Processing: A Remote Sensing Perspective, Second Edition. Prentice Hall, 1996.

Jensen, John R. "Spectral and Textural Features to Classify Elusive land Cover at the Urban Fringe." *The Professional Geographer*. Volume 31, Number 4, pp 400-409, November 1979.

Kruse, F.A., Taranik, Dan L., "The Spectral Image Processing (SIPS)-Interactive Visualization and Analysis of Imaging Spectrometer Data." *Remote Sensing of Environment*. Volume 44, pp 145-163, 1993.

Lillesand, Thomas M., and Keifer, Ralph W. Remote Sensing and Image Interpretation, Third Edition. John Wiley and Sons, Inc. 1994.

Marceau, Danielle J., Howarth, Philip J., Dubois, J.M., and Gratton, Denis J. "Evaluation of the Grey-Level Co-Occurrence Matrix Method for Land-Cover Classification Using SPOT Imagery." *IEEE Transactions on Geoscience and Remote Sensing*. Volume 28, Number 4, pp 513-519, July 1990.

Multispectral User's Guide. Department of Defense, August 1995.

Olsen, R.C. Remote Sensing from Air and Space. March 2002.

Olsen, R.C., Garner, Jamada, and Van Dyke, Eric. “Terrain Classification in Urban Wetlands with High-Resolution Multi-spectral Imagery.” *Proceedings of SPIE: Sensors, Systems, and Next-Generation Satellites VI.* Volume 4881, pp 686-691, September 2002.

Perry, David Robert. *Target Detection and Scene Classification with VNIR/SWIR Spectral Imagery*. Masters Thesis. Naval Postgraduate School, Monterey, CA. September 2000.

Research Systems Incorporated. ENVI User’s Guide. September 2001 Edition, pp 599-603, Research Systems, Inc. September 2001.

Richards, John A., and Xiuping, Jia. Remote Sensing Digital Image Analysis, Third Edition. Springer, 1999.

Russ, John C. The Image Processing Handbook, Second Edition. CRC Press, Inc. 1995.

Silberstein, Mark, and Campbell, Eileen. Elkhorn Slough. Monterey Bay Aquarium Foundation, 1989.

Wikantika, K., Tateishi, R., and Harto, A.B. “Spectral and Textural Information of Multisensor Data for Land Use Classification in Metropolitan Area.” IEEE 2000

THIS PAGE INTENTIONALLY LEFT BLANK

INITIAL DISTRIBUTION LIST

1. Defense Technical Information Center
   Ft. Belvoir, VA

2. Dudley Knox Library
   Naval Postgraduate School
   Monterey, CA

3. Dr. Richard C. Olsen, Code PH
   Naval postgraduate School
   Monterey, CA

4. Dr. Alan A. Ross, Code SP
   Naval postgraduate School
   Monterey, CA

5. Dr. William B Maier II, Code PH
   Naval postgraduate School
   Monterey, CA

6. Eric Van Dyke
   Elkhorn Slough Foundation
   Watsonville, CA

7. Dr. Donald Potts
   University of California, Santa Cruz
   Santa Cruz, CA

8. Brigette A. Martini
   HyVista Corporation
   Baulkham Hills NSW, Australia

9. Matthew D. Humphrey
   NAVAIR-Air 4.5
   Lexington Park, MD

10. Dr. James Luscombe, Code PH
    Naval Postgraduate School
    Monterey, CA